REPORT 1154

CONTENTS

REPORT 1154

ANALYSIS OF LANDING-GEAR BEHAVIOR [1]

By BENJAMIN MILWITZKY and FRANCIS E. COOK

SUMMARY

This report presents a theoretical study of the behavior of the conventional type of oleo-pneumatic landing gear during the process of landing impact. The basic analysis is presented in a general form and treats the motions of the landing gear prior to and subsequent to the beginning of shock-strut deflection. In the analysis of the first phase of the impact the landing gear is treated as a single-degree-of-freedom system in order to determine the conditions of motion at the instant of initial shock-strut deflection, after which instant the landing gear is considered as a system with two degrees of freedom. The equations for the two-degree-of-freedom system consider such factors as the hydraulic (velocity square) resistance of the orifice, the forces due to air compression and internal friction in the shock strut, the nonlinear force-deflection characteristics of the tire, the wing lift, the inclination of the landing gear, and the effects of wheel spin-up drag loads.

The applicability of the analysis to actual landing gears has been investigated for the particular case of a vertical landing gear in the absence of drag loads by comparing calculated results with experimental drop-test data for impacts with and without tire bottoming. The calculated behavior of the landing gear was found to be in good agreement with the drop-test data.

Studies have also been made to determine the effects of variations in such parameters as the dynamic force-deflection characteristics of the tire, the orifice discharge coefficient, and the polytropic exponent for the air-compression process, which might not be known accurately in practical design problems.

The study of the effects of variations in the tire characteristics indicates that in the case of a normal impact without tire bottoming reasonable variations in the force-deflection characteristics have only a relatively small effect on the calculated behavior of the landing gear. Approximating the rather complicated force-deflection characteristics of the actual tire by simplified exponential or linear-segment variations appears to be adequate for practical purposes. Tire hysteresis was found to be relatively unimportant. In the case of a severe impact involving tire bottoming, the use of simplified exponential and linear-segment approximations to the actual tire force-deflection characteristics, which neglect the effects of tire bottoming, although adequate up to the instant of bottoming, fails to indicate the pronounced increase in landing-gear load that results from bottoming of the tire. The use of exponential and linear-segment approximations to the tire characteristics which take into account the increased stiffness of the tire which results from bottoming, however, yields good results.

The study of the importance of the discharge coefficient of the orifice indicates that the magnitude of the discharge coefficient has a marked effect on the calculated behavior of the landing gear; a decrease in the discharge coefficient (or the product of the discharge coefficient and the net orifice area) results in an approximately proportional increase in the maximum upper-mass acceleration.

The study of the importance of the air-compression process in the shock strut indicates that the air springing is of only minor significance throughout most of the impact and that variations in the effective polytropic exponent n between the isothermal value of 1.0 and the near-adiabatic value of 1.3 have only a secondary effect on the calculated behavior of the landing gear. Even the assumption of constant air pressure in the strut equal to the initial pressure, that is, n=0, yields fairly good results which may be adequate for many practical purposes.

In addition to the more exact treatment, an investigation has been made to determine the extent to which the basic equations of motion can be simplified and still yield acceptable results. This study indicates that, for many practical purposes, the air-pressure force in the shock strut can be completely neglected, the tire force-deflection relationship can be assumed to be linear, and the lower or unsprung mass can be taken equal to zero. Generalization of the equations of motion for this simplified system shows that the behavior of the system is completely determined by the magnitude of one parameter, namely the dimensionless initial-velocity parameter. Solutions of these generalized equations are presented in terms of dimensionless variables for a wide range of landing-gear and impact parameters which may be useful for rapidly estimating landing-gear performance in preliminary design.

[1] Supersedes NACA TN 2755, "Analysis of Landing-Gear Behavior" by Benjamin Milwitzky and Francis E. Cook, 1952.

INTRODUCTION

The shock-absorbing characteristics of airplane landing gears are normally developed largely by means of extensive trial-and-error drop testing. The desire to reduce the expense and time required by such methods, as well as to provide a more rational basis for the prediction of wheel-inertia drag loads and dynamic stresses in flexible airframes during landing, emphasizes the need for suitable theoretical methods for the analysis of landing-gear behavior. Such theoretical methods should find application in the design of landing gears and complete airplane structures by permitting

(a) the determination of the behavior of a given landing-gear configuration under varying impact conditions (velocity at contact, weight, wing lift, etc.)

(b) the development of a landing-gear configuration to obtain a specified behavior under given impact conditions

(c) a more rational approach to the determination of wheel spin-up and spring-back loads which takes into account the shock-absorbing characteristics of the particular landing gear under consideration

(d) improved determination of dynamic loads in flexible airplane structures during landing. This problem may be treated either by calculating the response of the elastic system to landing-gear forcing functions determined under the assumption that the airplane is a rigid body or by the simultaneous solution of the equations of motion for the landing gear coupled with the equations representing the additional degrees of freedom of the structure. In many cases the former approach should be sufficiently accurate, but in some instances, particularly when the landing-gear attachment points experience large displacements relative to the nodal points of the flexible system, the latter approach, which takes into account the interaction between the deformations of the structure and the landing gear, may be required in order to represent the system adequately.

Since many aspects of the landing-impact problem are so intimately connected with the mechanics of the landing gear, the subject of landing-gear behavior has received analytical treatment at various times (see bibliography). Many of the earlier investigations, in order to reduce the mathematical complexity of the analysis, were limited to consideration of highly simplified linear systems which have little relation to practical landing gears. Some of the more recent papers consider, with different degrees of simplification, more realistic nonlinear systems. The present report represents an attempt at a more complete analysis of the mechanics of practical landing gears and, in addition, investigates the importance of the various elements which make up the landing gear, as well as the extent to which the system can be reasonably simplified for the purpose of rapid analysis.

The basic analysis is presented in a general form and takes into account such factors as the hydraulic (velocity square) resistance of the orifice, the forces due to air compression and internal friction in the shock strut, the nonlinear force-deflection characteristics of the tire, the wing lift, the inclination of the landing gear and the effects of wheel spin-up drag loads. An evaluation of the applicability of the analysis to actual landing gears is presented for the case of a vertical landing gear in the absence of drag loads by comparing calculated results with drop-test data.

Since some parameters, such as the dynamic force-deflection characteristics of the tire, the orifice discharge coefficient, and the polytropic exponent for the air-compression process, may not be accurately known in practical design problems, a study is made to assess the effects of variations in these parameters on the calculated landing-gear behavior.

Studies are also presented to evaluate the extent to which the dynamical system can be simplified without greatly impairing the validity of the calculated results. In addition to the investigations for specific cases, generalized solutions for the behavior of a simplified system are presented for a wide range of landing-gear and impact parameters which may be useful in preliminary design.

SYMBOLS

A_a	pneumatic area
A_h	hydraulic area
A_o	area of opening in orifice plate
A_1	internal cross-sectional area of shock-strut inner cylinder
A_2	external cross-sectional area of shock-strut inner cylinder
A_p	cross-sectional area of metering pin or rod in plane of orifice
A_n	net orifice area
C_d	orifice discharge coefficient
d	overall diameter of tire
F_a	pneumatic force in shock strut
F_h	hydraulic force in shock strut
F_f	friction force in shock strut
F_S	total axial shock-strut force
F_1	normal force on upper bearing (attached to inner cylinder)
F_2	normal force on lower bearing (attached to outer cylinder)
F_{N_a}	force normal to axis of shock strut, applied at axle
F_{V_a}	vertical force, applied at axle
F_{H_a}	horizontal force, applied at axle
F_{R_a}	resultant force, applied at axle
F_{S_g}	force parallel to axis of shock strut, applied to tire at ground
F_{N_g}	force normal to axis of shock strut, applied to tire at ground
F_{V_g}	vertical force, applied to tire at ground
F_{H_g}	horizontal force, applied to tire at ground
F_{R_g}	resultant force, applied to tire at ground
g	gravitational constant
K_L	lift factor, L/W
L	lift force
l_1	axial distance between upper and lower bearings, for fully extended shock strut
l_2	axial distance between axle and lower bearing (attached to outer cylinder), for fully extended shock strut
a,b,m,r	constants corresponding to the various regimes of the tire-deflection process
a'	combined constant, ad
m'	combined constant, md^r
n	polytropic exponent for air-compression process in shock strut

R Reynolds number
p_a air pressure in upper chamber of shock strut
p_h hydraulic pressure in lower chamber of shock strut
Q volumetric rate of discharge through orifice
r_d radius of deflected tire
s shock-strut axial stroke
T wheel inertia torque reaction
t time after contact
τ time after beginning of shock-strut deflection
v air volume of shock strut
I_w polar moment of inertia for wheel assembly about axle
V_V vertical velocity
V_H horizontal velocity
W total dropping weight
W_1 weight of upper mass above strut
W_2 weight of lower mass below strut
x_2 horizontal displacement of lower mass from position at initial contact
z_1 vertical displacement of upper mass from position at initial contact
z_2 vertical displacement of lower mass from position at initial contact
u_1 dimensionless upper-mass displacement from position at initial contact
u_2 dimensionless lower-mass displacement from position at initial contact
σ dimensionless shock-strut stroke, u_1-u_2
θ dimensionless time after contact
φ angle between shock-strut axis and vertical
η_s shock-strut effectiveness, $\dfrac{\int_0^{\sigma_{max}} u_1''\, d\sigma}{u_1''_{max}\sigma_{max}}$
η_{lg} landing-gear effectiveness, $\dfrac{\int_0^{u_{1_{max}}} u_1''\, du_1}{u_1''_{max}u_{1_{max}}}$
ϵ time interval in numerical integration procedures
μ coefficient of friction between tire and runway
μ_1 coefficient of friction for upper bearing (attached to inner cylinder)
μ_2 coefficient of friction for lower bearing (attached to outer cylinder)
ρ mass density of hydraulic fluid
α angular acceleration of wheel

Axes:

z vertical axis, positive downward
x horizontal axis, positive rearward

Subscripts:

0 at instant of initial contact
τ at instant of initial shock-strut deflection
su at instant of wheel spin-up
max maximum value

Notation:

$|(\ )|$ absolute value of ( )
$(\ )^*$ estimated value of ( )

The use of dots over symbols indicates differentiation with respect to time t or τ.

Prime marks indicate differentiation with respect to dimensionless time θ.

MECHANICS OF LANDING GEAR

DYNAMICS OF SYSTEM

In view of the fact that landing-gear performance appears to be relatively unaffected by the elastic deformations of the airplane structure (see, for example, refs. 1 and 2) particularly since in many cases the main gears are located fairly close to the nodal points of the fundamental bending mode of the wing, that part of the airplane which acts on a given gear can generally be considered as a rigid mass. As a result, landing-gear drop tests are often conducted in a jig where the mass of the airplane is represented by a concentrated weight. In particular instances, however, such as in the case of airplanes having large concentrated masses disposed in an outboard position in the wings, especially airplanes equipped with bicycle landing gear, consideration of the interaction between the deformation of the airplane structure and the landing gear may be necessary to represent the system adequately.

Since the present report is concerned primarily with the mechanics of the landing gear, it is assumed in the analysis that the landing gear is attached to a rigid mass which has freedom only in vertical translation. The gear is assumed infinitely rigid in bending. The combination of airplane and landing gear considered therefore constitutes a system having two degrees of freedom (see fig. 1(a)) as defined by the vertical displacement of the upper mass and the vertical displacement of the lower or unsprung mass, which is also the tire deflection. The strut stroke s is determined by the difference between the displacements z_1 and z_2 and, in the case of inclined gears, by the angle φ between the axis of the strut and the vertical. For inclined gears, compression of the shock strut produces a horizontal displacement of the axle x_2. From consideration of the kinematics of the system it can be seen that $s=\dfrac{z_1-z_2}{\cos\varphi}$ and $x_2=s\sin\varphi=(z_1-z_2)\tan\varphi$. In the analysis, external lift forces, corresponding to the aerodynamic lift, are assumed to act on the system throughout the impact. In addition to the vertical forces, arbitrary drag loads are considered to act between the tire and the ground.

The system treated in the analysis may therefore be considered to represent either a landing-gear drop test in a jig where wing lift and drag loads are simulated, or the landing impact of a rigid airplane if rotational motions are neglected. Rotational freedom of the airplane, where significant, may be taken into account approximately by use of an appropriate effective mass in the analysis.

Figure 1 (b) shows a schematic representation of a typical oleo-pneumatic shock strut used in American practice. The lower chamber of the strut contains hydraulic fluid and the upper chamber contains air under pressure. The outer cylinder of the strut, which is attached to the upper mass, contains a perforated tube which supports a plate with a small orifice, through which the hydraulic fluid is forced to flow at high velocity as a result of the telescoping of the strut. The hydraulic pressure drop across the orifice thus produced resists the closure of the strut, and the turbulence created provides a powerful means of absorbing and dissipating a large part of the impact energy. In some struts the orifice area is constant; whereas, in other cases a metering

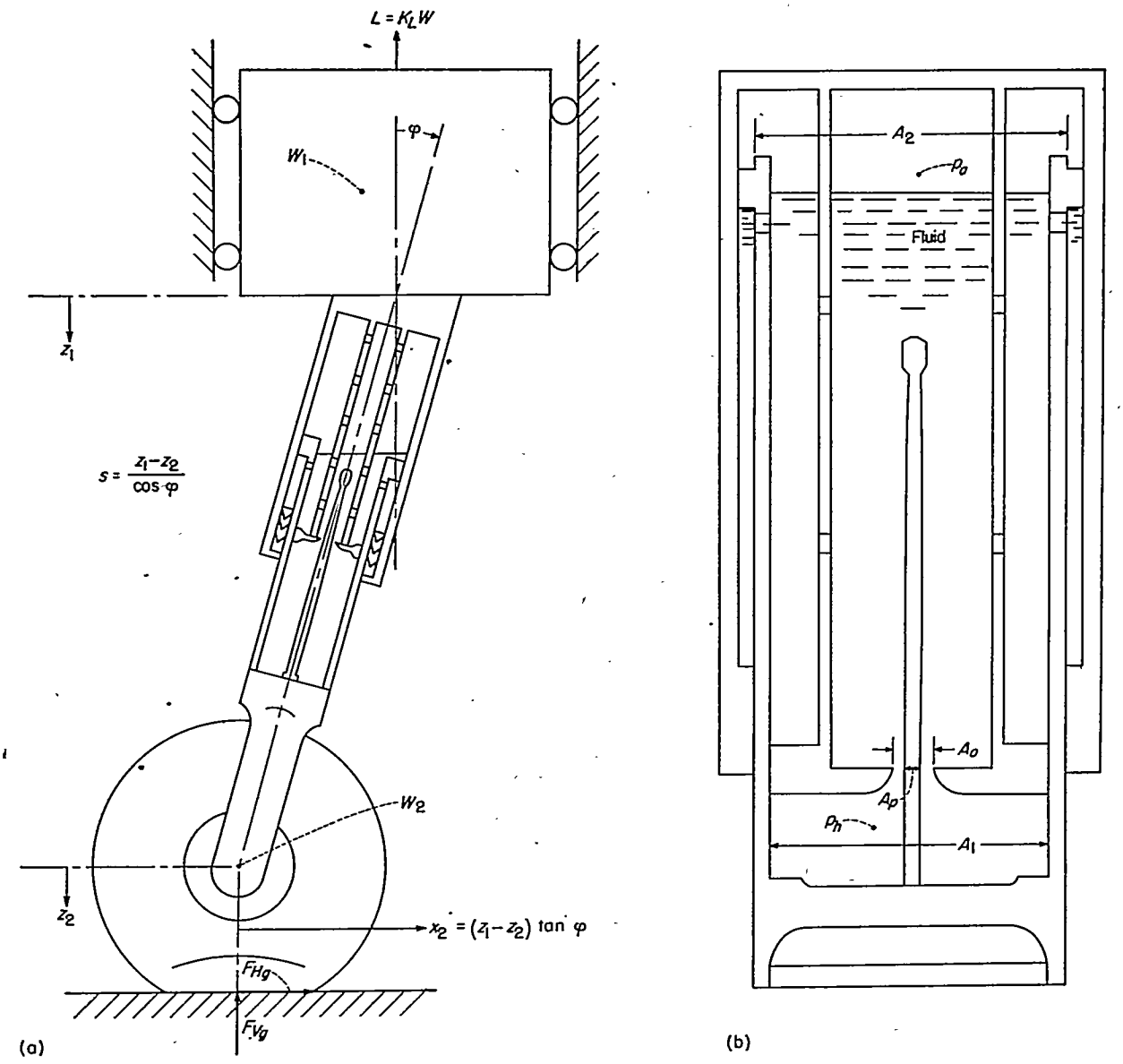

(a) System with two degrees of freedom.

(b) Schematic representation of shock strut.

FIGURE 1.—Dynamical system considered in analysis.

pin or rod is used to control the size of the orifice and govern the performance of the strut.

The compression of the strut produces an increase in the air pressure which also resists the closure of the strut. In figure 1 (b) p_h represents the oil pressure in the lower chamber and p_a represents the air pressure in the upper chamber.

In addition to the hydraulic resistance and air-pressure forces, internal bearing friction also contributes forces which can appreciably affect the behavior of the strut.

The forces created within the strut impart an acceleration to the upper mass and also produce an acceleration of the lower mass and a deflection of the tire. Figure 1 (c) shows the balance of forces and reactions for the wheel, the inner cylinder, and the outer cylinder. It is clear that the strut and the tire mutually influence the behavior of one another and must be considered simultaneously in analyzing the system.

FORCES IN SHOCK STRUT

From consideration of the pressures acting in the shock strut it can be readily seen from figure 1 (b) that the total axial force due to hydraulic resistance, air compression, and bearing friction can be expressed by

$$F_S = p_h(A_1 - A_p) + p_a(A_2 - A_1) + p_a A_p + F_f$$

where

A_1 internal cross-sectional area of inner cylinder
A_2 external cross-sectional area of inner cylinder
A_p cross-sectional area of metering pin or rod in plane of orifice

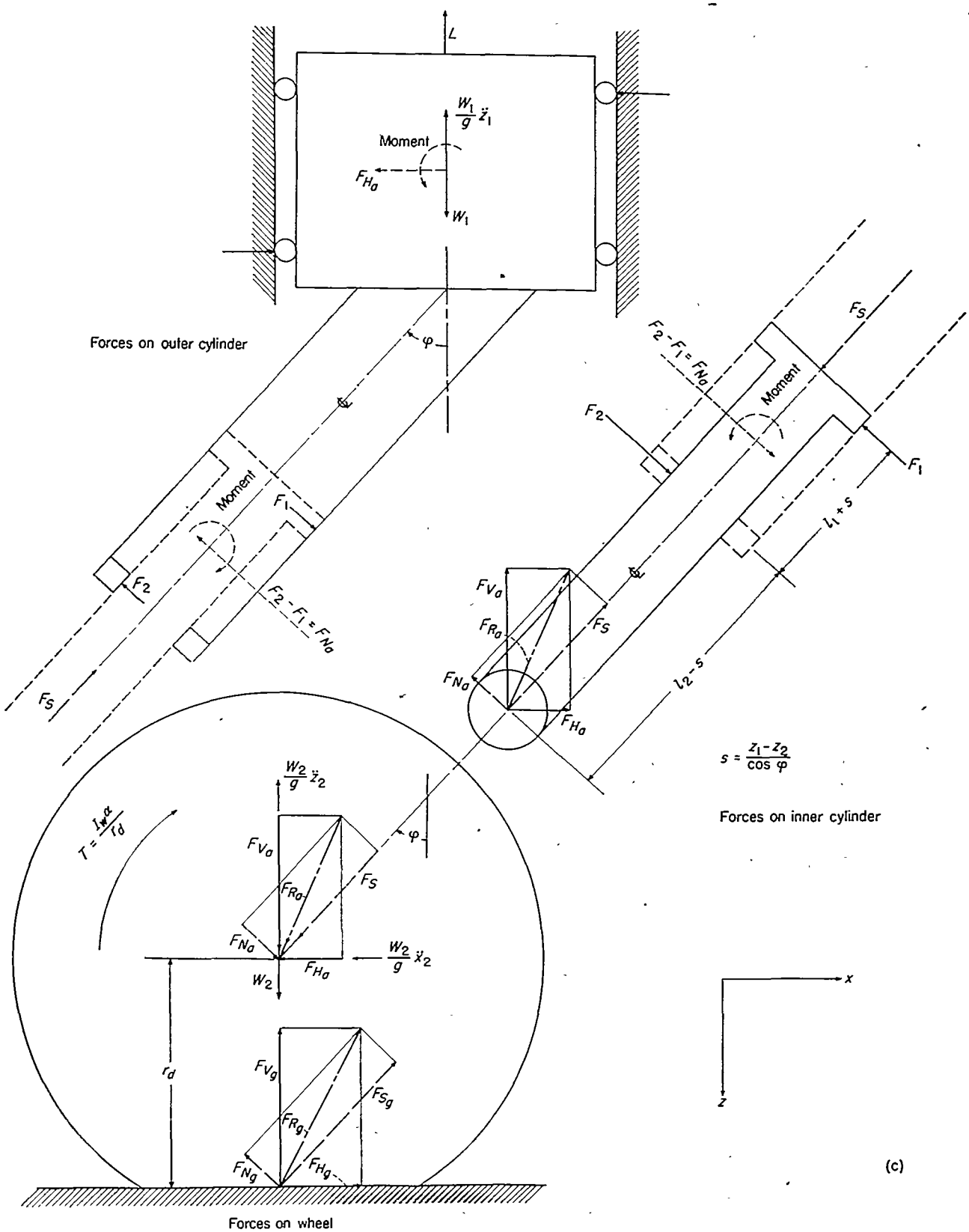

(c) Balance of forces and reactions for landing-gear components.

FIGURE 1.—Concluded.

This expression can also be written as

$$F_S=(p_h-p_a)(A_1-A_p')+p_aA_2+F_f$$
$$=(p_h-p_a)A_h+p_aA_a+F_f$$
$$=F_h+F_a+F_f \quad (1)$$

where

p_h-p_a pressure drop across the orifice
A_h hydraulic area (A_1-A_p for the strut shown in fig. 1)
A_a pneumatic area (A_2 for the strut shown in fig. 1)

In this report the terms $(p_h-p_a)A_h$ and p_aA_a are referred to as hydraulic force F_h and pneumatic force F_a, respectively. For the strut shown in figure 1, the hydraulic and pneumatic areas are related to the strut dimensions as previously noted. In the case of struts having different internal configurations, the hydraulic and pneumatic areas may bear somewhat different relations to the dimensions of the strut. In such cases, however, consideration of the pressures acting on the various components of the strut should permit these areas to be readily defined.

Hydraulic force.—The hydraulic resistance in the shock strut results from the pressure difference associated with the flow through the orifice. In a landing gear the orifice area is usually small enough in relation to the diameter of the strut so that the jet velocities and Reynolds numbers are sufficiently large that the flow is fully turbulent. As a result the damping force varies as the square of the telescoping velocity rather than linearly with the velocity. Since the hydraulic resistance is the major component of the total shock-strut force, viscous damping cannot be reasonably assumed, even though such an assumption would greatly simplify the analysis.

The hydraulic resistance can be readily derived by making use of the well-known equation for the discharge through an orifice, namely,

$$Q=C_dA_n\sqrt{\frac{2}{\rho}(p_h-p_a)}$$

where

Q volumetric rate of discharge
C_d coefficient of discharge
A_n net orifice area
p_h hydraulic pressure in lower chamber
p_a air pressure in upper chamber
ρ mass density of hydraulic fluid

From considerations of continuity, the volumetric rate of discharge can also be expressed as the product of the telescoping velocity $\dot{s}$ and the hydraulic area A_h

$$Q=A_h\dot{s}$$

Equating the preceding expressions for the discharge permits writing the following simple equation for the pressure drop across the orifice

$$p_h-p_a=\frac{\rho A_h^2\dot{s}^2}{2(C_dA_n)^2}$$

The hydraulic resistance F_h due to the telescoping of the strut is given by the product of the differential pressure p_h-p_a and the area A_h which is subjected to the hydraulic pressure, as previously noted. Thus

$$F_h=\frac{\rho A_h^3}{2(C_dA_n)^2}\dot{s}^2 \quad (2)$$

Equation (2) can be made applicable to both the compression and elongation strokes by introducing the factor $\frac{\dot{s}}{|\dot{s}|}$ to indicate the sign of the hydraulic resistance; thus

$$F_h=\frac{\dot{s}}{|\dot{s}|}\frac{\rho A_h^3}{2(C_dA_n)^2}\dot{s}^2 \quad (2a)$$

The net orifice area A_n may be either a constant or, when a metering pin is used, can vary with strut stroke; that is, $A_n=A_o-A_p=A_n(s)$, where A_o is the area of the opening in the orifice plate and A_p is the area of the metering pin in the plane of the orifice. At the present time there appears to be some tendency to eliminate the metering pin and use a constant orifice area, particularly for large airplanes, in which case $A_n=A_o$. In the general case, the orifice discharge coefficient might be expected to vary somewhat during an impact because of changes in the size and configuration of the net orifice area, changes in the exit conditions on the downstream face of the orifice due to variations in the amount of hydraulic fluid above the orifice plate, changes in the entry conditions due to variations in the length of the flow chamber upstream of the orifice, and because of variations in the Reynolds number of the flow, so that, in general, $C_d=C_d(s, R)$. Although the individual effects of these factors on the discharge coefficients for orifices in shock struts have not been evaluated, there is some experimental evidence to indicate appreciable variations of the discharge coefficient during impact, particularly in the case of struts with metering pins. It might be expected that such variations would be considerably smaller for gears having a constant orifice area.

In order to evaluate the precision with which the orifice discharge coefficient has to be known, a brief study is presented in a subsequent section which shows the effect of the discharge coefficient on the calculated behavior of a landing gear with a constant orifice area, under the assumption that the discharge coefficient is constant during the impact.

The foregoing discussion has been concerned primarily with the compression stroke of the shock strut. Most struts incorporate some form of pressure-operated rebound check valve, sometimes called a snubber valve, which comes into action after the maximum stroke has been attained and closes off the main orifice as soon as the strut begins to elongate, so that the fluid is forced to return to the lower chamber through small passages. The action of the snubber valve introduces greatly increased hydraulic resistance to dissipate the energy stored in the strut in the form of air pressure and to prevent excessive rebound. The product C_dA_n to be used in equation (2a) during the elongation stroke is generally uncertain. The exact area A_n during elongation is usually somewhat difficult to define from the geometry of the strut since in many cases the number of connecting passages varies with stroke and the

leakage area around the piston may be of the same order of magnitude as the area of the return passages. Furthermore, the magnitude of the orifice discharge coefficient, and even possibly the nature of the resistance, are questionable due to the foaming state of the returning fluid. Fortunately, the primary interest is in the compression process rather than the elongation process since the maximum load always occurs before the maximum strut stroke is reached.

Pneumatic force.—The air-pressure force in the upper chamber is determined by the initial strut inflation pressure, the area subjected to the air pressure (pneumatic area), and the instantaneous compression ratio in accordance with the polytropic law for compression of gases, namely $p_a v^n = \text{Constant}$, or

$$p_a = p_{a_0}\left(\frac{v_0}{v}\right)^n$$

where

p_a air pressure in upper chamber of shock strut
p_{a0} air pressure in upper chamber for fully extended strut
v air volume of shock strut
v_0 air volume for fully extended strut

Since the instantaneous air volume is equal to the difference between the initial air volume and the product of the stroke and pneumatic area A_a, $p_a = p_{a_0}\left(\frac{v_0}{v_0 - A_a s}\right)^n$. The force due to the air pressure is simply the product of the pressure and the pneumatic area:

$$F_a = p_{a_0} A_a \left(\frac{v_0}{v_0 - A_a s}\right)^n \tag{3}$$

In the preceding equations, the effective polytropic exponent n depends on the rate of compression and the rate of heat transfer from the air to the surrounding environment. Low rates of compression would be expected to result in values of n approaching the isothermal value of 1.0; whereas higher values of n, limited by the adiabatic value of 1.4, would be expected for higher rates of compression. The actual thermodynamic process is complicated by the violent mixing of the highly turbulent efflux of hydraulic fluid and the air in the upper chamber during impact. On the one hand, the dissipation of energy in the production of turbulence generates heat; on the other hand, heat is absorbed by the aeration and vaporization of the fluid. The effect of this mixing phenomenon on the polytropic exponent or on the equivalent air volume is not clear. A limited amount of experimental data obtained in drop tests (refs. 3 and 4), however, indicates that the effective polytropic exponent may be in the neighborhood of 1.1 for practical cases. A brief study of the importance of the air-compression process and the effects which different values of n may have on the calculated behavior of the landing gear is presented in a subsequent section.

Internal friction force.—In the literature on machine design the wide range of conditions under which frictional resistance can occur between sliding surfaces is generally classified in three major categories, namely, friction between dry surfaces, friction between imperfectly lubricated surfaces, and friction between perfectly lubricated surfaces. In the case of dry friction, the resistance depends on the physical characteristics of the sliding surfaces, is essentially proportional to the normal force, and is approximately independent of the surface area. The coefficient of friction μ, defined as the ratio of the frictional resistance to the normal force, is generally somewhat greater under conditions of rest (static friction) than under conditions of sliding (kinetic friction). Although the coefficient of kinetic friction generally decreases slightly with increasing velocity, it is usually considered, in first approximation, to be independent of velocity. If, on the other hand, the surfaces are completely separated by a fluid film of lubricant, perfect lubrication is said to exist. Under these conditions the resistance to relative motion depends primarily on the magnitude of the relative velocity, the physical characteristics of the lubricant, the area, and the film thickness, and is essentially independent of the normal force and the characteristics of the sliding surfaces. Perfect lubrication is rarely found in practice but is most likely under conditions of high velocity and relatively small normal pressure, where the shape of the sliding surfaces is conducive to the generation of fluid pressure by hydrodynamic action. In most practical applications involving lubrication, a state of imperfect lubrication exists and the resistance phenomenon is intermediate between that of dry friction and perfect lubrication.

In the case of landing-gear shock struts, the conditions under which internal friction is of concern usually involve relatively high normal pressures and relatively small sliding velocities. Moreover, the usual types of hydraulic fluid used in shock struts have rather poor lubricating properties, and the shape of the bearing surfaces is generally not conducive to the generation of hydrodynamic pressures. It would therefore appear that the lubrication of shock strut bearings is, at best, imperfect; in fact, the conditions appear to approach closely those for dry friction. In the present analysis, therefore, it is assumed, in first approximation, that the internal friction between the bearings and the cylinder walls follows laws similar to those for dry friction; that is, the friction force is given by the product of the normal force and a suitably chosen coefficient of friction.

With these assumptions the internal friction forces produced in the strut depend on the magnitude of the forces on the axle, the inclination of the gear, the spacing of the bearings, and the coefficient of friction between the bearings and the cylinder walls. Figure 1(c) schematically illustrates the balance of forces acting on the various components of the landing gear. The total axial friction in the shock strut is the sum of the friction forces contributed by each of the bearings:

$$F_f = \frac{\dot{s}}{|\dot{s}|}\left(\mu_1 |F_1| + \mu_2 |F_2|\right)$$

where

F_f axial friction force
μ_1 coefficient of friction for upper bearing (attached to inner cylinder)
F_1 normal force on upper bearing (attached to inner cylinder)
μ_2 coefficient of friction for lower bearing (attached to outer cylinder)

F_2 normal force on lower bearing (attached to outer cylinder)

$\frac{\dot{s}}{|\dot{s}|}$ factor to indicate sign of friction force

During the interval prior to the beginning of shock-strut motion the friction forces depend on the coefficients of static friction; after the strut begins to telescope the coefficients of kinetic friction apply.

From considerations of the balance of moments it can be seen from figure 1(c) that

$$F_1=F_{N_a}\left(\frac{l_2-s}{l_1+s}\right)$$

and

$$F_2=F_{N_a}\left(\frac{l_2-s}{l_1+s}+1\right)$$

so that

$$F_f=\frac{\dot{s}}{|\dot{s}|}|F_{N_a}|\left[(\mu_1+\mu_2)\frac{l_2-s}{l_1+s}+\mu_2\right] \quad (4)$$

where

$$F_{N_a}=F_{V_a}\sin\varphi-F_{H_a}\cos\varphi \quad (4a)$$

and

F_{N_a} force normal to strut applied at axle
F_{V_a} vertical force applied at axle
F_{H_a} horizontal force applied at axle
φ angle between strut axis and vertical
l_1 axial distance between upper and lower bearings, for fully extended strut
l_2 axial distance between axle and lower bearing (attached to outer cylinder), for fully extended strut

The quantities F_{N_a}, F_{V_a}, and F_{H_a} are forces applied at the axle and differ from the ground reactions by amounts equal to the inertia forces corresponding to the respective acceleration component of the lower mass. Since the inner cylinder generally represents only a relatively small fraction of the lower mass, the lower mass may reasonably be assumed to be concentrated at the axle. With this assumption, the relationships between the forces at the axle and the forces at the ground are given by

$$F_{V_a}=\left(F_{V_g}+\frac{W_2}{g}\ddot{z}_2-W_2\right) \qquad F_{H_a}=\left(F_{H_g}-\frac{W_2}{g}\ddot{x}_2\right)$$

The normal force at the axle can therefore be expressed in terms of the ground reactions and the component accelerations of the lower mass by

$$F_{N_a}=\left(F_{V_g}+\frac{W_2}{g}\ddot{z}_2-W_2\right)\sin\varphi-\left(F_{H_g}-\frac{W_2}{g}\ddot{x}_2\right)\cos\varphi \quad (4b)$$

where

F_{V_g} vertical force applied to tire at ground
F_{H_g} horizontal force applied to tire at ground
$\frac{W_2}{g}$ effective mass below shock strut, assumed concentrated at axle
$\ddot{x}_2$ horizontal acceleration of axle
$\ddot{z}_2$ vertical acceleration of axle

In the case of an inclined landing gear having infinite stiffness in bending, the horizontal displacement of the lower mass x_2 is related to the vertical displacements of the upper and lower masses by the kinematic relationship $x_2=(z_1-z_2)\tan\varphi$, as previously noted. Double differentiation of this relationship gives $\ddot{x}_2=(\ddot{z}_1-\ddot{z}_2)\tan\varphi$. Substitution of this expression into equation (4b) gives

$$F_{N_a}=F_{V_g}\sin\varphi-F_{H_g}\cos\varphi+\frac{W_2}{g}\ddot{z}_1\sin\varphi-W_2\sin\varphi \quad (4c)$$

In equation (4c) the quantity $\ddot{z}_1\sin\varphi$ represents the acceleration of the lower mass normal to the strut axis when the gear is rigid in bending. In the case of a gear flexible in bending, the normal acceleration of the lower mass is not completely determined by the vertical acceleration of the upper mass and the angle of inclination of the gear. If it should be necessary to take into account, in particular cases, the effects of gear flexibility on the relationship between the normal force on the axle and the ground reactions, the quantity $\ddot{z}_1\sin\varphi$ in equation (4c) may be replaced by estimated values of the actual normal acceleration of the lower mass as determined from consideration of the bending response of the gear to the applied forces normal to the gear axis. The effects of gear flexibility are not considered in more detail in the present analysis.

FORCES ON TIRE

Figure 2 (a) shows dynamic force-deflection characteristics for a 27-inch smooth-contour (type I) tire inflated to 32 pounds per square inch. These characteristics were determined from time-history measurements of vertical ground force and tire deflection in landing-gear drop tests with a nonrotating wheel at several vertical velocities. As can be seen, the tire compresses along one curve and unloads along another, the hysteresis loop indicating appreciable energy dissipation in the tire. There is some question as to whether the amount of hysteresis would be as great if the tire were rotating, as in a landing with forward speed. The force-deflection curve for a velocity of 11.63 feet per second is for a severe impact in which tire bottoming occurs and shows the sharp increase in force with deflection subsequent to bottoming.

In figure 2 (b) the same force-deflection characteristics are shown plotted on logarithmic coordinates. As can be seen, the force exhibits an exponential variation with deflection. A systematized representation of the force-deflection relationship can therefore be obtained by means of simple equations having the form

$$F_{V_g}=mz_2^r=m'\left(\frac{z_2}{d}\right)^r \quad (5)$$

where

F_{V_g} vertical force, applied to tire at ground
z_2 vertical displacement of lower mass from position at initial contact (radial deflection of tire)
d overall diameter of tire
m, r constants corresponding to the various regimes of the tire-deflection process
m' combined constant, md^r

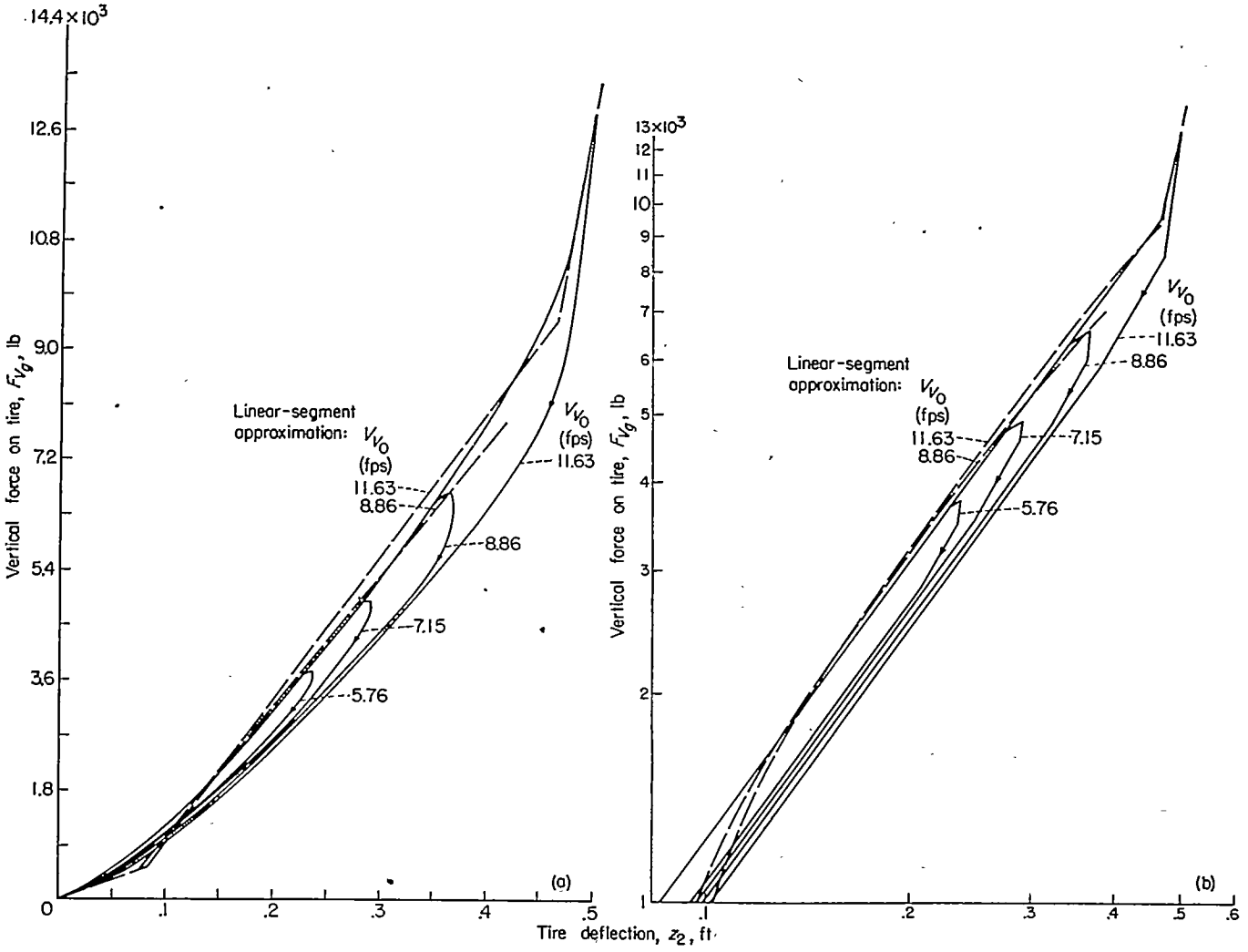

(a) Uniform coordinates. (b) Logarithmic coordinates

FIGURE 2.—Dynamic force-deflection characteristics of tire.

It may be noted from figure 2 that essentially the same force-deflection curve holds during compression for all impact velocities, up to the occurrence of tire bottoming, and that in figure 2 (b) the slopes of the curves in each of the several regimes of the tire-deflection process are also independent of velocity, except in the compression regime following tire bottoming.

Figure 2 also shows simple approximations to the tire characteristics which were obtained by fitting straight-line segments (long-dashed lines) to the actual force-deflection curves in figure 2 (a) for impacts at 8.86 and 11.63 feet per second. These approximations, hereinafter referred to as linear-segment approximations, are included in a study, presented in a subsequent section, to evaluate the degree of accuracy required for adequate representation of the tire characteristics. The various representations of the tire characteristics considered and the pertinent constants for each regime of tire deflection are shown in figure 3.

EQUATIONS OF MOTION

The internal axial force F_S produced by the shock strut was shown in a previous section to be equal to the sum of the hydraulic, pneumatic, and friction forces, as given by equation (1). Since these forces act along the axis of the strut, which may be inclined to the vertical by an angle φ, the vertical component of the axial shock-strut force is given by $F_S \cos \varphi$. The vertical component of the force normal to the shock strut is given by $F_{N_a} \sin \varphi$. These forces act in conjunction with the lift force and weight to produce an acceleration of the upper mass. The equation of motion for the upper mass is

$$F_S \cos \varphi + F_{N_a} \sin \varphi + L - W_1 = -\frac{W_1}{g} \ddot{z}_1 \qquad (6)$$

The vertical components of the axial and normal shock-strut forces also act, in conjunction with the weight of the lower mass, to produce a deformation of the tire and an acceleration of the lower mass. The equation of motion for the lower mass is

$$F_S \cos \varphi + F_{N_a} \sin \varphi + W_2 - \frac{W_2}{g} \ddot{z}_2 = F_{V_g}(z_2) \qquad (7)$$

where the vertical ground reaction F_{V_g} is expressed as a

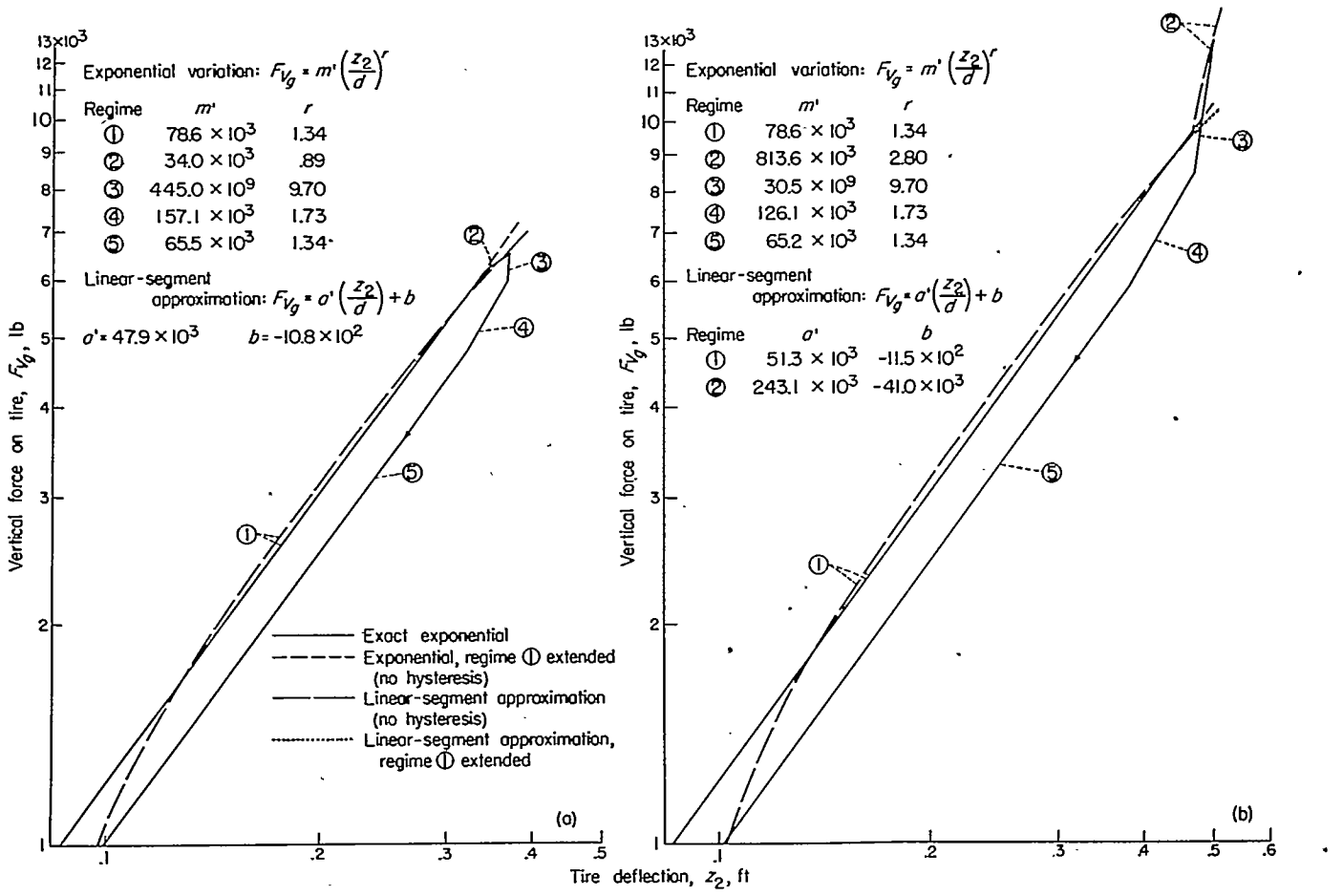

(a) Impact without tire bottoming, V_{V_0}=8.86 feet per second.

(b) Impact with tire bottoming, V_{V_0}=11.63 feet per second.

FIGURE 3.—Tire characteristics considered in solutions (logarithmic coordinates).

function of the tire deflection z_2. The relationship between F_{V_g} and z_2 has been discussed in the previous section on tire characteristics.

By combining equations (6) and (7), the vertical ground force can be written in terms of the inertia reactions of the upper and lower masses, the lift force, and the total weight. The overall dynamic equilibrium is given by

$$F_{V_g}(z_2) = -\frac{W_1}{g}\ddot{z}_1 - \frac{W_2}{g}\ddot{z}_2 - L + W \tag{8}$$

MOTION PRIOR TO SHOCK-STRUT DEFLECTION

Conventional oleo-pneumatic shock struts are inflated to some finite pressure in the fully extended position. Thus the strut does not begin to deflect in an impact until sufficient force is developed to overcome the initial preloading imposed by the air pressure and internal friction. Since the strut is effectively rigid in compression, as well as in bending, prior to this instant, the system may be considered to have only one degree of freedom during the initial stage of the impact. The equations of motion for the one-degree-of-freedom system are derived in order to permit determination of the initial conditions required for the analysis of the landing-gear behavior subsequent to the beginning of shock-strut deflection.

Since $\ddot{z}_1 = \ddot{z}_2 = \ddot{z}$ during this first phase of the impact, equation (8) may be written as

$$F_{V_g}(z) = -\frac{W}{g}\ddot{z} - W(K_L - 1) \tag{9}$$

where

$$K_L = \frac{L}{W}$$

For the general case of an exponential relationship between vertical ground force and tire deflection, equation (5) applies and the equation of motion becomes

$$\frac{W}{g}\ddot{z} + mz^r + W(K_L - 1) = 0 \tag{10}$$

The shock strut begins to telescope when the sum of the inertia, weight, and lift forces becomes equal to the vertical components of the axial and normal shock-strut forces. At this instant t_τ, $F_S=F_{a_0}+F_{f_\tau}$ and equation (6) can be written as

$$\ddot{z}_\tau=-\frac{(F_{a_0}+F_{f_\tau})\cos\varphi+F_{N_{a_\tau}}\sin\varphi+K_L W-W_1}{W_1/g} \tag{11}$$

where

F_{a_0} initial air-pressure preload force, $p_{a_0}A_a$

F_{f_τ} static friction at instant t_τ

At the instant t_τ, $s=0$ and equation (4) becomes

$$F_{f_\tau}=\left|F_{N_{a_\tau}}\right|K_\mu \tag{11a}$$

where

$$K_\mu=\left[(\mu_1+\mu_2)\frac{l_2}{l_1}+\mu_2\right]$$

and μ_1 and μ_2 are coefficients of static friction.

Since the strut is assumed essentially rigid in compression (and also rigid in bending), there is no kinematic displacement of the lower mass in the horizontal direction up to the beginning of shock-strut deflection, so that $x_2=0$ and equation (4b) becomes

$$F_{N_{a_\tau}}=\left(F_{V_{g_\tau}}+\frac{W_2}{g}\ddot{z}_\tau-W_2\right)\sin\varphi-F_{H_{g_\tau}}\cos\varphi \tag{11b}$$

Incorporating equations (11a), (11b), and (9) into equation (11) gives

$$\ddot{z}_\tau=\frac{F_{a_0}-(\pm K_\mu\sin\varphi-\cos\varphi)(K_L W-W_1)-F_{H_g}(\pm K_\mu\cos\varphi+\sin\varphi)}{\frac{W_1}{g}(\pm K_\mu\sin\varphi-\cos\varphi)} \tag{12}$$

In equation (12) wherever the $\pm$ sign appears, the plus signs apply when $F_{N_{a_\tau}}>0$ and the minus signs apply when $F_{N_{a_\tau}}<0$.

From equation (10) the vertical displacement of the system at the instant t_τ is given in terms of the corresponding acceleration by

$$z_\tau=\left\{\frac{1}{m}\left[W(1-K_L)-\frac{W}{g}\ddot{z}_\tau\right]\right\}^{1/r} \tag{13}$$

Integrating equation (10) and noting that $z_0=0$ provides the relationship between the vertical velocity and the vertical displacement of the system at the beginning of shock-strut deflection

$$\dot{z}_\tau=\sqrt{\dot{z}_0{}^2-\frac{2g}{W}\left[\frac{m}{r+1}z_\tau{}^{r+1}+W(K_L-1)z_\tau\right]} \tag{14}$$

In view of the fact that the tire force-deflection curve is essentially linear for small deflections, it may be reasonably assumed that $r=1$ for the purpose of determining the time after contact at which the strut begins to telescope. With this assumption t_τ can be determined from the relationship

$$t_\tau=\int_0^{z_\tau}\frac{dz}{\dot{z}}=\int_0^{z_\tau}\frac{dz}{\sqrt{\dot{z}_0{}^2-\frac{2g}{W}\left[\frac{m}{2}z^2+W(K_L-1)z\right]}}$$

where the general expression for the variable $\dot{z}$ is obtained from equation (14) without the subscripts τ. Performing the indicated integration gives

$$t_\tau=\sqrt{\frac{W}{mg}}\left\{\sin^{-1}C(1-K_L)-\sin^{-1}C\left[(1-K_L)-\frac{mz_\tau}{W}\right]\right\} \tag{15}$$

where

$$C=\frac{g}{\sqrt{\dot{z}_0{}^2\frac{mg}{W}+[(1-K_L)g]^2}}$$

The computation of t_τ can be greatly simplified by use of the following approximation which assumes a linear relationship between velocity and time:

$$t_\tau=\frac{2z_\tau}{\dot{z}_0+\dot{z}_\tau} \tag{15a}$$

Equation (15a) should be a fairly good approximation in view of the relatively short time interval between initial contact and the beginning of shock-strut motion.

Equations (12), (13), and (14) permit the determination of the vertical acceleration, displacement, and velocity, respectively, of the system (upper and lower masses) at the

beginning of shock-strut deflection. Equation (15) or (15a) permits calculation of the time interval between initial contact and this instant. These equations provide the initial conditions required for the analysis of the behavior of the landing gear as a system with two degrees of freedom after the shock strut begins to deflect.

If drag loads are considered, the solution of equation (12) requires knowledge of the horizontal ground force $F_{H_{g_\tau}}$ at the instant t_τ. Since the present analysis does not explicitly treat the determination of drag loads, values of $F_{H_{g_\tau}}$ have to be estimated, either from other analytical considerations, experimental data, or on the basis of experience.

MOTION SUBSEQUENT TO BEGINNING OF SHOCK-STRUT DEFLECTION

Once the sum of the inertia, weight, and lift forces becomes sufficiently large to overcome the preloading force in the shock strut due to initial air pressure and internal friction, the shock strut can deflect and the system becomes one having two degrees of freedom. Incorporating the expressions for the hydraulic, pneumatic, and friction forces (eqs. (2a), (3), and (4)) into equation (6) permits the equation of motion for the upper mass to be written as follows:

$$\frac{W_1}{g}\ddot{z}_1+\left\{\frac{\dot{s}}{|\dot{s}|}\frac{\rho A_h^3}{2(C_dA_a)^2}\dot{s}^2+p_{a_0}A_a\left(\frac{v_0}{v_0-A_as}\right)^n+\frac{\dot{s}}{|\dot{s}|}|F_{N_a}|\left[(\mu_1+\mu_2)\frac{l_2-s}{l_1+s}+\mu_2\right]\right\}\cos\varphi+K_LW-W_1+F_{N_a}\sin\varphi=0 \tag{16}$$

where

$$s=\frac{z_1-z_2}{\cos\varphi}$$

$$\dot{s}=\frac{\dot{z}_1-\dot{z}_2}{\cos\varphi}$$

and, since $F_{V_g}=F_{V_g}(z_2)$, equation (4c) becomes

$$F_{N_a}=F_{V_g}(z_2)\sin\varphi-F_{H_g}\cos\varphi+\frac{W_2}{g}\ddot{z}_1\sin\varphi-W_2\sin\varphi$$

where $F_{V_g}(z_2)$ is determined from the force-deflection characteristics of the tire. For the usual type of pneumatic tire, $F_{V_g}(z_2)=mz_2^r$, as previously noted.

Similarly, the equation of motion for the lower mass follows from equation (7):

$$\frac{W_2}{g}\ddot{z}_2-\left\{\frac{\dot{s}}{|\dot{s}|}\frac{\rho A_h^3}{2(C_dA_a)^2}\dot{s}^2+p_{a_0}A_a\left(\frac{v_0}{v_0-A_as}\right)^n+\frac{\dot{s}}{|\dot{s}|}|F_{N_a}|\left[(\mu_1+\mu_2)\frac{l_2-s}{l_1+s}+\mu_2\right]\right\}\cos\varphi+F_{V_g}(z_2)-F_{N_a}\sin\varphi-W_2=0 \tag{17}$$

The overall dynamic equilibrium equation is still, of course, as given by equation (8)

$$\frac{W_1}{g}\ddot{z}_1+\frac{W_2}{g}\ddot{z}_2+W(K_L-1)+F_{V_g}(z_2)=0$$

Any two of the preceding equations (eqs. (16), (17), and (8)) are sufficient to describe the behavior of the landing gear subsequent to the beginning of shock-strut motion. These equations may be used to calculate the behavior of a given landing-gear configuration or to develop orifice and metering-pin characteristics required to produce a specified behavior for given impact conditions. They may also be used as a basis for the calculation of dynamic loads in flexible airplane structures either by (a) determining the landing-gear forcing function under the assumption that the upper mass is a rigid body and then using this forcing function to calculate the response of the elastic system or (b) combining the preceding equations with the equations representing the additional degrees of freedom of the structure; the simultaneous solution of the equations for such a system would then take into account the interaction between the deformation of the structure and the landing gear.

SOLUTION OF EQUATIONS OF MOTION

In the general case the analysis of a landing gear involves the solution of the equations of motion given in the section entitled "Motion Subsequent to the Beginning of Shock-Strut Deflection," with the initial conditions taken as the conditions of motion at the beginning of shock-strut deflection, as determined in accordance with the initial impact conditions and the equations given in the section entitled "Motion Prior to Shock-Strut Deflection."

NUMERICAL INTEGRATION PROCEDURES

In view of the fact that the equations of motion for the landing gear subsequent to the beginning of shock-strut deflection are highly nonlinear, analytical solution of these equations does not appear feasible. In the present report, therefore, finite-difference methods are resorted to for the step-by-step integration of the equations of motion. Al-

though such numerical methods lack the generality of analytical solutions and are especially time consuming if the calculations are carried out manually, the increasing availability of automatic calculating machines largely overcomes these objections.

Most of the solutions presented in this report were obtained with a procedure, hereinafter referred to as the "linear procedure," which assumes changes in the motion variables to be linear over finite time intervals. A few of the solutions presented were obtained with a procedure, hereinafter referred to as the "quadratic procedure," which assumes a quadratic variation of displacement with time for successive intervals. The generalized solutions for the simplified equations discussed in a subsequent section were obtained by means of the Runge-Kutta procedure. The application of these procedures is described in detail in appendix A.

USE OF TIRE FORCE-DEFLECTION CHARACTERISTICS

In order to obtain solutions for particular cases, it is, of course, necessary to have, in addition to information regarding the physical characteristics of the landing gear, some knowledge of the force-deflection characteristics of the tire.

If extensive data regarding the dynamic tire characteristics, such as shown in figures 2 and 3, are available, an accurate solution can be obtained which takes into account the various breaks in the force-deflection curves (logarithmic coordinates), as well as the effects of hysteresis. In view of the fact that the constants m' and r have the same values throughout practically the entire tire compression process regardless of the initial impact velocity or the maximum load attained, these values of m' and r, as determined from the force-deflection curves, can be used in the calculation of the motion subsequent to the beginning of shock-strut deflection until the first break in the force-deflection curve is reached prior to the attainment of the maximum force. If the conditions for the calculations are the same as those for which force-deflection curves are available, the values of m' and r for each of the several regimes subsequent to the first break can also be determined directly from the force-deflection curves. In general, however, the conditions will not be the same and interpolation will be necessary to estimate the values of m' for the subsequent regimes. Such interpolation is facilitated, particularly after the maximum force-deflection point has been calculated, by the fact that each subsequent regime has a fixed value of r, regardless of the initial impact conditions.

The use of the tire-deflection characteristics in the calculations is greatly simplified if hysteresis is neglected since the values of m' and r which apply prior to the first break in the force-deflection curves are then used throughout the entire calculation, except in the case of severe impacts where tire bottoming occurs, in which case new values of m' and r are employed in the tire-bottoming regime. A similar situation exists with respect to the constants a' and b when the linear approximations which neglect hysteresis are used. These simplifications would normally be employed when only the tire manufacturer's static or so-called impact load-deflection data are available, as is usually the case.

EFFECT OF DRAG LOADS

Although the present analysis permits taking into account the effects of wheel spin-up drag loads on the behavior of the landing gear, the determination of the drag-load time history is not treated explicitly. Thus, if it is desired to consider the effects of the drag load on the gear behavior, such as in the case of a drop test in which drag loads are simulated by reverse wheel rotation or in a landing with forward speed, it is necessary to estimate the drag load, either by means of other analytical considerations or by recourse to experimental data. As a first approximation the instantaneous drag force may be assumed to be equal to the vertical ground reaction multiplied by a suitable coefficient of friction μ; that is, $F_{H_g}=F_{V_g}\mu$, up to the instant when the wheel stops skidding, after which the drag force may be assumed equal to zero. (The current ground-loads requirements specify a skidding coefficient of friction $\mu=0.55$; limited experimental evidence, on the other hand, indicates that μ may be as high as 0.7 or as low as 0.4.) In some cases experimental data indicate that representation of the drag-load time history can be simplified even further by assuming a linear variation of the drag force with time during the period of wheel skidding.

The instant at which the wheel stops skidding can be estimated from the simple impulse-momentum relationship

$$\int_0^{t_{su}} F_{H_g}\,dt=\mu\int_0^{t_{su}} F_{V_g}\,dt=\frac{I_w V_{H_0}}{r_d^2}$$

where

I_w polar moment of inertia of wheel assembly about axle
V_{H_0} initial horizontal velocity
r_d radius of deflected tire
t_{su} time of wheel spin-up

When the drag force is expressed in terms of the vertical force, the value of the integral $\int_0^t F_{H_g}\,dt$ can be determined as the step-by-step calculations proceed and the drag-force term eliminated from the equations of motion after the required value of the integral at the instant of spin-up is reached.

EVALUATION OF ANALYSIS BY COMPARISON OF CALCULATED RESULTS WITH EXPERIMENTAL DATA

In order to evaluate the applicability of the foregoing analytical treatment to actual landing gears, tests were conducted in the Langley impact basin with a conventional oleo-pneumatic landing gear originally designed for a small military training airplane. A description of the test specimen and apparatus used is given in appendix B.

In this section calculated results are compared with experimental data for a normal impact and a severe impact with tire bottoming. The vertical velocities at the instant of ground contact used in the calculations correspond to

the vertical velocities measured in the tests. Equations (12), (13), (14), and (15a) were used to calculate the values of the variables at the instant of initial shock-strut deflection. Numerical integration of equations (16) and (17) provided the calculated results for the two-degree-of-freedom system subsequent to the beginning of shock-strut deflection.

In these calculations the discharge coefficient for the orifice and the polytropic exponent for the air-compression process were assumed to have constant values throughout the impact. Consideration of the shape of the orifice and examination of data for rounded approach orifices in pipes suggested a value of C_d equal to 0.9. Evaluation of data for other landing gears indicated that the air-compression process could be represented fairly well by use of an average value of the effective polytropic exponent $n=1.12$. In view of the fact that the landing gear was mounted in a vertical position and drag loads were absent in the tests, friction forces in the shock strut were assumed to be negligible in the calculations. Since the weight was fully balanced by lift forces in the tests, the lift factor K_L was taken equal to 1.0. The appropriate exact tire characteristics (see fig. 3) were used for each case.

NORMAL IMPACT

Figure 4 presents a comparison of calculated results with experimental data for an impact without tire bottoming at a vertical velocity of 8.86 feet per second at the instant of ground contact. The exact dynamic force-deflection characteristics of the tire, including hysteresis, were used in the calculations. These tire characteristics are shown by the solid lines in figure 2 (a) and values for the tire constants m' and r are given in figure 3 (a).

Calculated time histories of the total force on the upper mass and the acceleration of the lower mass are compared with experimental data in figure 4 (a). Similar comparisons for the upper-mass displacement, upper-mass velocity, lower-mass displacement, strut stroke, and strut telescoping velocity are presented in figure 4 (b). As can be seen, the agreement between the calculated and experimental results is reasonably good throughout most of the time history. Some of the minor discrepancies during the later stages of the impact appear to be due to errors in measurement since the deviations between the calculated and experimental upper-mass accelerations (as represented by the force on the upper mass) are incompatible with those for the upper-mass displacements, whereas the calculated upper-mass displacements are necessarily directly compatible with the calculated upper-mass accelerations. The maximum value of the experimental acceleration of the lower mass may be somewhat high because of overshoot of the accelerometer.

In addition to the total force on the upper mass, figure 4 (a) presents calculated time histories of the hydraulic and pneumatic components of the shock-strut force, as determined from equations (2) and (3), respectively. It can be seen that throughout most of the impact the force developed in the shock strut arises primarily from the hydraulic resistance of the orifice. Toward the end of the impact, however, because of the decreased telescoping velocities and fairly large strokes which correspond to high compression ratios, the air-pressure force becomes larger than the hydraulic force.

IMPACT WITH TIRE BOTTOMING

Figure 5 presents a comparison of calculated and experimental results for a severe impact ($V_{v_0}=11.63$ ft per sec) in which tire bottoming occurred. The tire force-deflection characteristics used in the calculations are shown by the solid lines in figure 3 (b). Region (1) of the tire force-deflection curve has the same values of the tire constants m' and r as for the case previously discussed. Following the occurrence of tire bottoming, however, different values of m' and r apply. These values are given in figure 3 (b).

It can be seen from figure 5 that the agreement between the calculated and experimental results for this case is similar to that for the comparison previously presented.

The calculated instant of tire bottoming is indicated in figure 5. When tire bottoming occurs, the greatly increased stiffness of the tire causes a marked increase in the shock-strut telescoping velocity, as is shown in the right-hand portion of figure 5 (b). Since the strut is suddenly forced to absorb energy at a much higher rate, an abrupt increase in the hydraulic resistance takes place. The further increase in shock-strut force immediately following the occurrence of tire bottoming is evident from the left-hand portion of figure 5 (a). The sudden increase in lower-mass acceleration at the instant of tire bottoming can also be seen.

In this severe impact the hydraulic resistance of the orifice represents an even greater proportion of the total shock-strut force than was indicated by the calculated results for an initial vertical velocity of 8.86 feet per second previously discussed.

The foregoing comparisons indicate that the analytical treatment presented, in conjunction with reasonably straightforward assumptions regarding the parameters involved in the equations, provides a fairly accurate representation of the behavior of a conventional oleo-pneumatic landing gear.

PARAMETER STUDIES

In the previous section comparisons of calculated results with experimental data showed that the equations which have been developed provide a fairly good representation of the behavior of the landing gear for the impact conditions considered. In view of the fact that the equations are somewhat complicated and require numerical values for several parameters such as the tire force-deflection constants m' and r, the orifice discharge coefficient C_d, and the polytropic exponent n, which may not be readily or accurately known in the case of practical engineering problems, it appears desirable (a) to determine the relative accuracy with which these various parameters have to be known and (b) to investigate the extent to which the equations can be simplified and still yield useful results. In order to accomplish these objectives, calculations have been made to evaluate the effect of simplifying the force-deflection characteristics of the tire, as well as to determine the effects which different values of the orifice discharge coefficient and the effective polytropic exponent have on the calculated behavior. The results of these calculations are discussed in the present section. The question of simplification of the equations of motion is considered in more detail in a subsequent section.

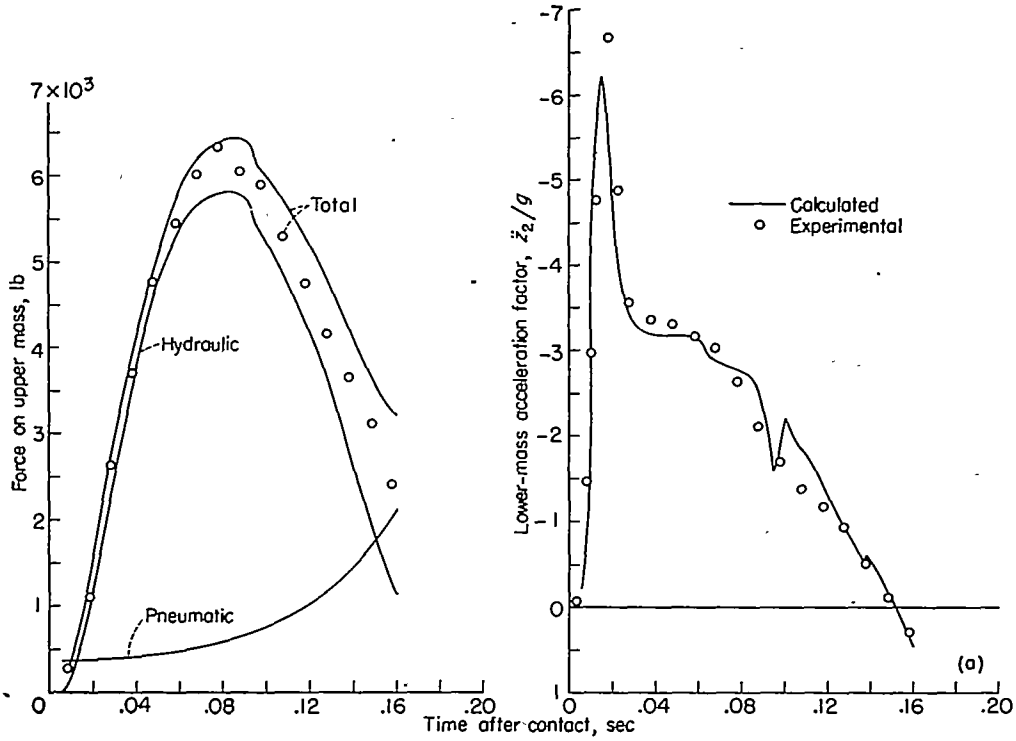

(a) Time histories of forces on upper mass and lower-mass acceleration.

FIGURE 4.—Comparisons between calculated results and experimental data for normal impact; solution with exact exponential tire characteristics. V_{V_0}=8.86 feet per second; C_d=0.9; n=1.12.

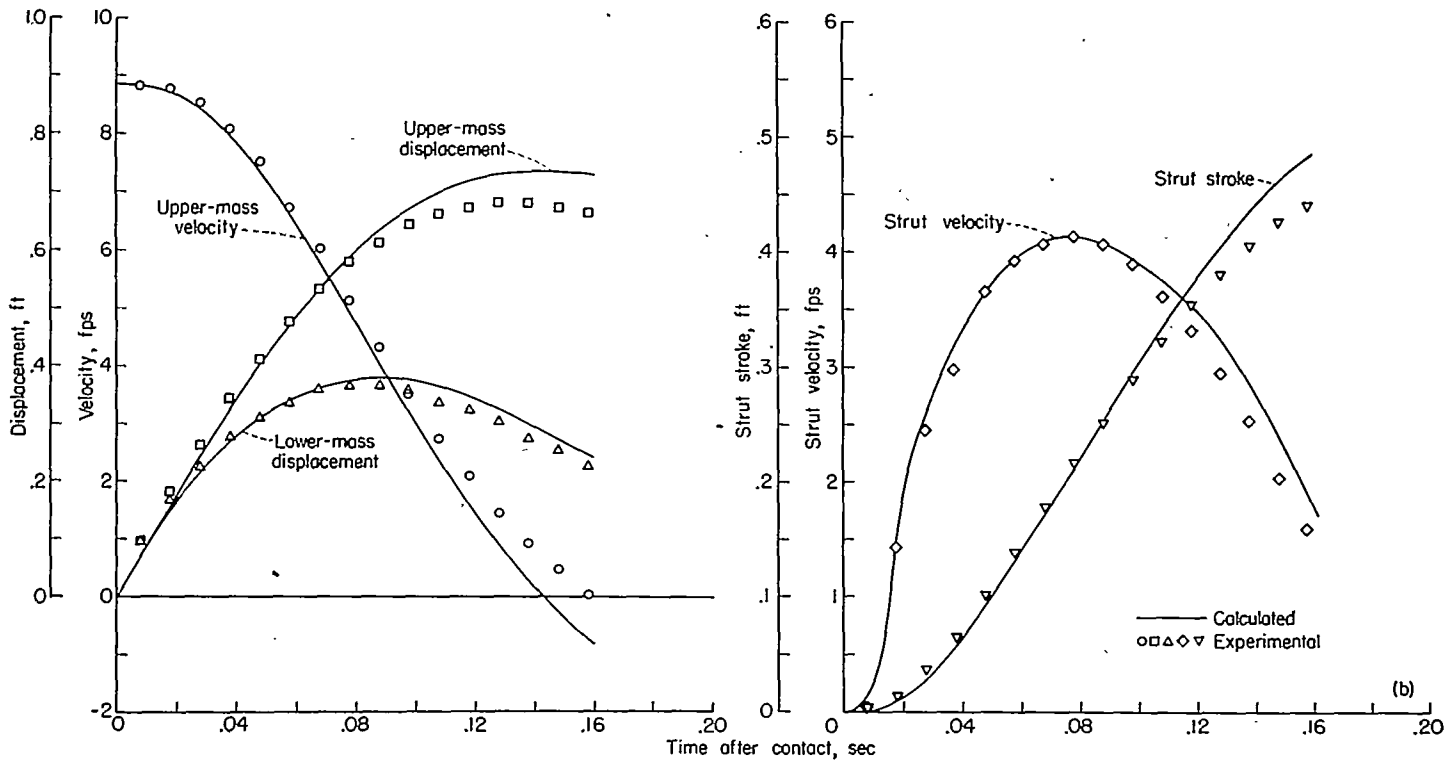

(b) Time histories of landing-gear velocities and displacements.

FIGURE 4.—Concluded.

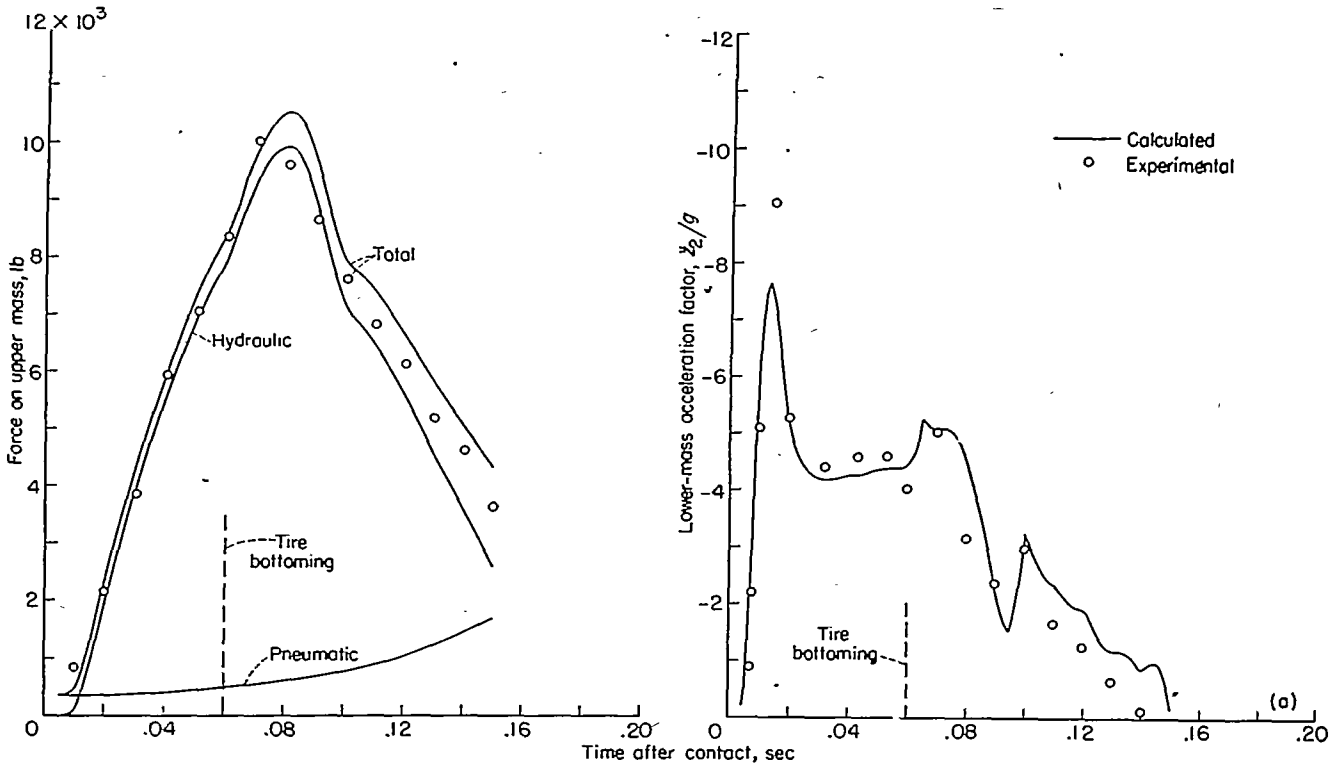

(a) Time histories of forces on upper mass and lower-mass acceleration.

FIGURE 5.—Comparisons between calculated results and experimental data for impact with tire bottoming; solution with exact exponential tire characteristics. V_{v_0}=11.63 feet per second; C_d=0.9; n=1.12.

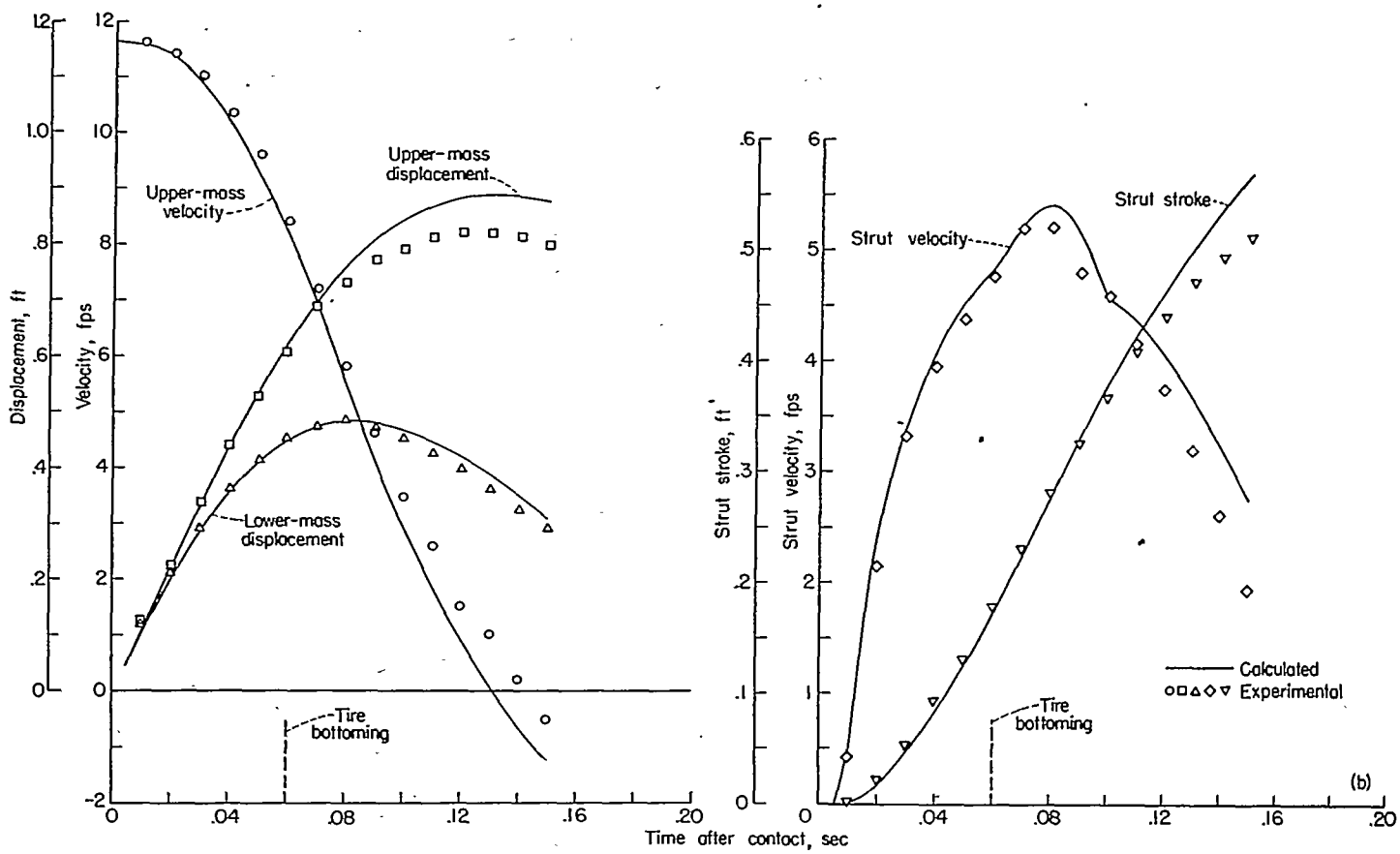

(b) Time histories of landing-gear velocities and displacements.

FIGURE 5.—Concluded.

REPRESENTATION OF TIRE FORCE-DEFLECTION CHARACTERISTICS

In order to evaluate the degree of accuracy required for adequate representation of the tire force-deflection characteristics, comparisons are made of the calculated behavior of the landing gear for normal impacts and impacts with tire bottoming when the tire characteristics are represented in various ways. First, the force-deflection characteristics will be assumed to be exactly as shown by the solid-line curves in figure 2 (b), including the various breaks in the curve and the effects of hysteresis. These characteristics are referred to hereinafter as the exact exponential tire characteristics. The effects of simplifying the representation of the tire characteristics will then be investigated by considering (a) the exponential characteristics without hysteresis; that is, the tire will be assumed to deflect and unload along the same exponential curve, (b) the linear-segment approximations to the tire characteristics (long-dashed lines), which also neglect hysteresis, and (c) errors introduced by neglecting the effects of tire bottoming in the case of severe impacts. The calculated results presented in this study make use of the relationships between vertical force on the tire and tire deflection, as shown in figures 3 (a) and 3 (b).

Figure 6 presents a comparison of the calculated results for a normal impact at a vertical velocity of 8.86 feet per second, whereas figure 7 permits comparison of the solutions for a severe impact, involving tire bottoming, at a vertical velocity of 11.63 feet per second. In figures 6 and 7 the solid-line curves represent solutions of the landing-gear equations when the exact exponential relationships between force and tire deflection are considered. Since these solutions were previously shown to be in fairly good agreement with experimental data (figs. 4 and 5), they are used as a basis for evaluating the results obtained when tire hysteresis is neglected and the force-deflection characteristics are represented by either simplified exponential or linear-segment relationships.

As in the calculations previously described, the solutions were obtained in two parts. During the first stage of the impact the shock strut was considered to be rigid until sufficient force was developed to overcome the initial air-pressure force. The calculations for the landing-gear behavior subsequent to this instant were based on the equations which consider the gear to have two degrees of freedom. Time histories of the upper-mass acceleration calculated on the basis of a rigid shock strut are shown by the dotted curves in figures 6 and 7. These solutions show the greatest rate of increase of upper-mass acceleration possible with the exponential tire force-deflection characteristics considered. Comparison of these solutions with those for the two-degree-of-freedom system indicates the effect of the shock strut in attenuating the severity of the impact.

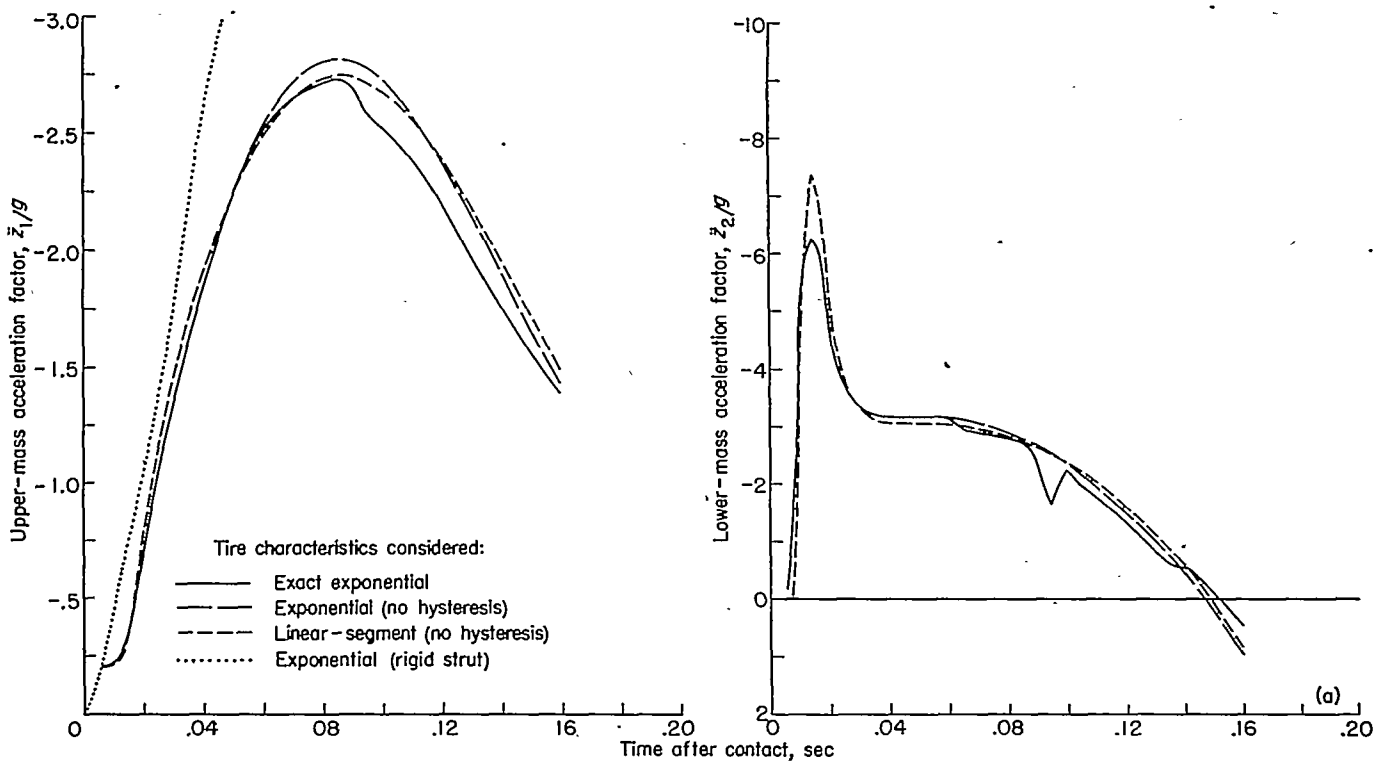

(a) Time histories of upper-mass acceleration and lower-mass acceleration.

FIGURE 6.—Effect of tire characteristics on calculated landing-gear behavior in normal impact. V_{v_0}=8.86 feet per second; C_d=0.9; n=1.12.

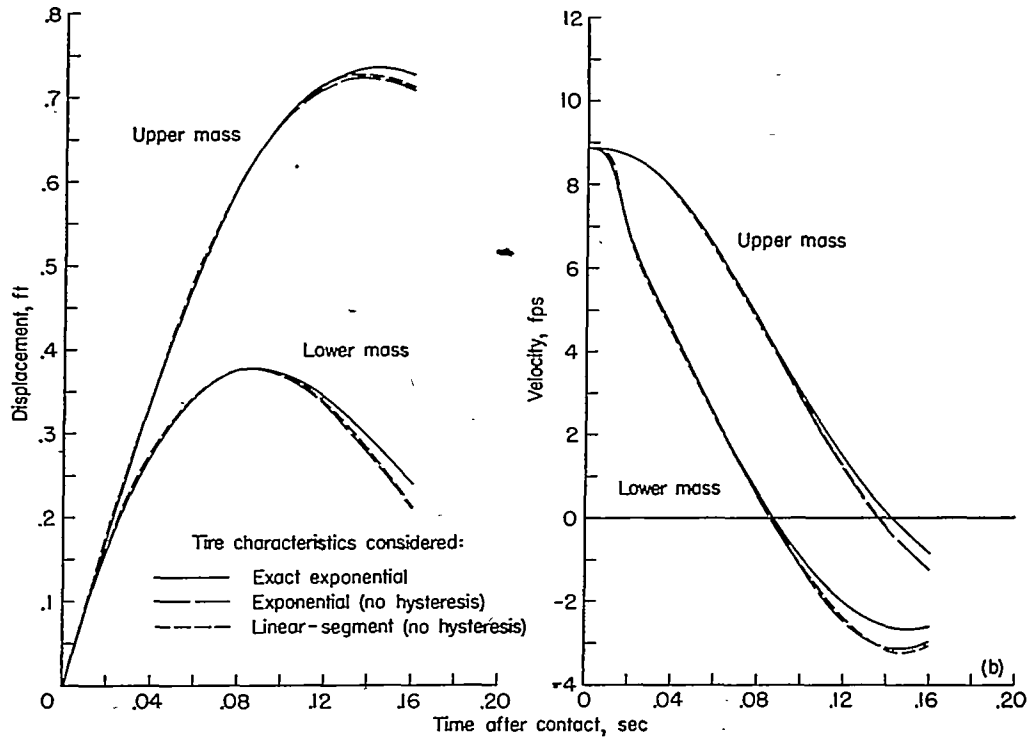

(b) Time histories of landing-gear displacements and velocities.

FIGURE 6.—Continued.

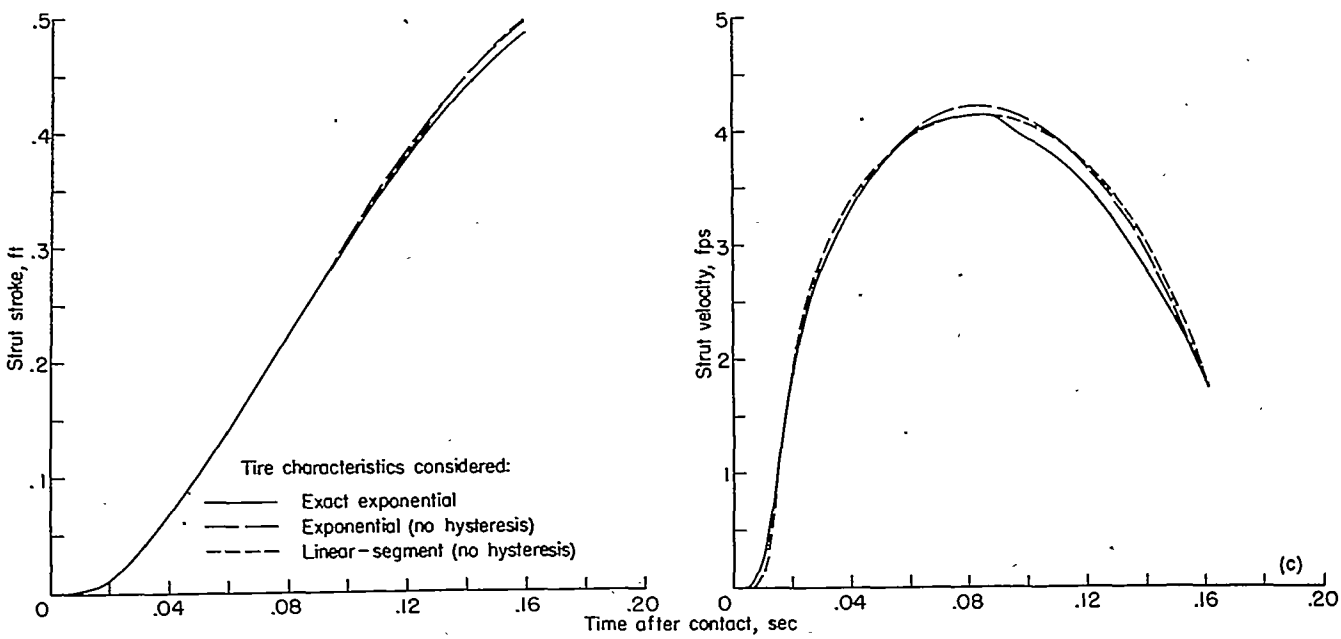

(c) Time histories of shock-strut stroke and velocity.

FIGURE 6.—Concluded.

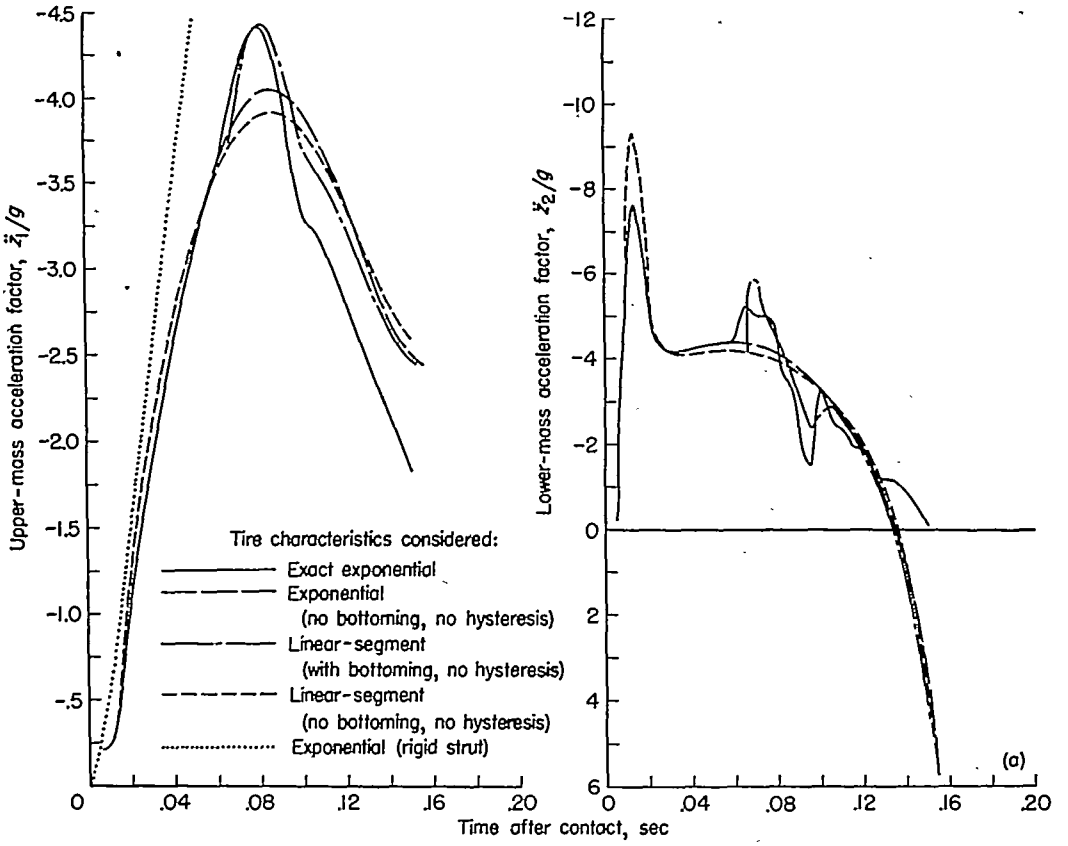

(a) Time histories of upper-mass acceleration and lower-mass acceleration.

FIGURE 7.—Effect of tire characteristics on calculated landing-gear behavior for impact with tire bottoming. $V_{v_0}=11.63$ feet per second; $C_d=0.9$; $n=1.12$.

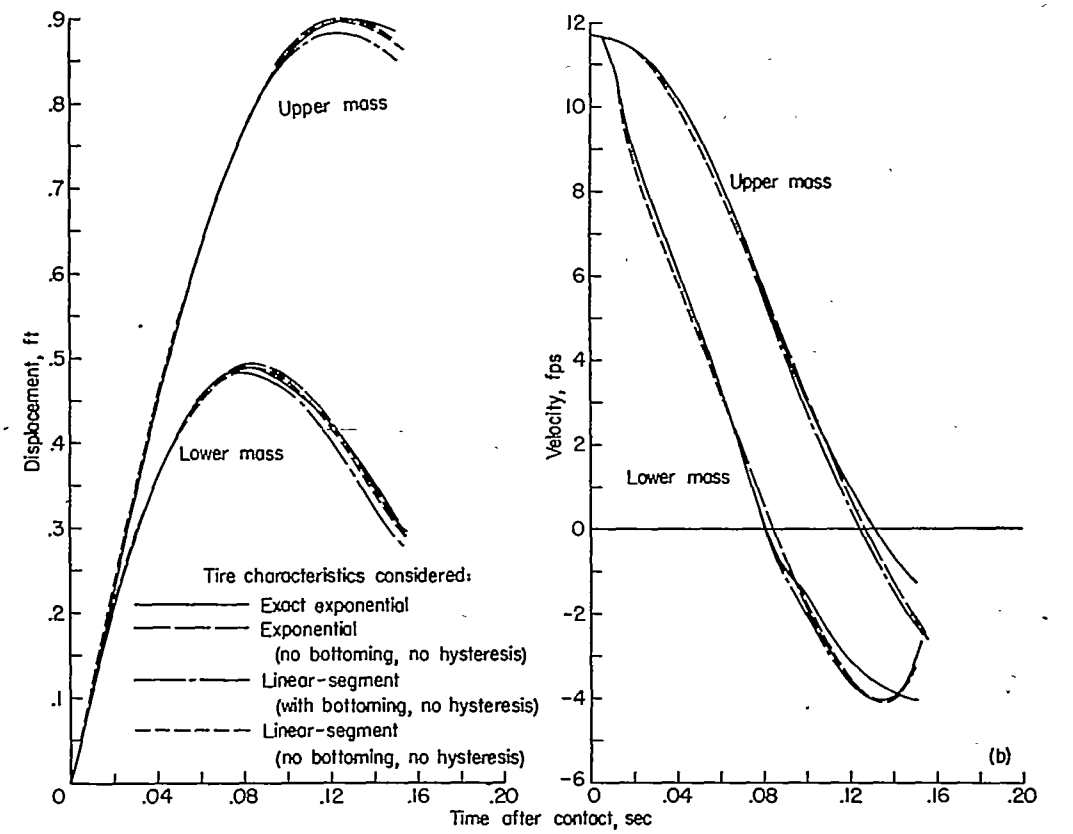

(b) Time histories of landing-gear displacements and velocities

FIGURE 7.—Continued.

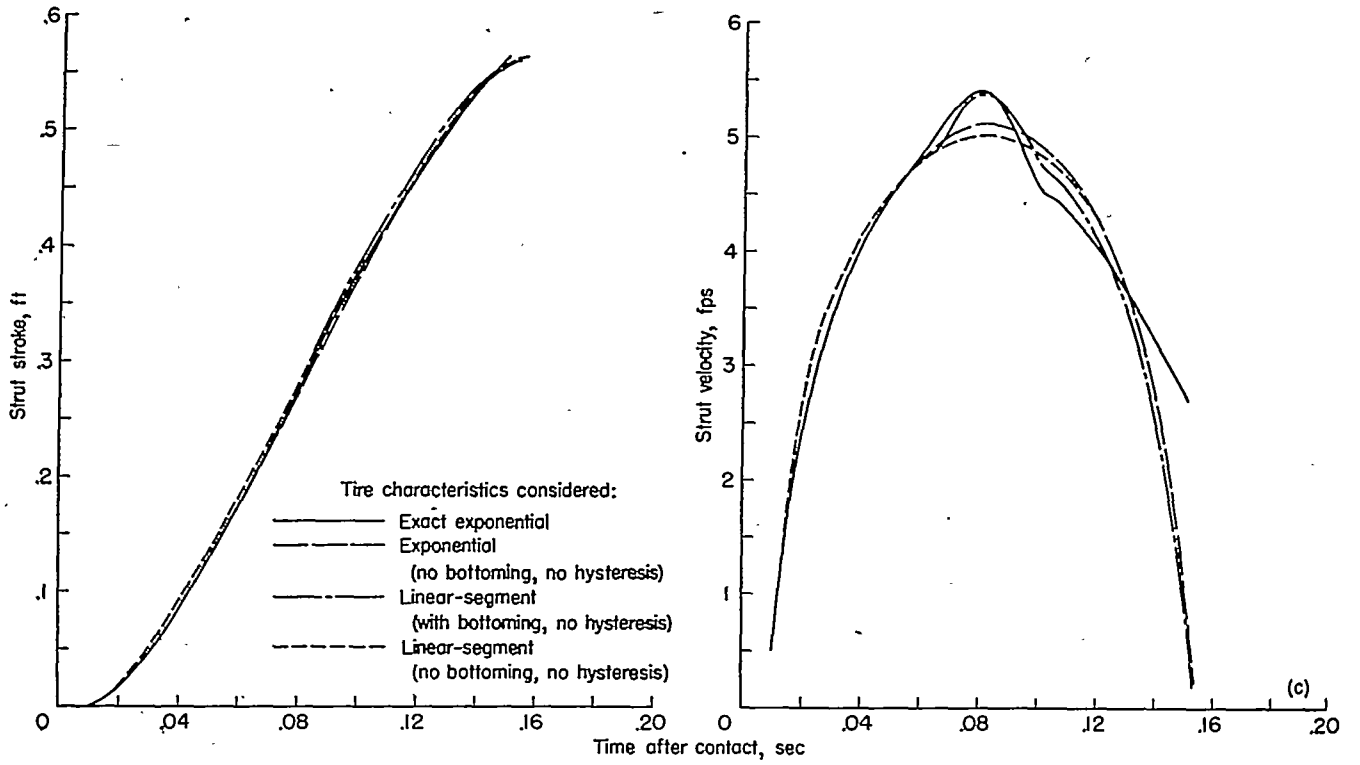

(c) Time histories of shock-strut stroke and velocity.

FIGURE 7.—Concluded.

Normal impact.—In the case of the normal impact at a vertical velocity of 8.86 feet per second, figure 6 shows that the solution obtained with the exponential force-deflection variation which neglects hysteresis and the solution with the linear-segment approximation to the tire characteristics are in fairly good agreement with the results of the calculation based on the exponential representation of the exact tire characteristics. The greatest differences between the solutions are evident in the time histories of upper-mass and lower-mass accelerations; considerably smaller differences are obtained for the lower-order derivatives, as might be expected. With regard to the upper-mass acceleration, the three solutions are in very good agreement during the early stages of the impact. In the case of the simplified exponential characteristics, neglect of the decreased slope of the force-deflection curve between the first break and the maximum (regime ② in fig. 3 (a)) resulted in the calculation of a somewhat higher value of the maximum upper-mass acceleration than was obtained with the exact tire characteristics. For the simplified exponential and linear-segment characteristics, neglect of hysteresis resulted in the calculation of somewhat excessive values of upper-mass acceleration subsequent to the attainment of the maximum vertical load. It is of interest to note that the calculated results for the exponential and linear-segment characteristics without hysteresis were generally in quite good agreement with each other throughout the entire duration of the impact, although the assumption of linear-segment tire force-deflection characteristics did result in somewhat excessive values for the maximum lower-mass acceleration. On the whole, the simplified tire force-deflection characteristics considered permit calculated results to be obtained which represent the behavior of the landing gear in normal impacts fairly well.

Impact with tire bottoming.—In the case of the severe impact at a vertical velocity of 11.63 feet per second, the effects of tire bottoming on the upper-mass acceleration, the lower-mass acceleration, and the strut telescoping velocity are clearly indicated in figure 7 by the calculated results based on the exact tire characteristics. As can be seen, the linear-segment approximation to the tire deflection characteristics which takes into account the effects of tire bottoming resulted in a reasonably good representation of the landing-gear behavior throughout most of the time history. On the other hand, as might be expected, the calculations which neglected the effects of bottoming on the tire force-deflection characteristics did not reveal the marked increase in the upper-mass acceleration due to the increased stiffness of the tire subsequent to the occurrence of bottoming. It is also noted that the discrepancies in the calculated upper-mass acceleration due to neglect of hysteresis in the later stages of the impact are more pronounced in this case than in the impact without tire bottoming previously considered, again as might be expected.

EFFECT OF ORIFICE DISCHARGE COEFFICIENT

In view of the fact that there is very little information available regarding the magnitude of discharge coefficients for orifices in landing gears, it appears desirable to evaluate the effect which differences in the magnitude of the orifice coefficient can have on the calculated results. Figure 8 presents comparisons of calculated results for a range of values of the orifice discharge coefficient C_d between 1.0 and 0.7. The four solutions presented are for the same set of initial conditions as the normal impact without tire bottoming previously considered and are based on the exponential tire force-deflection characteristics which neglect hysteresis.

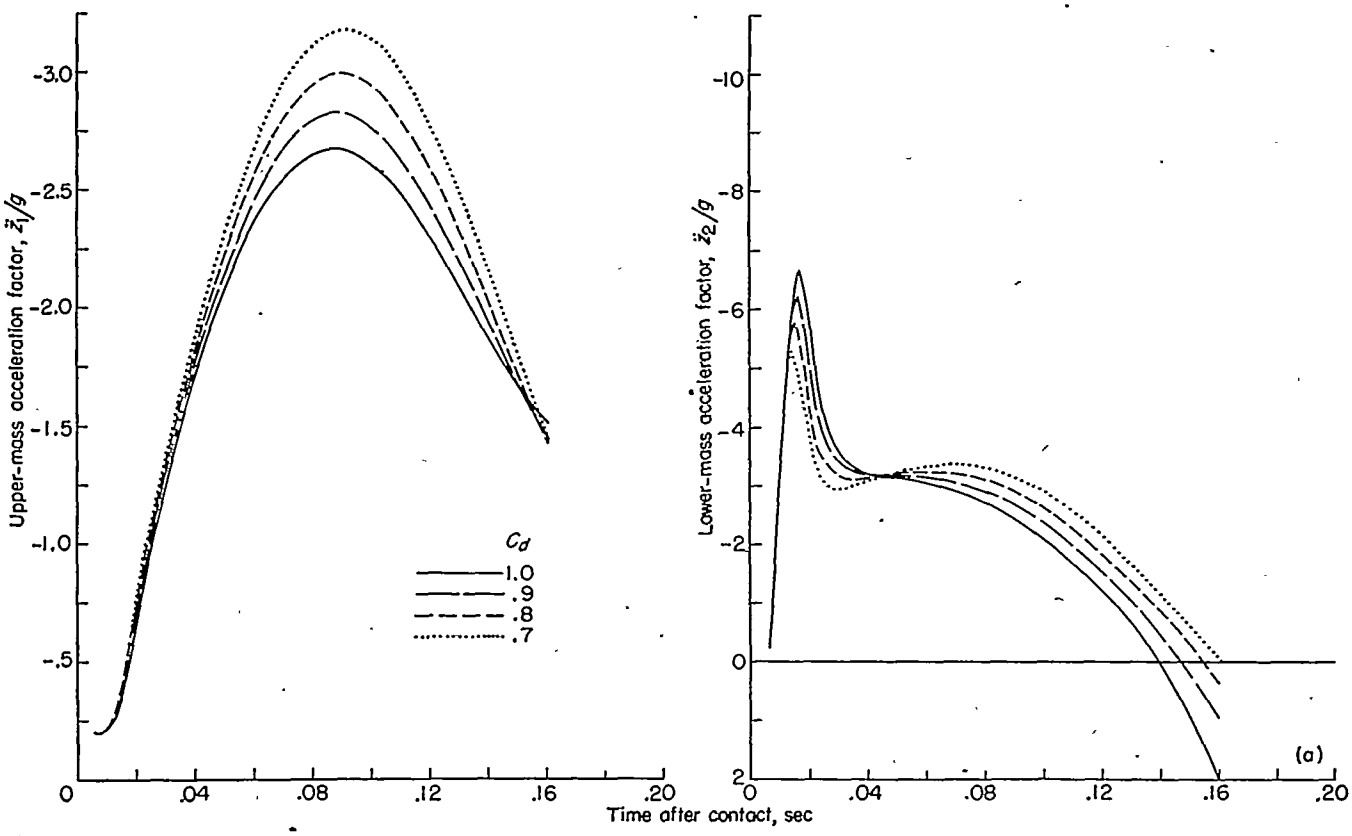

(a) Time histories of upper-mass acceleration and lower-mass acceleration.

FIGURE 8.—Effect of orifice discharge coefficient on landing-gear behavior; calculations with exponential tire characteristics without hysteresis. V_{V_0}=8.86 feet per second; n=1.12.

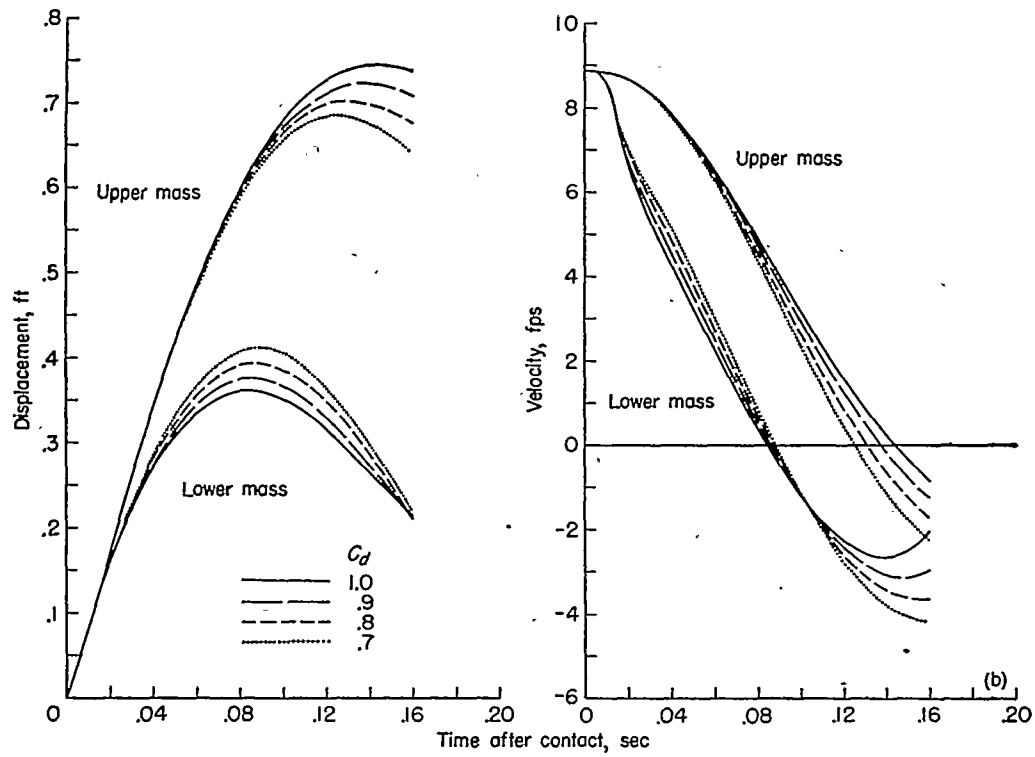

(b) Time histories of landing-gear displacements and velocities.

FIGURE 8.—Continued.

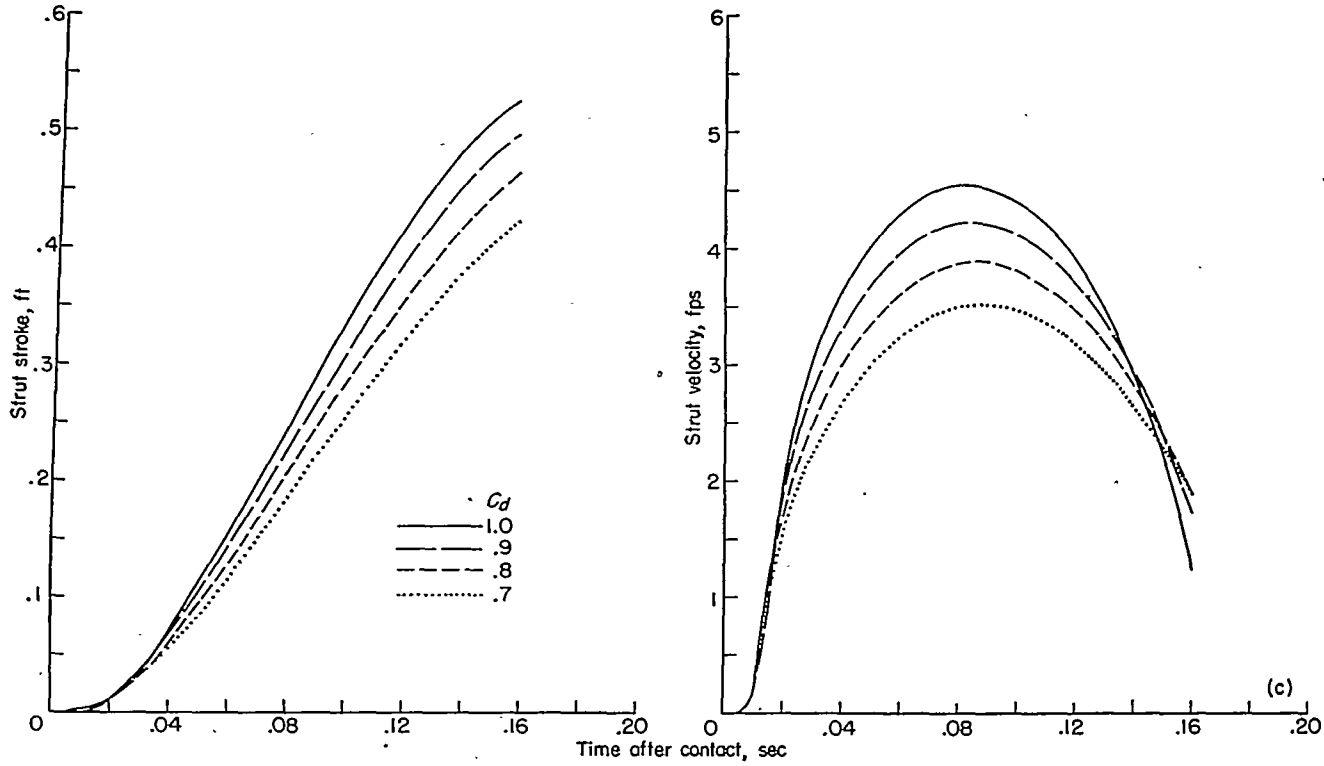

(c) Time histories of shock-strut stroke and velocity.

FIGURE 8.—Concluded.

These calculations show that a decrease in the orifice discharge coefficient results in an approximately proportional increase in the upper-mass acceleration. This variation is to be expected since the smaller coefficients correspond to reduced effective orifice areas which result in greater shock-strut forces due to increased hydraulic resistance. As a result of the increased shock-strut force acting downward on the lower mass, the maximum upward acceleration of the lower mass is reduced with decreasing values of the discharge coefficient. The increase in shock-strut force with decreasing discharge coefficient also results in a decrease in the strut stroke and telescoping velocity but an increase in the lower-mass velocity and displacement, as might be expected. However, since the increases in lower-mass displacement and velocity are smaller than the decreases in strut stroke and telescoping velocity, the upper-mass displacement and velocity are reduced with decreasing orifice discharge coefficient.

These comparisons show that the magnitude of the orifice coefficient has an important effect on the behavior of the landing gear and indicates that a fairly accurate determination of the numerical value of this parameter is necessary to obtain good results.

EFFECT OF AIR-COMPRESSION PROCESS

Since the nature of the air-compression process in a shock strut is not well-defined and different investigators have assumed values for the polytropic exponent ranging anywhere between the extremes of 1.4 (adiabatic) and 1.0 (isothermal), it appeared desirable to evaluate the importance of the air-compression process and to determine the extent to which different values of the polytropic exponent can influence the calculated results. Consequently, solutions have been obtained for three different values of the polytropic exponent; namely, $n=1.3$, 1.12, and 0.

The value $n=1.3$ corresponds to a very rapid compression in which an adiabatic process is almost attained. The value $n=1.12$ corresponds to a relatively slow compression in which the process is virtually isothermal. The value $n=0$ is completely fictitious since it implies constant air pressure within the strut throughout the impact. The assumption $n=0$ has been considered since it makes one of the terms in the equations of motion a constant and permits simplification of the calculations. The three solutions presented are for the same set of initial conditions as the normal impact without tire bottoming previously considered and are based on the exponential tire force-deflection characteristics which neglect hysteresis.

Figure 9 shows that the air pressure contributes only a relatively small portion of the total shock-strut force throughout most of the impact since the compression ratio is relatively small until the later stages of the impact. Toward the end of the impact, however, the air-pressure force becomes a large part of the total force since the compression ratio becomes large, whereas the hydraulic resistance decreases rapidly as the strut telescoping velocity is reduced to zero.

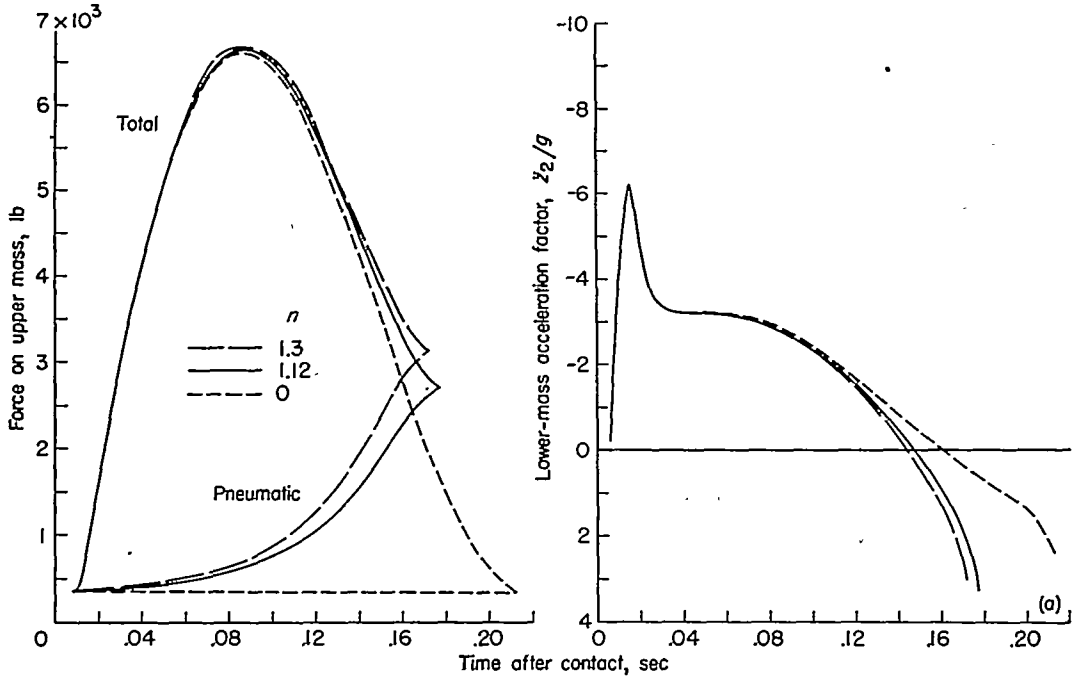

(a) Time histories of upper-mass force and lower-mass acceleration.

FIGURE 9.—Effect of polytropic exponent; calculations with exponential tire characteristics without hysteresis. V_{r_0}=8.86 feet per second; C_d=0.9.

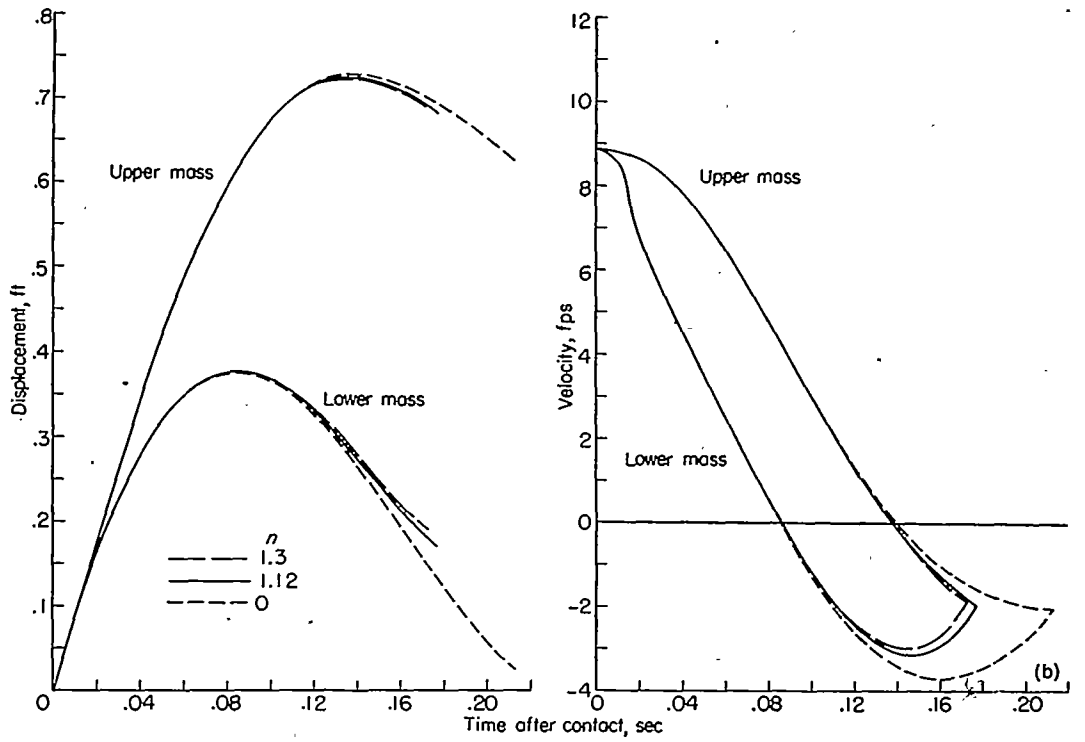

(b) Time histories of landing-gear displacements and velocities.

FIGURE 9.—Continued.

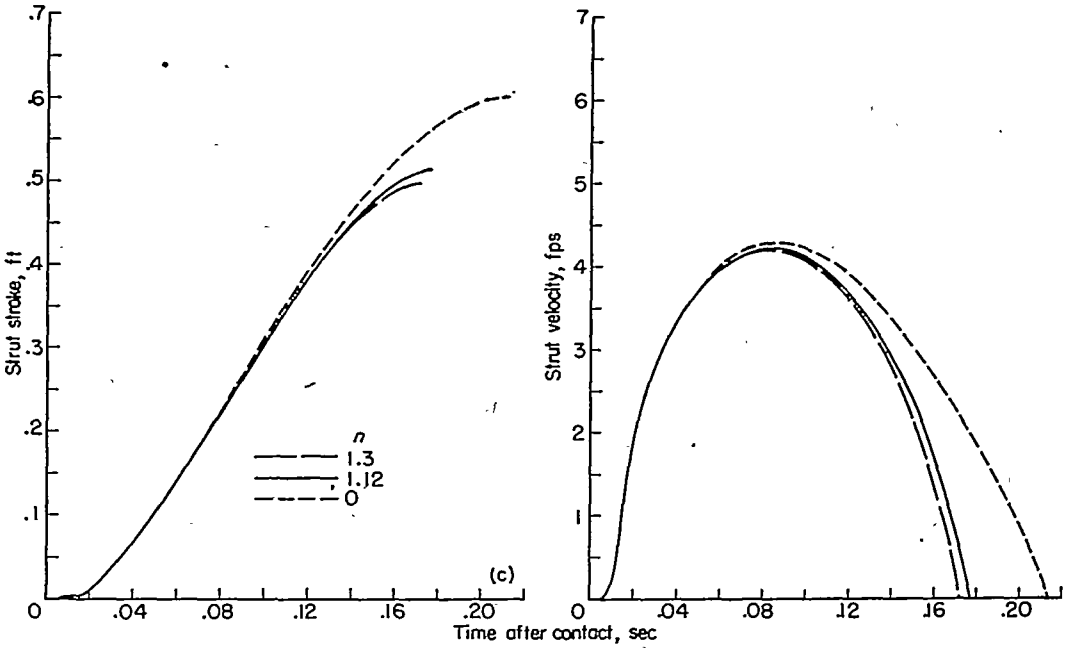

(c) Time histories of shock-strut stroke and velocity.

FIGURE 9.—Concluded.

As a result, the calculations show that the magnitude of the polytropic exponent has only a very small effect on the behavior of the landing gear throughout most of the impact. For the practical range of polytropic exponents, variations in the air-compression process result in only minor differences in landing-gear behavior, even during the very latest stages of the impact. The assumption of constant air pressure in the strut throughout the impact ($n=0$), however, does lead to the calculation of excessive values of stroke and of the time to reach the maximum stroke. The time history of the shock-strut force calculated on the basis of this assumption is, on the other hand, in quite good agreement with the results for the practical range of air-compression processes.

On the whole it appears that the behavior of the landing gear is relatively insensitive to variations in the air-compression process. The foregoing results suggest that, in many cases, fairly reasonable approximations for the landing-gear force-time variation might be obtained even if the air-pressure term in the equations of motion were completely neglected.

SIMPLIFICATION OF EQUATIONS OF MOTION

The preceding studies have indicated that variations in the tire force-deflection characteristics and in the air-compression process individually have only a relatively minor effect on the calculated behavior of the landing gear. These results suggest that the equations of motion for the landing gear might be simplified by completely neglecting the internal air-pressure forces in the shock strut and by considering the tire force-deflection characteristics to be linear. With these assumptions, the equations of motion for the upper mass, lower mass, and complete system (eqs. (16), (17), and (8)) can be written as follows for the case where the wing lift is equal to the weight and the internal friction is neglected:

$$\left.\begin{aligned} &\frac{W_1}{g}\ddot{z}_1+A(\dot{z}_1-\dot{z}_2)^2+W_2=0 \\ &\frac{W_2}{g}\ddot{z}_2-A(\dot{z}_1-\dot{z}_2)^2+az_2+b-W_2=0 \\ &\frac{W_1}{g}\ddot{z}_1+\frac{W_2}{g}\ddot{z}_2+az_2+b=0 \end{aligned}\right\} \quad (18)$$

where

$$A=\frac{\dot{s}}{|\dot{s}|}\frac{\rho A_h^3}{2(C_d A_n)^2\cos\varphi}$$

and

a slope of linear approximation to tire force-deflection characteristics

b value of force corresponding to zero tire deflection, as determined from the linear-segment approximation to the tire force-deflection characteristics

The motion variables at the beginning of shock-strut deflection can be readily determined in a manner similar to that employed in the more general treatment previously discussed. For the simplified equations the variables at the instant t_τ are given by

$$\left.\begin{aligned} \ddot{z}_\tau&=-\frac{W_2}{W_1}g \\ z_\tau&=\frac{W_2}{a}\left(1+\frac{W_2}{W_1}\right) \\ \dot{z}_\tau&=\sqrt{\dot{z}_0^2-\frac{ag}{W}z_\tau^2} \end{aligned}\right\} \quad (19)$$

In most cases the term $\frac{ag}{W}z_\tau^2$ is small in comparison with $\dot{z}_0^2$ so that $\dot{z}_\tau\approx\dot{z}_0$.

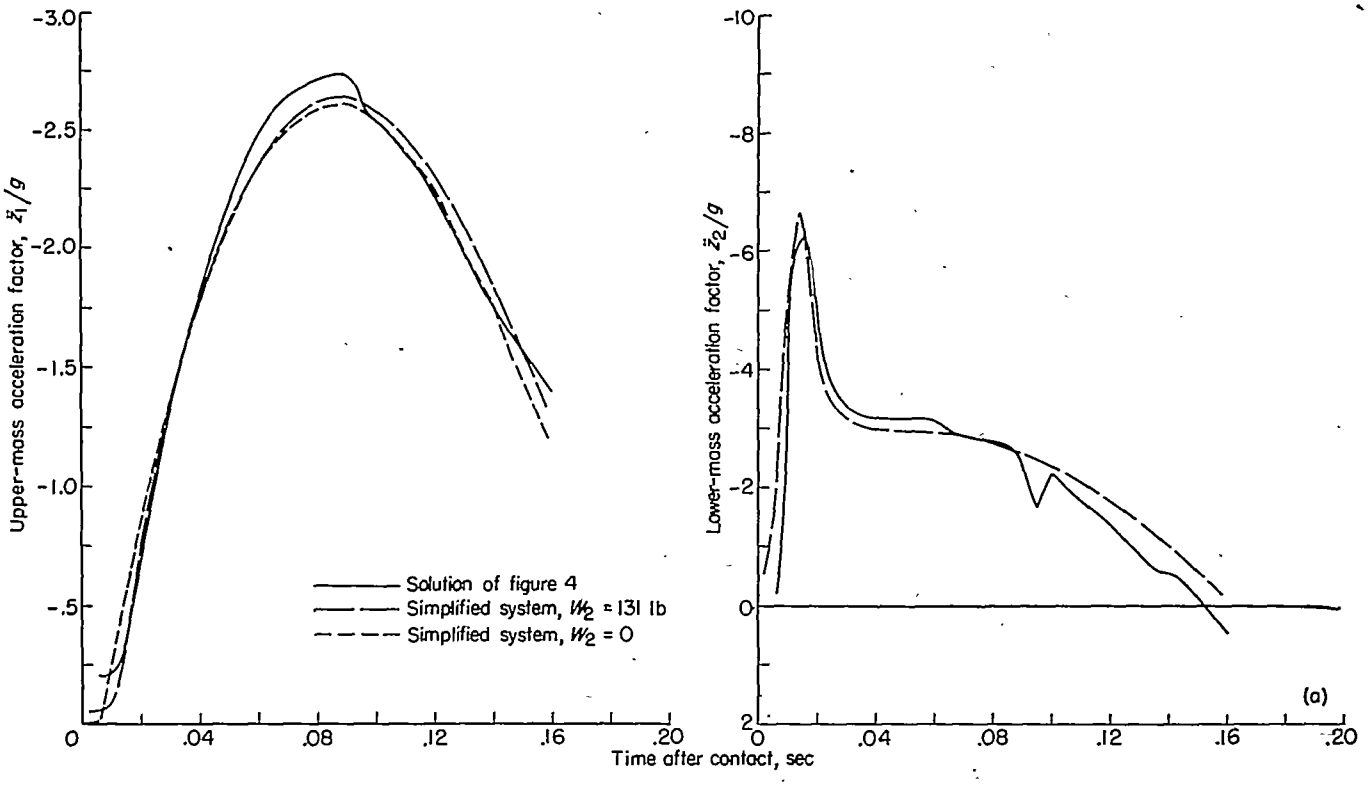

(a) Time histories of upper-mass acceleration and lower-mass acceleration.

FIGURE 10.—Evaluation of calculated results for simplified systems. V_{T_0}=8.86 feet per second; C_d=0.9.

The values determined from equations (19) are used as initial conditions in the solution of equations (18).

The fact that the lower mass is a relatively small fraction of the total mass suggests that the system might be simplified even further without greatly modifying the calculated results by assuming the lower mass to be equal to zero. With this assumption t_τ=0 and the initial values of the variables in equations (18) correspond to the conditions at initial contact.

EVALUATION OF SIMPLIFICATION

In order to evaluate the applicability of these simplifications, the behavior of the landing gear has been calculated in accordance with equations (18) for an impact with an initial vertical velocity of 8.86 feet per second. A similar calculation has been made with the assumption W_2=0. These results are compared in figure 10 with the more exact solutions previously presented in figure 4, which include consideration of the air-compression springing and the exact exponential tire characteristics. A time history of the lower-mass acceleration is not presented for the case where W_2 is assumed equal to zero since the values of $\ddot{z}_2/g$ have no significance in this case.

Figure 10 shows that the two simplified solutions are in quite good agreement with each other, as might be expected, and are also in fairly good agreement with the more exact results. Neglecting the air-pressure forces and assuming a linear tire force-deflection variation resulted in the calculation of slightly lower values for the maximum upper-mass acceleration and somewhat higher values for the maximum stroke than were obtained with the more exact equations. The effect of neglecting the lower mass was primarily to reduce the lower-mass displacement (tire deflection), as a result of the elimination of the lower-mass inertia reaction.

On the whole, it appears that the assumptions considered permit appreciable simplification of the equations of motion without greatly impairing the validity of the calculated results.

GENERALIZED TREATMENT

Equations and solutions.—By writing the simplified equations of motion in terms of dimensionless variables, generalized solutions can be obtained for a wide range of landing-gear and impact parameters which may be useful in preliminary design. If W_2 is taken equal to zero and it is further assumed that the tire force-deflection curve is represented by a single straight line through the origin (b=0 throughout the impact), equations (18) reduce to

$$\left.\begin{aligned} &\frac{W_1}{g}\ddot{z}_1+A(\dot{z}_1-\dot{z}_2)^2=0 \\ &A(\dot{z}_1-\dot{z}_2)^2-az_2=0 \\ &\frac{W_1}{g}\ddot{z}_1+az_2=0 \end{aligned}\right\} \qquad (20)$$

where $\frac{W_1}{g}$, A, and a are constants, as previously defined, and any two of the foregoing equations are sufficient to describe completely the behavior of the system. With this representation of the system, the shock strut begins to deflect at the instant of initial contact (t_τ=0). Thus, the initial conditions for equations (20) are the initial impact conditions; namely, $z_{1_0}=z_{2_0}=0$ and $\dot{z}_{1_0}=\dot{z}_{2_0}=\dot{z}_0$.

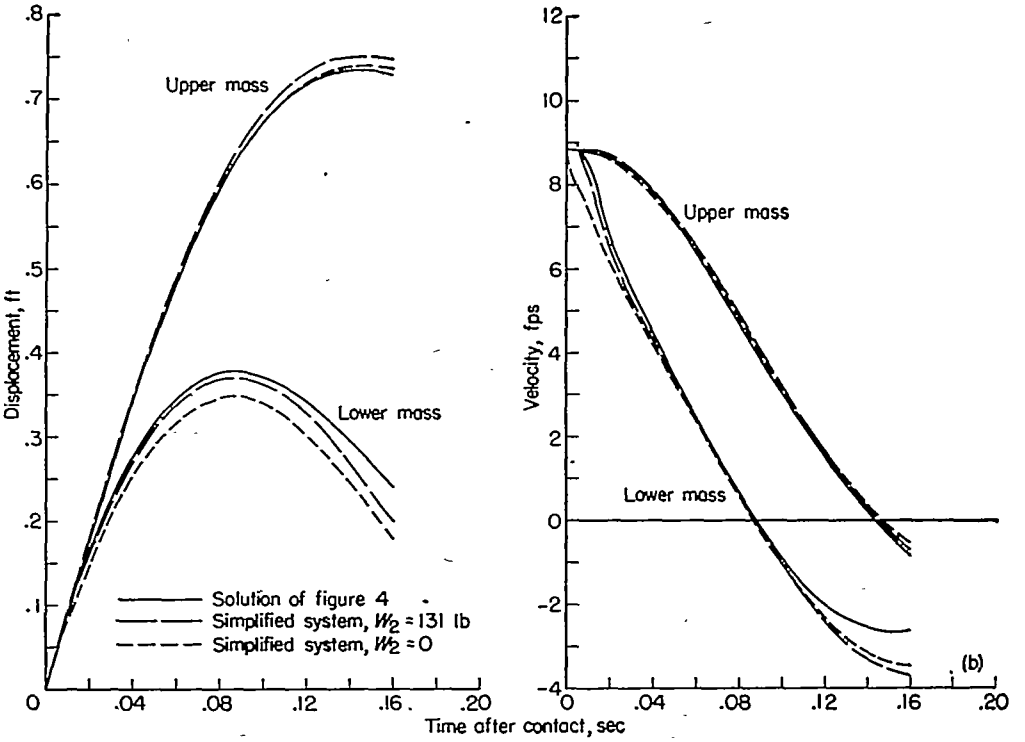

(b) Time histories of landing-gear displacements and velocities.

FIGURE 10.—Continued.

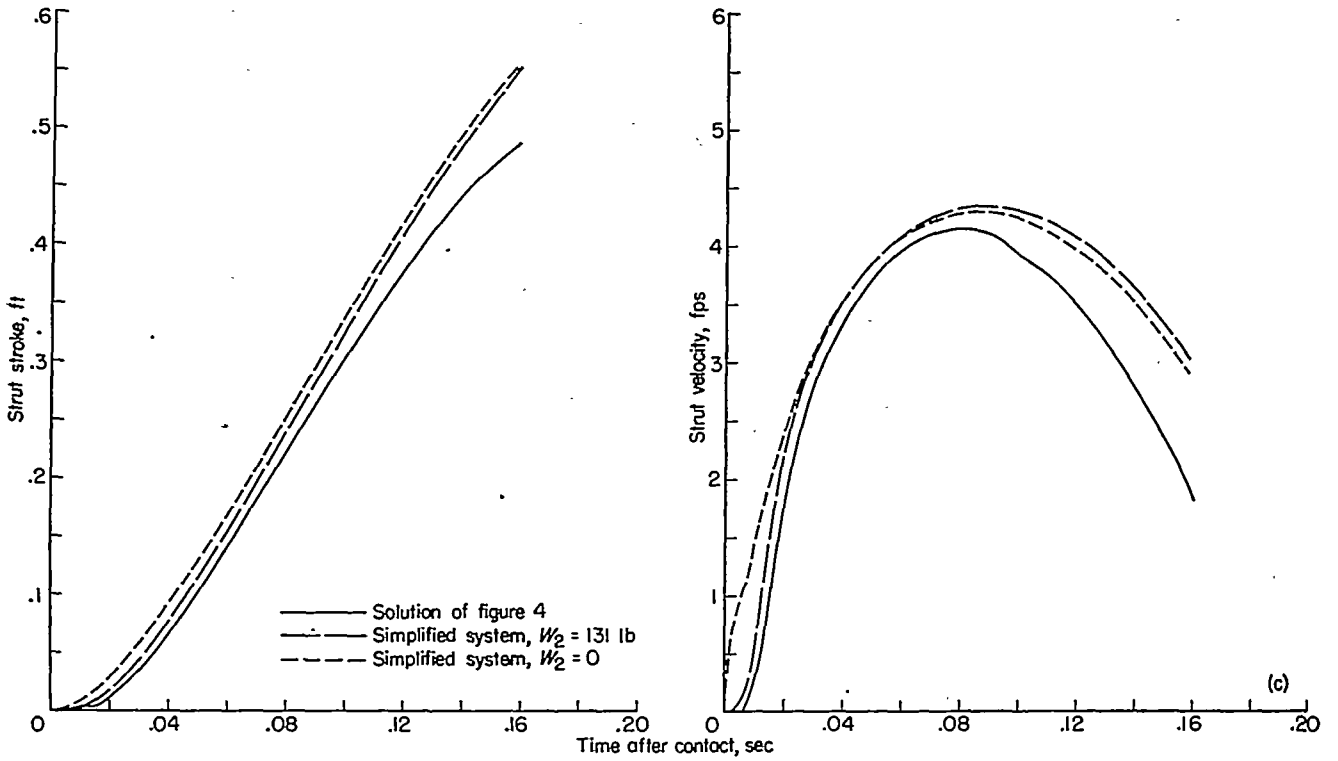

(c) Time histories of shock-strut stroke and velocity.

FIGURE 10.—Concluded.

As can be seen, with the equations in this form, the solution depends on five parameters, namely, $\frac{W_1}{g}$, A, a, and the initial conditions $\dot{z}_0$ and z_0. However, since $z_0=0$ in all cases, the number of variable parameters is reduced to four. In view of the fact that these parameters are independent of one another and each may take on a large range of values, a great many solutions and a large number of graphs would be required to cover the entire range of landing-gear and impact parameters with the equations in the form of equations (20).

The number of independent parameters which have to be considered may be greatly decreased by the introduction of generalized dimensionless variables and the corresponding transformations of equations (20). In this case, generalized variables can be obtained which permit transformation of the equations of motion to a form which does not involve any constants. With the equations in this form, there is only one variable parameter, namely, the initial velocity parameter. To determine the generalized variables which satisfy the aforementioned requirements, let

$$u=z\alpha$$

and

$$\theta=t\beta$$

Thus,

$$u'=\frac{du}{d\theta}=\dot{z}\,\frac{\alpha}{\beta}$$

and

$$u''=\frac{du'}{d\theta}=\ddot{z}\,\frac{\alpha}{\beta^2}$$

Substituting these new variables permits equations (20) to be written as

$$\left.\begin{aligned}(u_1'-u_2')^2+\left(\frac{\alpha}{A}\frac{W_1}{g}\right)u_1''=0\\(u_1'-u_2')^2-\left(\frac{a}{A}\frac{\alpha}{\beta^2}\right)u_2=0\\u_1''+\left(\frac{a/\beta^2}{W_1/g}\right)u_2=0\end{aligned}\right\} \tag{20a}$$

The number of independent parameters will be reduced if all the combined constants in equations (20a) are set equal to one another, that is, let

$$\frac{\alpha}{A}\frac{W_1}{g}=\frac{a}{A}\frac{\alpha}{\beta^2}=\frac{a/\beta^2}{W_1/g}$$

From this relationship, it can be seen that

$$\alpha=\frac{A}{W_1/g}$$

and

$$\beta=\sqrt{\frac{a}{W_1/g}}$$

Thus the generalized variables become

$$u_1=z_1\left(\frac{A}{W_1/g}\right) \qquad u_2=z_2\left(\frac{A}{W_1/g}\right)$$

$$u_1'=\frac{du_1}{d\theta}=\dot{z}_1\sqrt{\frac{A^2/a}{W_1/g}} \qquad u_2'=\frac{du_2}{d\theta}=\dot{z}_2\sqrt{\frac{A^2/a}{W_1/g}}$$

and

$$u_1''=\frac{d^2u_1}{d\theta^2}=\ddot{z}_1\left(\frac{A}{a}\right).$$

where

$$\theta=t\sqrt{\frac{a}{W_1/g}}$$

With these new variables equations (20) can be written as [2]

$$\left.\begin{aligned}(u_1'-u_2')^2+u_1''=0\\(u_1'-u_2')^2-u_2=0\\u_1''+u_2=0\end{aligned}\right\} \tag{21}$$

where any two of these equations are sufficient to describe the behavior of the system.

Inasmuch as equations (21) do not involve any constants, their solutions are completely determined by the initial values of the variables. Since the displacements at initial contact u_{1_0} and u_{2_0} are equal to zero and the initial velocities u_{1_0}' and u_{2_0}' are equal, the only parameter is the initial dimensionless velocity

$$u_0'=\dot{z}_0\sqrt{\frac{A^2g}{W_1a}}$$

where $u_0'=u_{1_0}'=u_{2_0}'$.

Generalized solutions of equations (21) are presented in figure 11 for values of u_0' corresponding to a wide range of landing-gear and impact parameters. Parts (a) to (e) of figure 11 show the variations of the dimensionless variables during the impact; parts (f) and (g) show the maximum values of the more important variables as functions of u_0'. Part (h) shows the shock-strut effectiveness η_s and the landing-gear effectiveness η_{lg}. The shock-strut effectiveness, sometimes called "efficiency" and, in Europe, "planimetric ratio," is defined as

$$\eta_s=\frac{\int_0^{\sigma_{max}}u_1''\,d\sigma}{u_{1_{max}}''\,\sigma_{max}}$$

where $\sigma=u_1-u_2$ is the dimensionless shock-strut stroke. Since η_s represents the ratio of the energy actually absorbed by the shock strut to the maximum energy which the strut could possibly absorb for any combination of maximum acceleration (or load) and maximum stroke, it serves as a measure of the extent to which a given combination of maximum load and stroke has been utilized to absorb the energy of an impact. A similar measure of the energy absorption effectiveness of the landing gear as a whole is given by η_{lg} which is defined by

$$\eta_{lg}=\frac{\int_0^{u_{1_{max}}}u_1''\,du_1}{u_{1_{max}}''\,u_{1_{max}}}$$

[2] Equations (21) may be reduced to a single equation in one variable by differentiating the last equation and substituting for u_2' in the first equation. This gives $(u_1'+u_1'')^2+u_1''=0$.

By introducing the new variable $w=u_1'$, this equation may be reduced to the second-order equation $(w+w')^2+w'=0$, subject to the initial conditions $w_0=u_0'$ and $w_0'=0$.

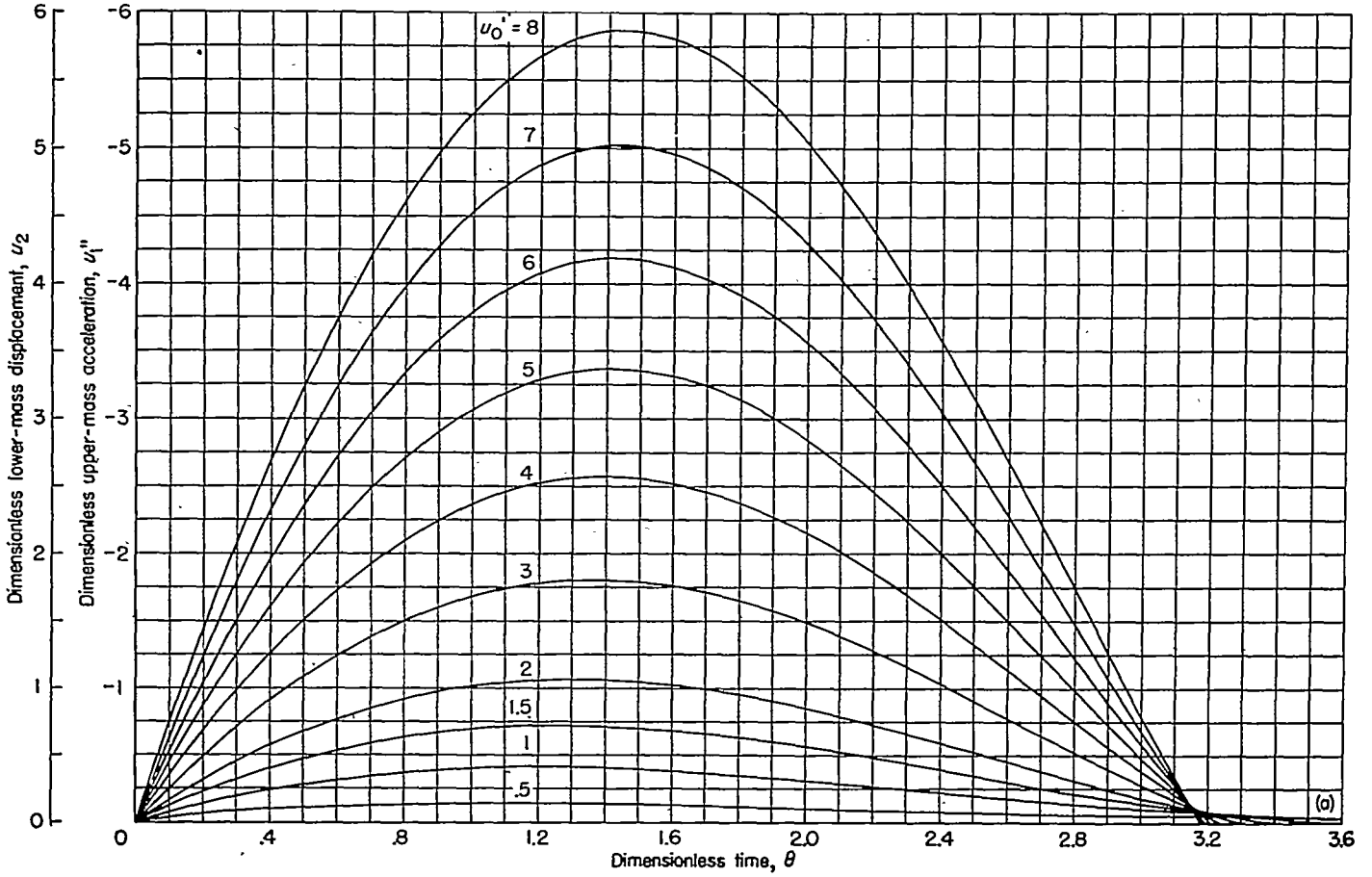

(a) Relationship between upper-mass acceleration, lower-mass displacement, and time.

FIGURE 11.—Generalized solutions for simplified system.

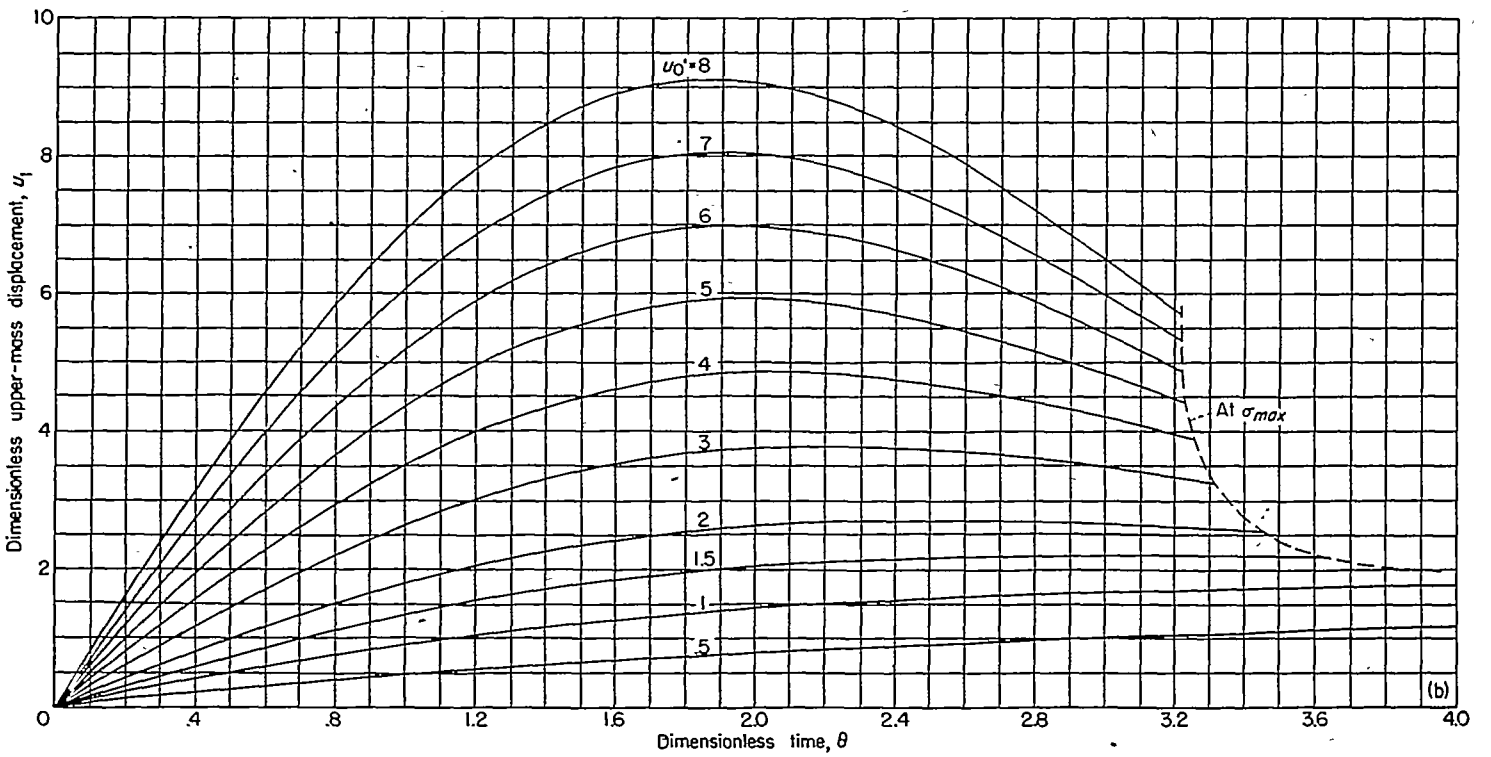

(b) Relationship between upper-mass displacement and time.

FIGURE 11.—Continued.

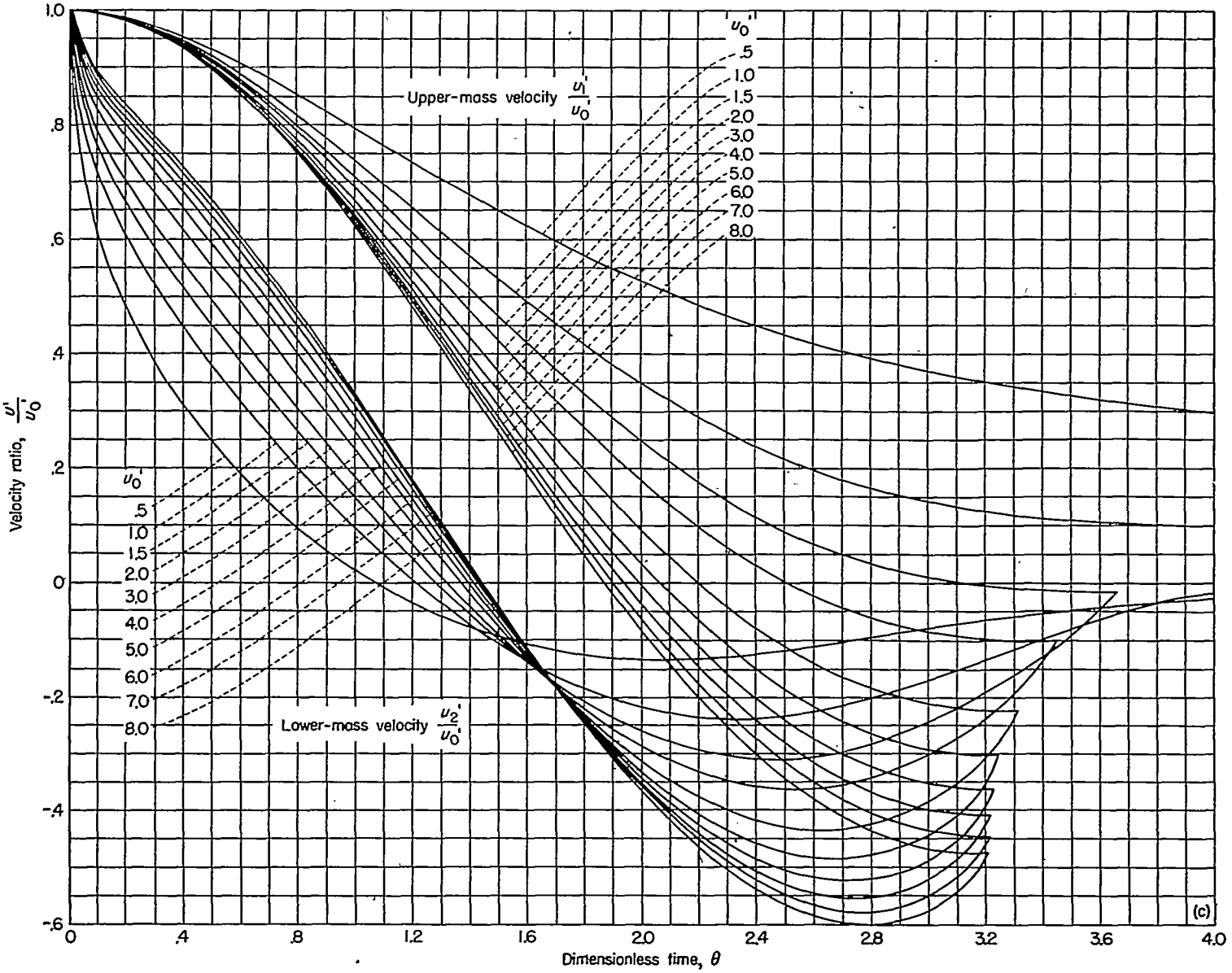

(c) Relationship between upper-mass velocity, lower-mass velocity, and time.

FIGURE 11.—Continued.

The generalized results presented in figure 11 [3] can be used to estimate the performance of a given landing gear of known configuration for particular impact conditions or to choose the dimensions for a landing gear when the impact conditions and desired performance are specified.

Applicability of solutions.—To illustrate the applicability of the generalized solutions, the curves of figure 11 have been applied to the previously considered case of the normal impact at an initial vertical velocity of 8.86 feet per second for comparison with the more exact solution presented in figure 4. In order to make use of the generalized solutions it is first necessary to approximate the tire force-deflection characteristics by a simple linear variation. Two such linear approximations which might be considered suitable for this purpose are shown in figure 12. Linear approximation I is a straight line through the origin having a slope $a=18.5\times10^3$ pounds per foot ($a'=ad=41.6\times10^3$ lb). This value of a and the other pertinent landing-gear and impact parameters result in a value of the initial dimensionless velocity parameter $u_0'=2.57$. Linear approximation II is a straight line with slope $a=21.3\times10^3$ pounds per foot ($a'=47.9\times10^3$ lb) which does not pass through the origin but intersects the displacement axis at a value of $z_{2(F_{V_g}=0)}=0.0508$ foot. With this value of a, $u_0'=2.39$.

Since the solutions of figure 11 have been calculated only for integral values of u_0', curves for the foregoing values of u_0' were graphically interpolated by cross plotting. These results were then converted to dimensional values by multi-

[3] Although time-history solutions are presented for values of u_0' as small as 0.5, it will be noted that values of $u_{1_{max}}$, σ_{max}, η_t, and η_{l_g} are not given for values of $u_0'<1.5$. It can be seen from the time histories that the characteristics of the solution in the later stages of the impact change as u_0' becomes small; in particular, u_1 increases and the curve of $u_{1_{max}}$ as a function of u_0' appears to reach a minimum at some value of $u_0'\leqq1.5$. Furthermore, the later stages of the solutions greatly stretch out in time and appear to be almost asymptotic in character. Several different analytical, numerical, and analogue methods were applied in an attempt to study this phase of the problem further but the extremely slow rate of change of the variables in this region prevented successful completion of the solutions.

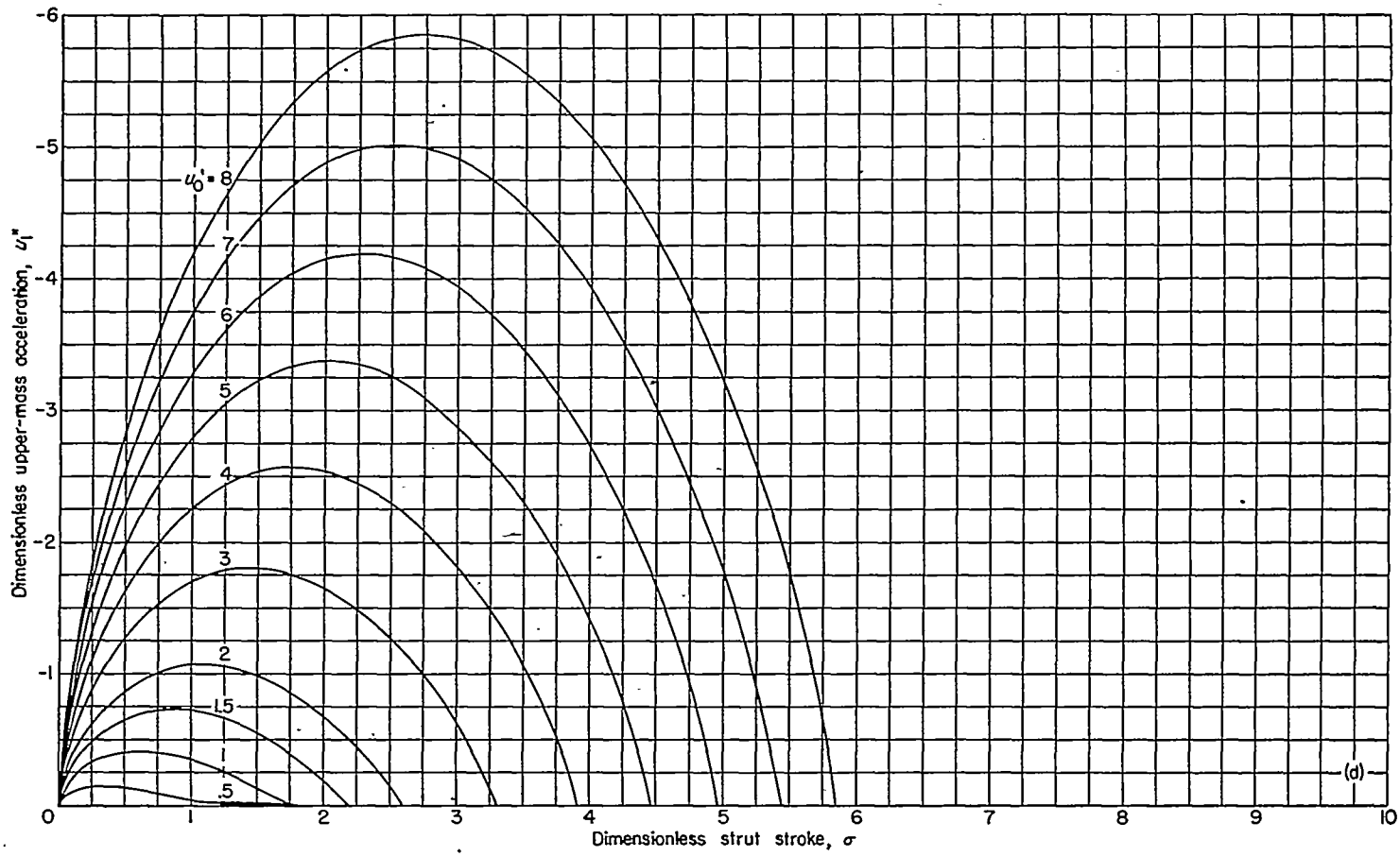

(d) Relationship between upper-mass acceleration and strut stroke.

FIGURE 11.—Continued.

plying the dimensionless variables by the appropriate constants. The results obtained are compared in figure 13 with the more exact solution presented in figure 4. The values based on linear approximation I have been plotted exactly as determined from the generalized solutions. The results for linear approximation II, however, have been displaced relative to the origin of coordinates as indicated in the following discussion.

The assumption of linear approximation II implies that the system must move a distance equal to $z_{2_{(F_{V_g}=0)}}$ after initial contact (at constant velocity since the wing lift is taken equal to the weight) before any finite ground reaction can develop. The derivation of the equations of motion, on the other hand, assumes that the ground reaction increases linearly with deflection from the instant of initial contact. As a result, the equations of motion do not apply until after the system has attained a displacement equal to $z_{2_{(F_{V_g}=0)}}$, which occurs at a time after initial contact $t=\frac{z_{2_{(F_{V_g}=0)}}}{V_{V_0}}$. In other words, the equations of motion apply to a coordinate system transformed so that the tire force-deflection relationship passes through the origin; that is, a coordinate system displaced by $z_{2_{(F_{V_g}=0)}}$ relative to the coordinate system originating at the point of initial contact. It therefore follows that the upper-mass and lower-mass displacements determined from the generalized solutions for the case of linear approximation II must be increased by a constant amount equal to $z_{2_{(F_{V_g}=0)}}$, in this case 0.0508 foot, and all results must be displaced in time by a constant increment $\Delta t=\frac{z_{2_{(F_{V_g}=0)}}}{V_{V_0}}$, in this case $\frac{0.0508}{8.86}=0.0057$ second, relative to the instant of initial contact. These corrections have been incorporated in plotting the curves for linear approximation II shown in figure 13.

As can be seen, the results obtained by application of the generalized solutions, particularly by the method employing linear approximation II, are in fairly good agreement with the more exact solution. The discrepancies which exist are attributable to the neglect of the shock-strut preloading and springing provided by the air-pressure force, neglect of the lower mass, and to differences between the very simple tire force-deflection relationships assumed and the exact tire characteristics. On the whole, it appears that the generalized results offer a means for rapidly estimating the behavior of the landing gear within reasonable limits of accuracy and may therefore be useful for preliminary design purposes.

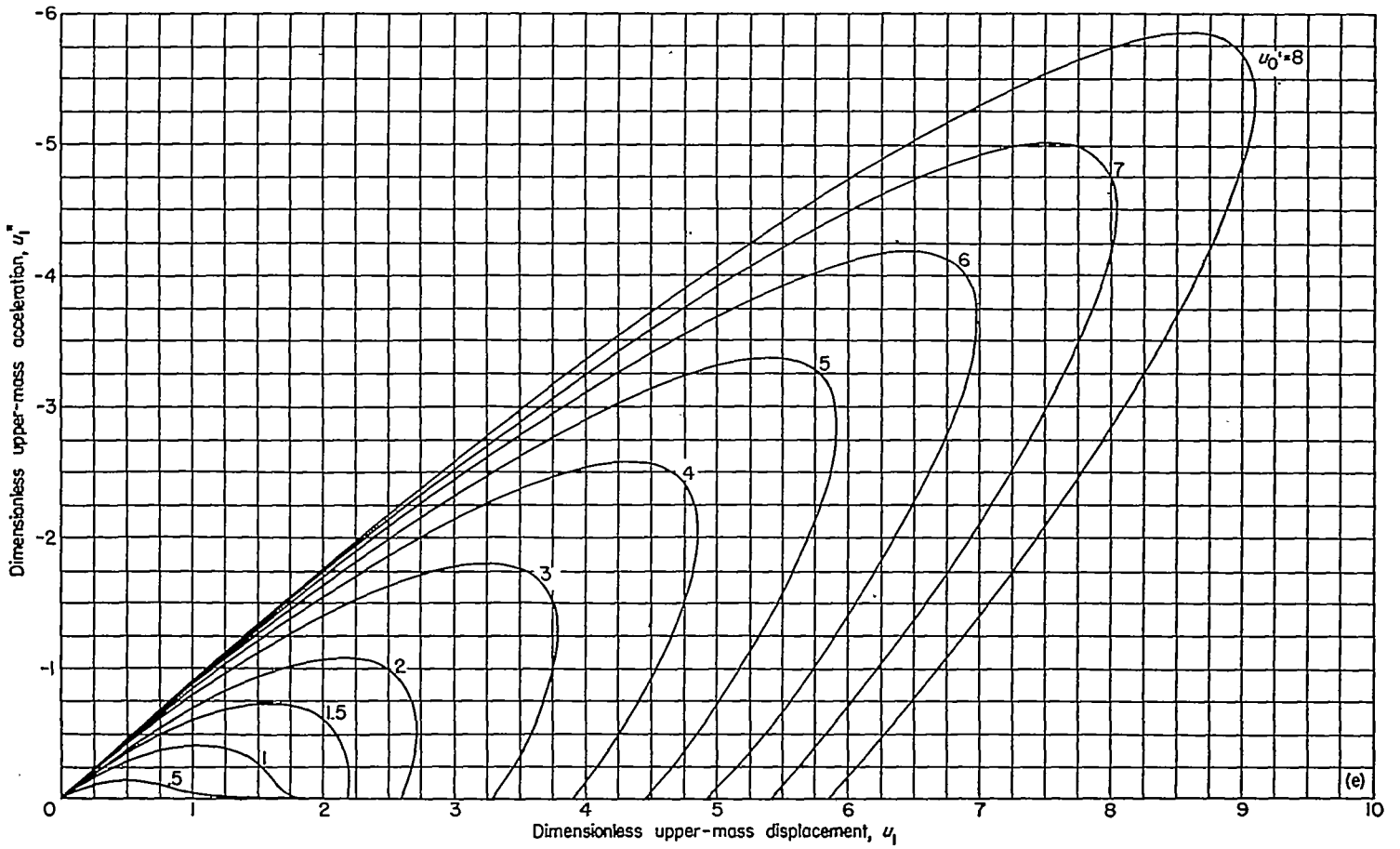

(e) Relationship between upper-mass acceleration and upper-mass displacement.

FIGURE 11.—Continued.

SUMMARY OF RESULTS AND CONCLUSIONS

A theoretical study has been made of the behavior of the conventional type of oleo-pneumatic landing gear during the process of landing impact. The basic analysis is presented in a general form and treats the motions of the landing gear prior to and subsequent to the beginning of shock-strut deflection. In the first phase of the impact the landing gear is treated as a single-degree-of-freedom system in order to determine the conditions of motion at the instant of initial shock-strut deflection, after which instant the landing gear is considered as a system with two degrees of freedom. The equations for the two-degree-of-freedom system consider such factors as the hydraulic (velocity square) resistance of the orifice, the forces due to air compression and internal friction in the shock strut, the nonlinear force-deflection characteristics of the tire, the wing lift, the inclination of the landing gear, and the effects of wheel spin-up drag loads.

The applicability of the analysis to actual landing gears has been investigated for the particular case of a vertical landing gear in the absence of drag loads by comparing calculated results with experimental drop-test data for corresponding impact conditions, for both a normal impact and a severe impact involving tire bottoming.

Studies have also been made to determine the effects of variations in such parameters as the dynamic force-deflection characteristics of the tire, the orifice discharge coefficient, and the effective polytropic exponent for the air-compression process, which might not be known accurately in practical design problems.

In addition to the more exact treatment an investigation has also been made to determine the extent to which the basic equations of motion can be simplified and still yield useful results. Generalized solutions of the simplified equations obtained are presented for a wide range of landing-gear and impact parameters.

On the basis of the foregoing studies the following conclusions are indicated:

1. The behavior of the landing gear as calculated from the basic equations of motion was found to be in good agreement with experimental drop-test data for the case of a vertical landing gear in the absence of drag loads, for both a normal impact and a severe impact involving tire bottoming.

2. A study of the effects of variations in the force-deflection characteristics of the tire indicates that

a. In the case of a normal impact without tire bottoming, reasonable variations in the force-deflection characteristics of the tire have only a relatively small effect on the calculated behavior of the landing gear. Approximating the rather complicated force-deflection characteristics of the actual tire by simplified exponential or linear-segment variations appears

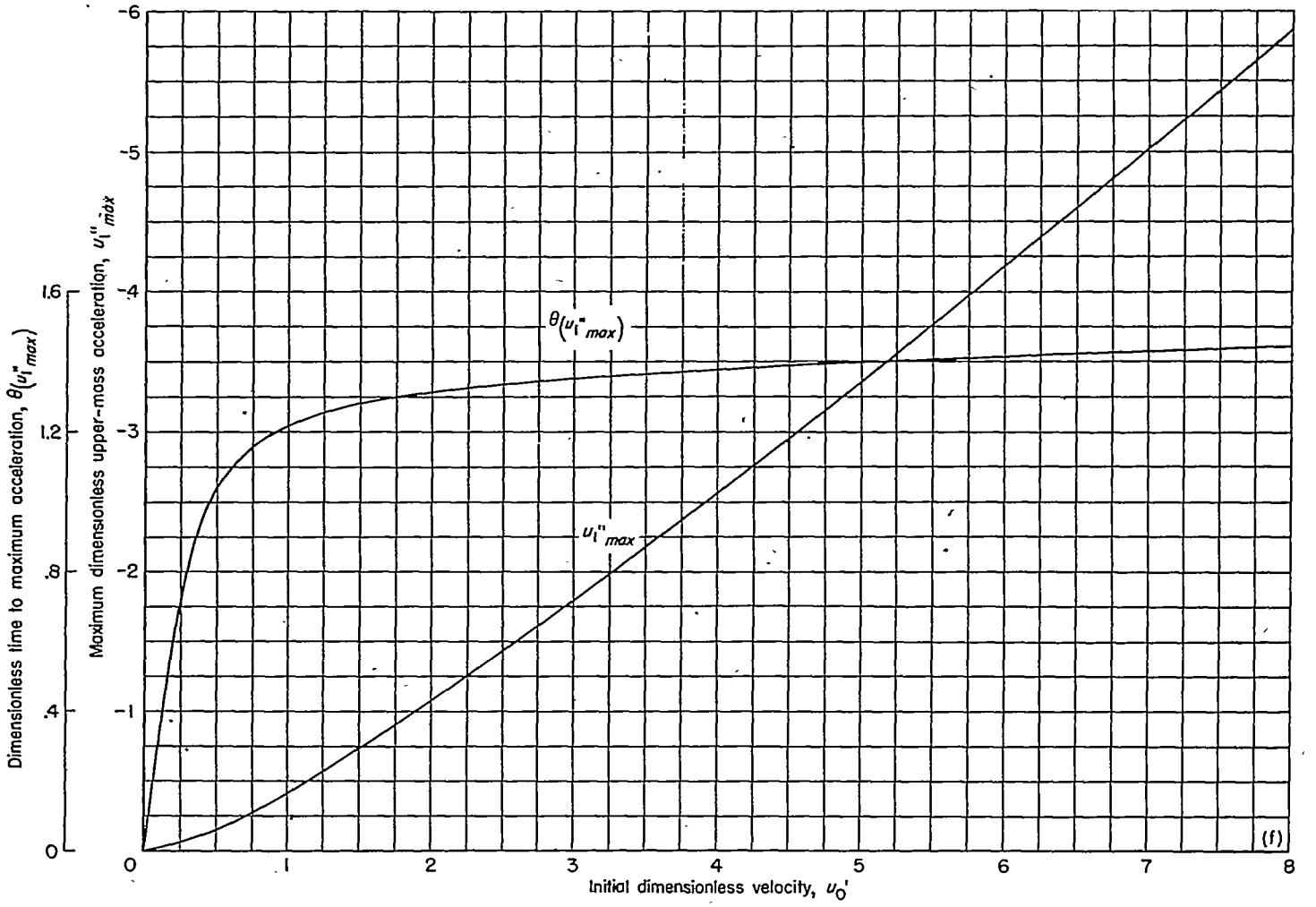

(f) Variation of maximum upper-mass acceleration and time to reach maximum upper-mass acceleration with initial velocity parameter.

FIGURE 11.—Continued.

to be adequate for practical purposes. Tire hysteresis was found to be relatively unimportant.

b. In the case of a severe impact involving tire bottoming, the use of simplified exponential and linear-segment approximations to the actual tire force-deflection characteristics which neglect the effects of tire bottoming, although adequate up to the instant of bottoming, fails to indicate the pronounced increase in landing-gear load which results from bottoming of the tire. The use of exponential or linear-segment approximations to the tire characteristics which take into account the increased stiffness of the tire that results from bottoming, however, yields good results.

3. A study of the importance of the discharge coefficient of the orifice indicates that the magnitude of the discharge coefficient has a marked effect on the calculated behavior of the landing gear; a decrease in the discharge coefficient (or the product of the discharge coefficient and the net orifice area) results in an approximately proportional increase in the maximum upper-mass acceleration.

4. A study of the importance of the air-compression process in the shock strut indicates that the air springing is of only minor significance throughout most of the impact, and that variations in the effective polytropic exponent n between the isothermal value of 1.0 and the near-adiabatic value of 1.3 have only a secondary effect on the calculated behavior of the landing gear. Even the assumption of constant air pressure in the strut equal to the initial pressure ($n=0$) yields fairly good results, which may be adequate for many practical purposes.

5. An investigation of the extent to which the equations of motion for the landing gear can be simplified and still yield acceptable calculated results indicates that, for many practical purposes, the air-pressure force in the shock strut can be completely neglected, the tire force-deflection relationship can be assumed to be linear, and the lower or unsprung mass can be taken equal to zero.

6. Generalization of the equations of motion for the simplified system described in the preceding paragraph shows that the behavior of this system is completely determined by the magnitude of one parameter, namely, the dimensionless initial-velocity parameter. Solution of these generalized equations in terms of dimensionless variables permits compact representation of the behavior of the system for a wide range of landing-gear and impact parameters, which may be useful for rapidly estimating landing-gear performance in preliminary design.

LANGLEY AERONAUTICAL LABORATORY,
NATIONAL ADVISORY COMMITTEE FOR AERONAUTICS,
LANGLEY FIELD, VA., *May 1, 1952.*

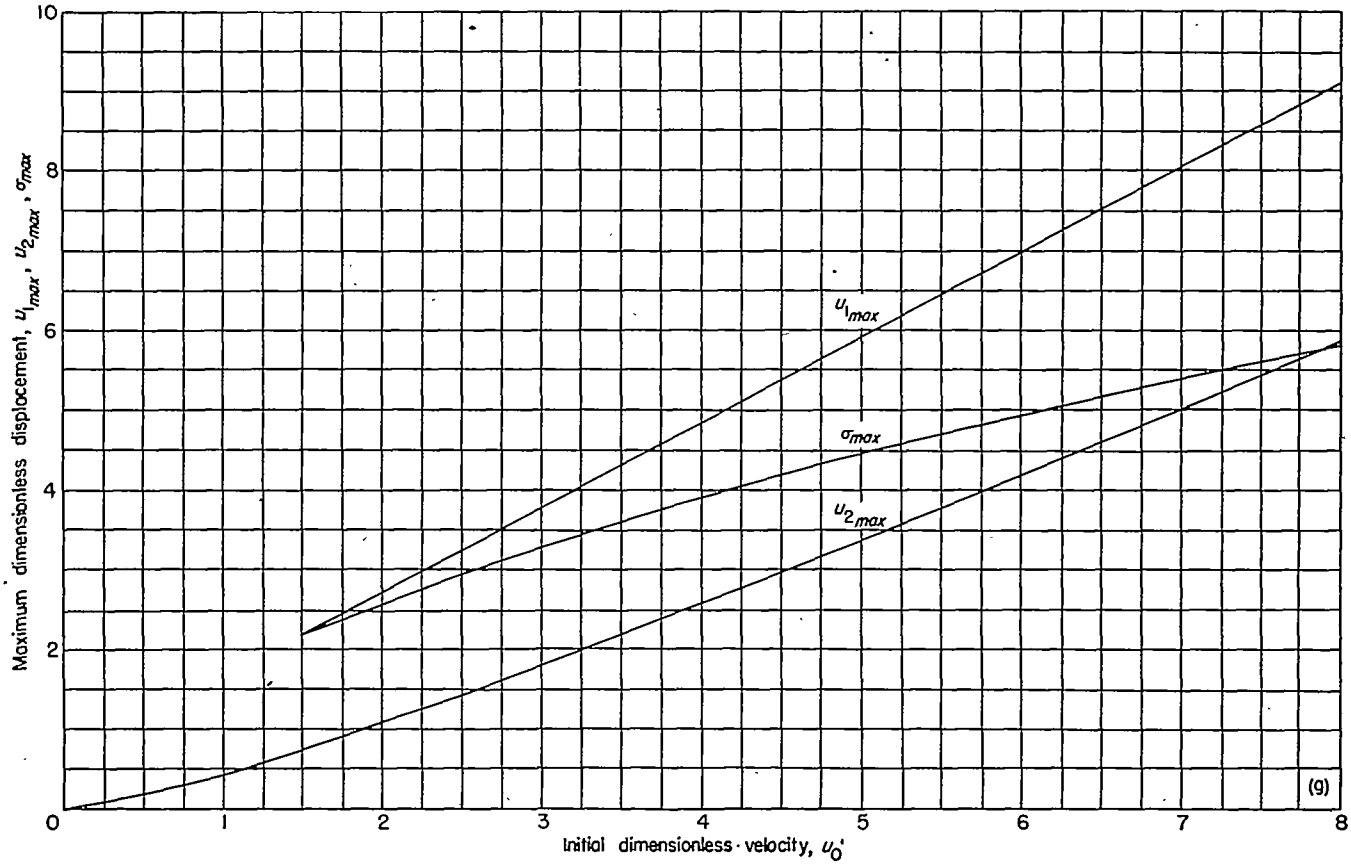

(g) Variation of maximum upper-mass displacement, maximum lower-mass displacement, and maximum strut stroke with initial velocity parameter.

FIGURE 11.—Continued.

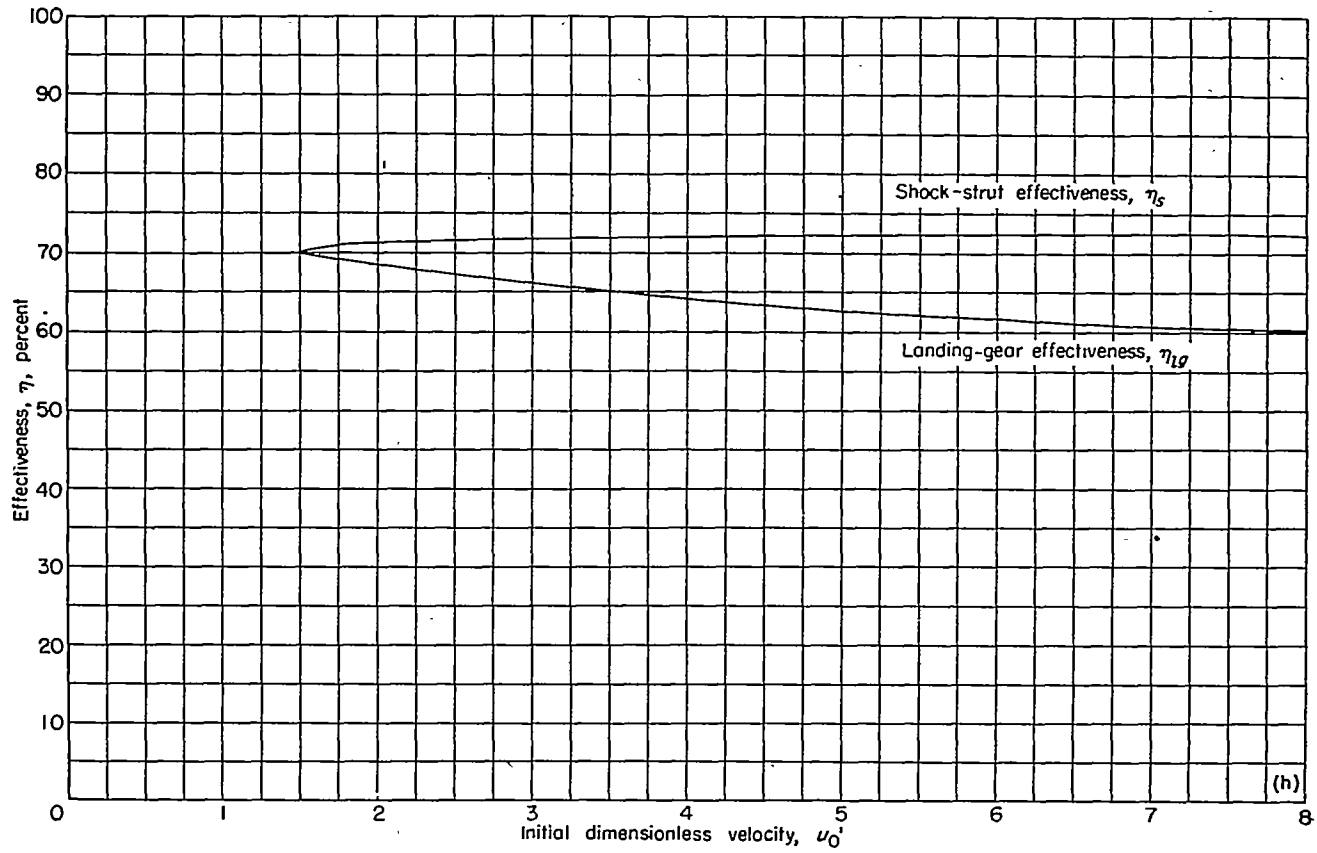

(h) Variation of shock-strut effectiveness and landing-gear effectiveness with initial velocity parameter.

FIGURE 11.—Concluded.

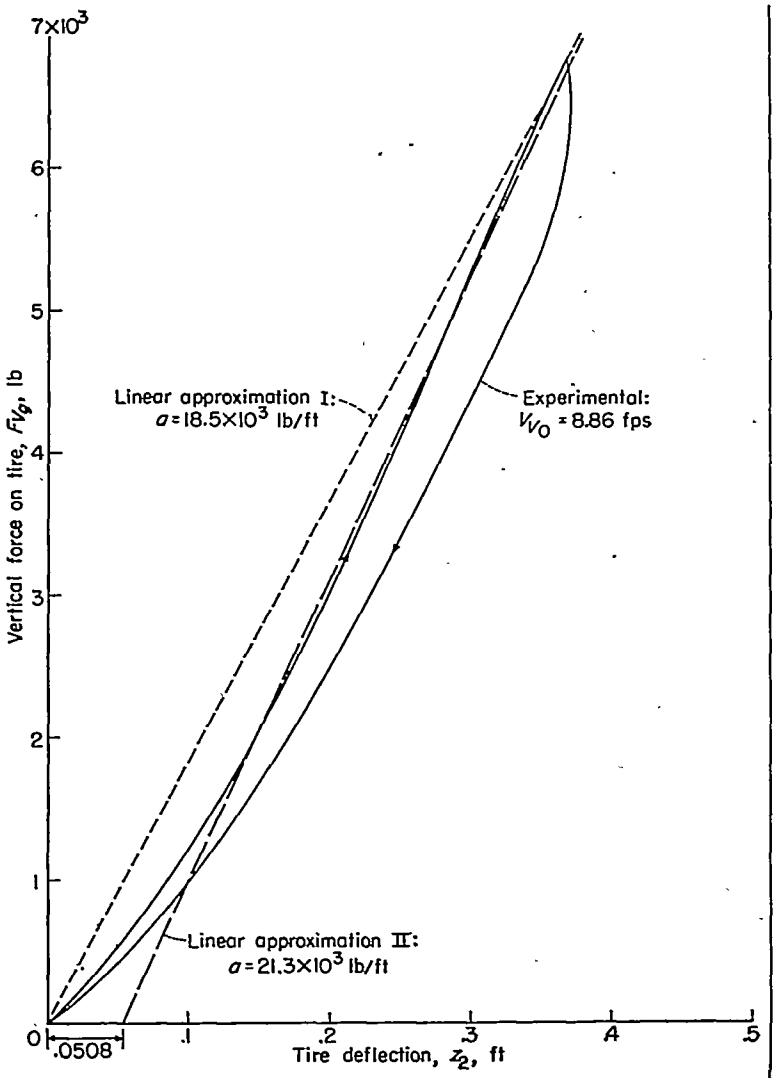

FIGURE 12.—Linear approximations to tire force-deflection characteristics used in application of generalized solutions.

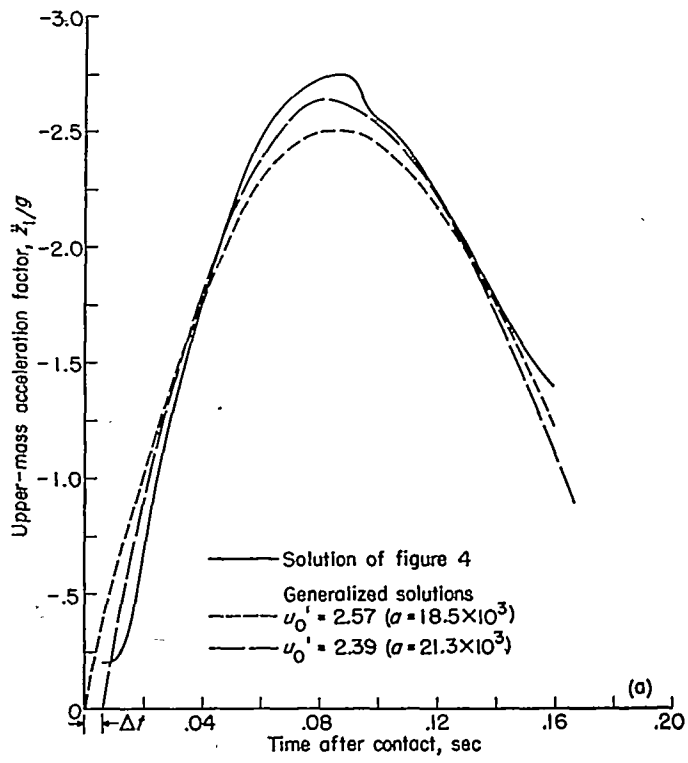

(a) Time history of upper-mass acceleration.

FIGURE 13.—Comparison of generalized results and more exact solution. V_{V_0}=8.86 feet per second; C_d=0.9.

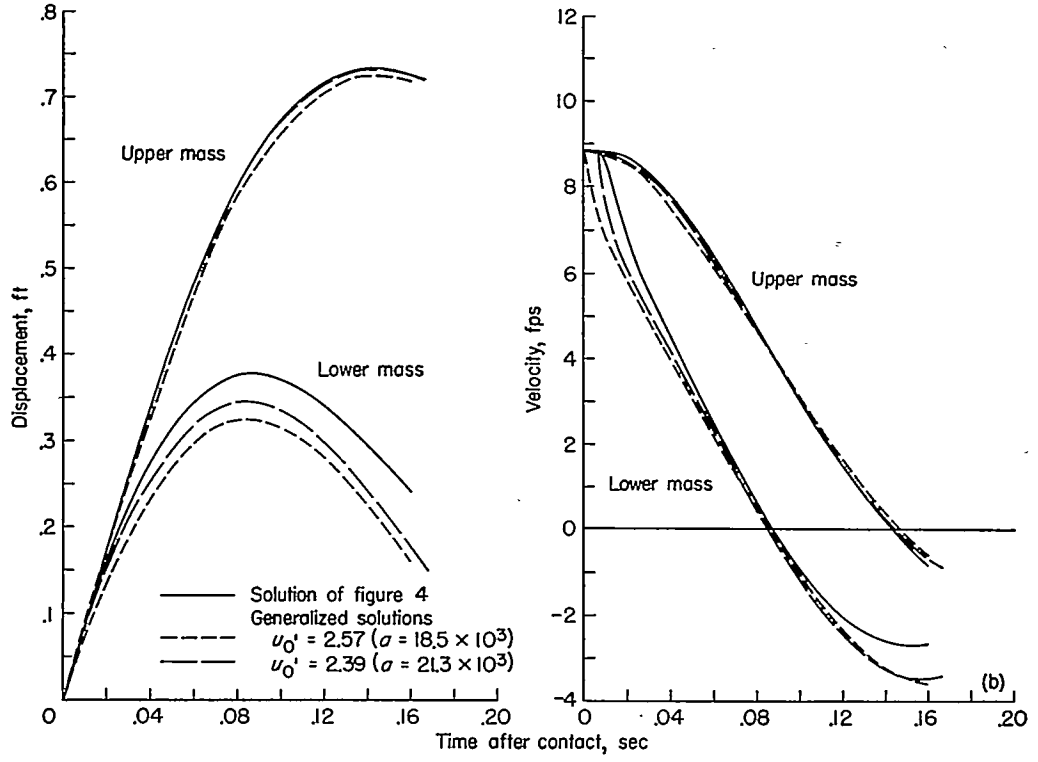

(b) Time histories of landing-gear displacements and velocities.

FIGURE 13.—Continued.

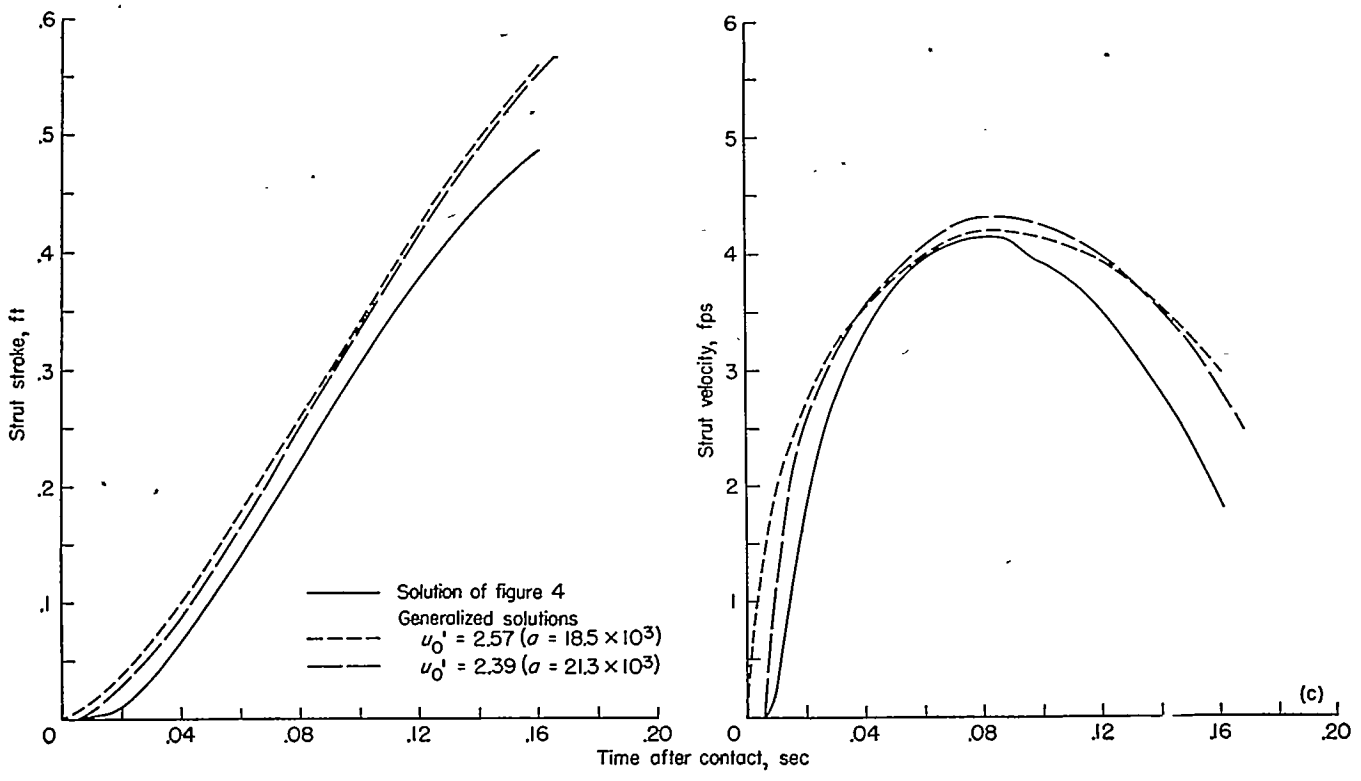

(c) Time histories of shock-strut stroke and velocity.

FIGURE 13.—Concluded.

APPENDIX A

NUMERICAL INTEGRATION PROCEDURES

As previously noted, most of the specific solutions presented in this report were obtained with a numerical integration procedure, termed the "linear procedure," which assumes changes in the variables to be linear over finite time intervals. With this procedure a time interval $\epsilon=0.001$ second was used in order to obtain the desired accuracy for the particular cases considered. A few of the specific solutions presented were obtained by means of a procedure, termed the "quadratic procedure," which assumes a quadratic variation of displacement with time for successive intervals. This procedure, although requiring somewhat more computing time per interval, may permit an increase in the interval size for a given accuracy, in some cases allowing a reduction in the total computing time required. In the case of the more exact equations of motion the accuracy of the quadratic procedure with a time interval of 0.002 second appears to be equal to that of the linear procedure with an interval of 0.001 second. Although the accuracy naturally decreases with increasing interval size, the loss in accuracy for proportionate increases in interval size appears to be smaller for the quadratic than for the linear procedure. In the case of the simplified equations of motion reasonably satisfactory results were obtained in test computations with the quadratic procedure for intervals as large as 0.01 second, whereas the linear procedure was considered questionable for intervals larger than 0.002 second.

The generalized solutions presented, because of the relatively simple form of the equations of motion, were obtained with the well-known Runge-Kutta procedure. A study of the allowable interval size resulted in the use of an interval $\Delta\theta=0.08$, which corresponds to a time interval of about 0.005 second for the landing gear under consideration.

LINEAR PROCEDURE

In this step-by-step procedure the variations in displacement, velocity, and acceleration are assumed to be linear over each finite time interval ϵ. The method, as used, involves one stage of iteration. Linear extrapolation of the velocity at the end of any interval is used to obtain estimated values of velocity and displacement for the next interval. These values are then used to calculate values of the acceleration in accordance with the equations of motion. Integration of the acceleration provides improved values of the velocity and, if desired, the displacement and acceleration. In this procedure all integrations are performed by application of the trapezoidal rule.

The following derivation illustrates the application of the linear procedure to the equations of motion for the landing gear, which apply subsequent to the beginning of shock-strut deflection at time t_τ. In the example presented internal friction forces are neglected in order to simplify the derivation. However, the same general procedure can be used if these, or other complicating effects, are included in the equations.

For the case under consideration the equations of motion (eqs. (16), (17), and (8)) can be written as follows:

$$\frac{W_1}{g}\ddot{z}_1+A(\dot{z}_1-\dot{z}_2)^2+B[1-C(z_1-z_2)]^{-n}+D=0 \tag{A1}$$

$$\frac{W_2}{g}\ddot{z}_2-A(\dot{z}_1-\dot{z}_2)^2-B[1-C(z_1-z_2)]^{-n}+F_{V_g}(z_2)-W_2=0 \tag{A2}$$

$$\frac{W_1}{g}\ddot{z}_1+\frac{W_2}{g}\ddot{z}_2+F_{V_g}(z_2)+E=0 \tag{A3}$$

where

$$A=\frac{\dot{s}}{|\dot{s}|}\frac{\rho A_h^3}{2(C_d A_n)^2\cos\varphi}$$

$$B=p_{a_0}A_a\cos\varphi$$

$$C=\frac{A_a}{v_0\cos\varphi}$$

$$D=K_L W-W_1$$

$$E=W(K_L-1)$$

Solving equation (A3) for $\ddot{z}_1$ gives

$$\frac{\ddot{z}_1}{g}=[F-G\ddot{z}_2-HF_{V_g}(z_2)]\frac{1}{g} \tag{A4}$$

where

$$F=\frac{W}{W_1}(1-K_L)g$$

$$G=\frac{W_2}{W_1}$$

$$H=\frac{g}{W_1}$$

Integrating equation (A4) with respect to t between the limits t_τ and t and noting that $\dot{z}_{1_\tau}=\dot{z}_{2_\tau}=\dot{z}_\tau$ gives

$$\dot{z}_1=\dot{z}_\tau+F\tau-G(\dot{z}_2-\dot{z}_\tau)-H\int_0^\tau F_{V_g}(z_2)d\tau \tag{A5}$$

where $\tau=(t-t_\tau)$.

Integrating again and noting that $z_{1_\tau}=z_{2_\tau}=z_\tau$ gives

$$z_1=(1+G)(z_\tau+\dot{z}_\tau\tau)+\frac{F\tau^2}{2}-Gz_2-H\int_0^\tau\int_0^\tau F_{V_g}(z_2)\,d\tau\,d\tau \tag{A6}$$

Substituting for $\dot{z}_1$ and z_1 in equation (A2) gives

$$\frac{\ddot{z}_2}{g}=\frac{1}{W_2}\left(A\left[(1+G)(\dot{z}_\tau-\dot{z}_2)+F_\tau-H\int_0^\tau F_{V_g}(z_2)\,d\tau\right]^2+B\left\{1-C\left[(1+G)(z_\tau+\dot{z}_\tau\tau-z_2)+\frac{F_\tau{}^2}{2}-H\int_0^\tau\int_0^\tau F_{V_g}(z_2)\,d\tau\,d\tau\right]\right\}^{-n}-F_{V_g}(z_2)+W_2\right) \tag{A7}$$

The motion of the landing gear subsequent to the beginning of shock-strut deflection is determined by means of a step-by-step solution of equation (A7). This numerical procedure yields time histories of the lower-mass motion variables z_2, $\dot{z}_2$, and $\ddot{z}_2$, from which the motion variables for the upper mass $\ddot{z}_1$, $\dot{z}_1$, and z_1 can be calculated by means of equations (A4), (A5), and (A6).

The initial conditions for the step-by-step procedure are

$$\left.\begin{aligned} z_{1_{n=0}}&=z_{2_{n=0}}=z_\tau\\ \dot{z}_{1_{n=0}}&=\dot{z}_{2_{n=0}}=\dot{z}_\tau\\ \ddot{z}_{1_{n=0}}&=\ddot{z}_{2_{n=0}}=\ddot{z}_\tau \end{aligned}\right\} \tag{A8}$$

where z_τ, $\dot{z}_\tau$, and $\ddot{z}_\tau$ are the conditions of motion at the beginning of shock-strut deflection as determined from the solution for the one-degree-of-freedom system.

Estimated values of the lower-mass velocity at the end of the first time increment ϵ following the beginning of shock-strut deflection can be obtained from the expression

$$\dot{z}^*_{2_{n=1}}=\dot{z}_\tau+\epsilon\ddot{z}_\tau \tag{A9}$$

or, as a first approximation,

$$\dot{z}^*_{2_{n=1}}=\dot{z}_\tau$$

The corresponding displacement is given by

$$z_{2_{n=1}}=z_\tau+\frac{\epsilon}{2}(\dot{z}_{2_1}+\dot{z}_\tau) \tag{A10}$$

After the initial conditions and the conditions at the end of the first time increment are established, a step-by-step calculation of the motion can be obtained by routine operations as indicated by the following general procedure which applies at any time $\tau=n\epsilon$ after the beginning of the process. The operations indicated are based on integration by application of the trapezoidal rule:

$$\dot{z}^*_{2_n}=\dot{z}_{2_{n-1}}+(\dot{z}_{2_{n-1}}-\dot{z}_{2_{n-2}})=\dot{z}_{2_{n-1}}+\frac{\epsilon}{2}(\ddot{z}_{2_{n-1}}+\ddot{z}_{2_{n-2}}) \tag{A11}$$

$$z^*_{2_n}=z_{2_{n-1}}+\frac{\epsilon}{2}(\dot{z}_{2_{n-1}}+\dot{z}^*_{2_n})=z_{2_{n-1}}+\epsilon\dot{z}_{2_{n-1}}+\frac{\epsilon^2}{4}(\ddot{z}_{2_{n-1}}+\ddot{z}_{2_{n-2}}) \tag{A12}$$

With the estimated values $\dot{z}^*_{2_n}$ and $z^*_{2_n}$ the acceleration of the lower mass can be determined by substitution in the appropriate integrodifferential equation for the system, equation (A7) in the present case. Thus

$$\ddot{z}_{2_n}=f(\dot{z}^*_{2_n},\,z^*_{2_n},\,\tau_n) \tag{A13}$$

In equation (A7) the integral expressions can also be evaluated by application of the trapezoidal rule. For example, when $F_{V_g}(z_2)=mz_2{}^r$,

$$\int_0^{n\epsilon} z_2{}^r d\tau\approx\frac{\epsilon}{2}(z_\tau{}^r+2z_{2_1}{}^r+\ldots 2z_{2_{n-1}}{}^r+z_n{}^r)\approx\int_0^{(n-1)\epsilon} z_2{}^r d\tau+\frac{\epsilon}{2}(z_{2_{n-1}}{}^r+z_{2_n}{}^r) \tag{A14}$$

and

$$\int_0^{n\epsilon}\int_0^{n\epsilon} z_2{}^r d\tau\,d\tau\approx\int_0^{(n-1)\epsilon}\int_0^{(n-1)\epsilon} z_2{}^r d\tau\,d\tau+\frac{\epsilon}{2}\left(\int_0^{(n-1)\epsilon} z_2{}^r d\tau+\int_0^{n\epsilon} z_2{}^r d\tau\right) \tag{A15}$$

An improved value for the velocity is obtained from the expression

$$\dot{z}_{2_n}=\dot{z}_{2_{n-1}}+\frac{\epsilon}{2}(\ddot{z}_{2_{n-1}}+\ddot{z}_{2_n}) \tag{A16}$$

This value is used in the calculation of the estimated velocity $\dot{z}^*_{2_{n+1}}$ and displacement $z^*_{2_{n+1}}$ for the next interval.

If desired, improved values of the displacement and acceleration for the nth interval subsequent to the beginning of shock-strut deflection can be obtained as follows:

$$z_{2_n}=z_{2_{n-1}}+\frac{\epsilon}{2}(\dot{z}_{2_{n-1}}+\dot{z}_{2_n})=z_{2_{n-1}}+\epsilon\dot{z}_{2_{n-1}}+\frac{\epsilon^2}{4}(\ddot{z}_{2_{n-1}}+\ddot{z}_{2_n}) \tag{A17}$$

and

$$\ddot{z}_{2_n}=f(\dot{z}_{2_n},\,z_{2_n},\,\tau_n) \tag{A18}$$

where $f(\dot{z}_{2_n},\,z_{2_n},\,\tau_n)$ is an appropriate equation for the system, such as equation (A7).

With the values of z_{2_n}, $\dot{z}_{2_n}$, and $\ddot{z}_{2_n}$, the motion variables for the upper mass $\ddot{z}_{1_n}$, $\dot{z}_{1_n}$, and z_{1_n} can be calculated separately from equations (A4), (A5), and (A6), as previously noted.

In setting up the numerical procedure used in obtaining the solutions presented in this report, an evaluation of the errors introduced by the procedure indicated that it would not be necessary to calculate the improved values of the displacement z_{2_n} (eq. (A17)) or the acceleration $\ddot{z}_{2_n}$ (eq. (A18)). However, improved values of the velocity $\dot{z}_{2_n}$ were calculated by

means of equation (A16) for the purpose of determining estimated values of the velocity $\dot{z}_2$ and the displacement z_2 (eqs. (A11) and (A12)) for the increment immediately following.

In order to illustrate the application of the method, a tabular computing procedure for the solution of the system represented by equations (A1), (A2), and (A3) is presented in table I.

QUADRATIC PROCEDURE

In this step-by-step procedure a quadratic variation of displacement is assumed over successive equal finite time intervals for the purpose of extrapolating values of the motion variables from one interval to the next. With this assumption the displacement variation over two successive equal time intervals is completely determined by the three values of displacement at the beginning and end of each of the two intervals. By writing the quadratic variation in difference form, the velocity and acceleration at the midpoint of the double interval can be expressed in terms of the three displacement values previously mentioned. Substituting for the velocity and acceleration in the differential equations for the system yields difference equations of motion in terms of successive displacement values which can be evaluated interval by interval.

TABLE I

LINEAR PROCEDURE

Row	Quantity	Equation	Procedure†
⓪	τ	----------	----------
①	$\dot{z}^*_{2_n}$	$\dot{z}_{2_{n-1}}+\frac{\epsilon}{2}(\ddot{z}_{2_{n-2}}+\ddot{z}_{2_{n-1}})$	$⑨_p$
②	$z^*_{2_n}$	$z_{2_{n-1}}+\frac{\epsilon}{2}(\dot{z}_{2_{n-1}}+\dot{z}^*_{2_n})$	$②_p+\epsilon⑧_p$
③	$F_{V_g}(z^*_{2_n})$	----------	Determined from tire force-deflection characteristics.
④	$\int_0^\tau F_{V_g}(z^*_{2_n})d\tau$	Equation (A14)	$④_p+\frac{\epsilon}{2}[③+③_p]$
⑤	$\int_0^\tau\int_0^\tau F_{V_g}(z^*_{2_n})d\tau\,d\tau$	Equation (A15)	$⑤_p+\frac{\epsilon}{2}[④+④_p]$
⑥	$\frac{\ddot{z}_{2_n}}{g}$	Equation (A7)	Given by equation (A7).
⑦	$\dot{z}_{2_n}$	$\dot{z}_{2_{n-1}}+\frac{\epsilon}{2}(\ddot{z}_{2_{n-1}}+\ddot{z}_{2_n})$	$⑦_p+\frac{\epsilon}{2}[⑥+⑥_p]g$
⑧	$\frac{1}{2}(\dot{z}_{2_n}+\dot{z}^*_{2_{n+1}})$	$\dot{z}_{2_n}+\frac{\epsilon}{4}(\ddot{z}_{2_{n-1}}+\ddot{z}_{2_n})$	$⑦+\frac{\epsilon}{4}[⑥+⑥_p]g$
⑨	$\dot{z}^*_{2_{n+1}}$	$\dot{z}_{2_n}+\frac{\epsilon}{2}(\ddot{z}_{2_{n-1}}+\ddot{z}_{2_n})$	$⑦+\frac{\epsilon}{2}[⑥+⑥_p]g$
⑩	$\frac{\ddot{z}_{1_n}}{g}$	Equation (A4)	Given by equation (A4).
⑪	$\dot{z}_{1_n}$	Equation (A5)	Given by equation (A5).
⑫	z_{1_n}	Equation (A6)	Given by equation (A6).

† $\bigcirc_p$ denotes value for previous time interval.

The following derivation shows how the procedure can be applied to the determination of the behavior of the landing gear subsequent to the beginning of shock-strut deflection at time t_τ. In order to simplify the derivation, internal friction forces are again neglected in setting-up the equations of motion.

The assumption of a quadratic variation of displacement with time (constant acceleration) over two successive intervals, each of duration ϵ, permits expressing the velocity and acceleration at the midpoints of the double interval (see sketch) in terms of the displacement values at the beginning, midpoint, and end of the double interval by the equations (see ref. 5, p. 16):

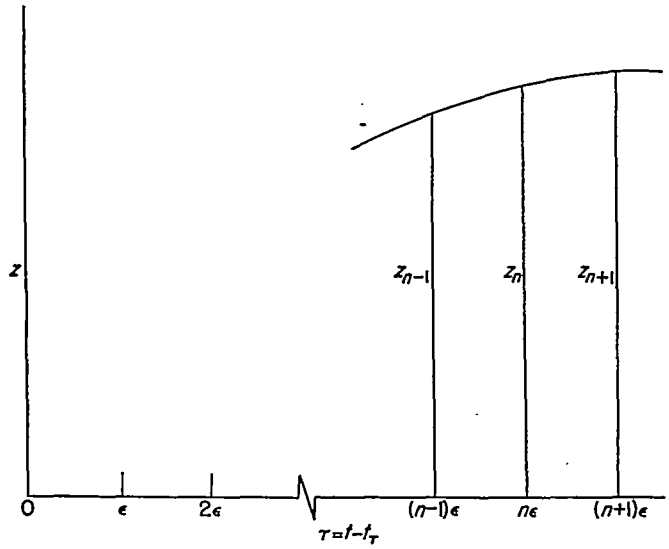

$$\dot{z}_n=\frac{z_{n+1}-z_{n-1}}{2\epsilon} \tag{A19}$$

and

$$\ddot{z}_n=\frac{z_{n+1}-2z_n+z_{n-1}}{\epsilon^2} \tag{A20}$$

where $\dot{z}_n$, $\ddot{z}_n$, and z_n are the velocity, acceleration, and displacement at the end of the nth interval ($\tau=n\epsilon$) after the beginning of shock-strut deformation and z_{n-1} and z_{n+1} are the displacements at the end of intervals $n-1$ and $n+1$, respectively.

Substituting the difference relations for $\dot{z}_1$, $\dot{z}_2$, $\ddot{z}_1$, and $\ddot{z}_2$ into equations (A1) and (A3) permits writing the equations of motion for the landing gear in difference form as follows:

$$\frac{W_1}{g\epsilon^2}(z_{1_{n+1}}-2z_{1_n}+z_{1_{n-1}})+\frac{A}{4\epsilon^2}(z_{1_{n+1}}-z_{1_{n-1}}-z_{2_{n+1}}+z_{2_{n-1}})^2+B[1-C(z_{1_n}-z_{2_n})]^{-n}+D=0 \tag{A21}$$

and

$$z_{1_{n+1}}=2z_{1_n}-z_{1_{n-1}}-G(z_{2_{n+1}}-2z_{2_n}+z_{2_{n-1}})-H\epsilon^2[F_{V_g}(z_{2n})+E] \tag{A22}$$

where the constants are as defined in the previous section.

Substituting for $z_{1_{n+1}}$ in equation (A21) gives

$$z_{2_{n+1}}=\frac{\beta_{n+1}}{W}+\frac{1}{gAW^2}\left[2W_1^2W_2-\sqrt{4W_1^2W_2(gAW\beta_{n+1}+W_1^2W_2)-gAW^2(4W_1^2\alpha_{n+1}+gA\gamma_{n+1})}\right] \tag{A23}$$

where

$$\alpha_{n+1}=2W_2z_{2_n}-W_2z_{2_{n-1}}-g\epsilon^2[F_{V_g}(z_{2_n})+E]$$

$$\beta_{n+1}=2W_2z_{2_n}+(W_1-W_2)z_{2_{n-1}}+2W_1(z_{1_n}-z_{1_{n-1}})-g\epsilon^2[F_{V_g}(z_{2_n})+E]$$

and

$$\gamma_{n+1}=\frac{4W_1^2\epsilon^2}{A}\{B[1-C(z_{1_n}-z_{2_n})]^{-n}+D\}$$

Equations (A22) and (A23) are essentially extrapolation formulas which permit the determination of values for the upper-mass and lower-mass displacements to come from the values of displacement already calculated. These equations thus permit step-by-step calculation of the displacements as the impact progresses, starting with the initial conditions, from which the upper-mass and lower-mass velocities and accelerations can be determined by means of equations (A19) and (A20).

Since the calculation of the displacements z_1 and z_2 at any instant by means of equations (A22) and (A23) requires values for the displacements at two previous instants, the routine application of these equations can begin only at the end of the second interval ($\tau=2\epsilon$) following the beginning of shock-strut deflection. Before the displacements at the end of the second interval can be calculated, however, it is necessary to determine the displacements at the end of the first interval. These values can be obtained from the conditions of motion at the instant of initial shock-strut deflection by applying equations (A19) and (A20) to the instant $t=t_\tau$.

At the instant of initial shock-strut deflection

$$\left.\begin{aligned} z_{1_{n=0}} &= z_{2_{n=0}} = z_\tau \\ \dot{z}_{1_{n=0}} &= \dot{z}_{2_{n=0}} = \dot{z}_\tau \\ \ddot{z}_{1_{n=0}} &= \ddot{z}_{2_{n=0}} = \ddot{z}_\tau \end{aligned}\right\} \tag{A24}$$

Application of the difference equations (A19) and (A20) to the instant $t=t_\tau$ (that is, $n=0$) gives the following equations:

$$\left.\begin{aligned} \dot{z}_\tau &= \frac{z_{n=1} - z_{n=-1}}{2\epsilon} \\ \ddot{z}_\tau &= \frac{z_{n=1} - 2z_\tau + z_{n=-1}}{\epsilon^2} \end{aligned}\right\} \tag{A25}$$

Since the landing gear is considered as a one-degree-of-freedom system from initial contact up to the instant $t=t_\tau$, the foregoing application of the difference equations results in identical values for the upper-mass displacement and lower-mass displacement at the end of the first interval. Simultaneous solution of equations (A25) gives the following expression for the displacement at the end of the first interval:

$$z_{2_{n=1}} = z_{1_{n=1}} = z_\tau + \epsilon \dot{z}_\tau + \frac{\epsilon^2}{2} \ddot{z}_\tau \tag{A26}$$

With the values for z_τ and $z_{n=1}$, equations (A22) and (A23) permit the step-by-step calculation of the upper-mass and lower-mass displacements subsequent to the first interval following the beginning of shock-strut deflection. The corresponding velocities and accelerations of the upper and lower masses can be determined from the calculated displacements by means of equations (A19) and (A20), as previously noted.

A tabular computing procedure illustrating the application of the method is presented in table II.

TABLE II

QUADRATIC PROCEDURE

Row	Quantity	Equation	Procedure †
⓪	τ	----------	----------
①	z_{2_n}	----------	③$_p$
②	z_{1_n}	----------	④$_p$
③	$z_{2_{n+1}}$	Equation (A23)	Given by equation (A23).
④	$z_{1_{n+1}}$	Equation (A22)	Given by equation (A22).
⑤	$\dot{z}_{2_n}$	$\frac{z_{2_{n+1}} - z_{2_{n-1}}}{2\epsilon}$	$\frac{③ - ①_p}{2\epsilon}$
⑥	$\ddot{z}_{2_n}$	$\frac{z_{2_{n+1}} - 2z_{2_n} + z_{2_{n-1}}}{\epsilon^2}$	$\frac{③ - 2① + ①_p}{\epsilon^2}$
⑦	$\dot{z}_{1_n}$	$\frac{z_{1_{n+1}} - z_{1_{n-1}}}{2\epsilon}$	$\frac{④ - ②_p}{2\epsilon}$
⑧	$\ddot{z}_{1_n}$	$\frac{z_{1_{n+1}} - 2z_{1_n} + z_{1_{n-1}}}{\epsilon^2}$	$\frac{④ - 2② + ②_p}{\epsilon^2}$

† ○ denotes value for previous time interval.

RUNGE-KUTTA PROCEDURE

In this step-by-step procedure the differences in the dependent variables over any given interval of the independent variable are calculated from a definite set of formulas, the same set of formulas being used for all increments. Thus the values of the variables at the end of any given interval are completely determined by the values at the end of the preceding interval. Unfortunately, however, unless the equations to be integrated are relatively simple, the method can become quite lengthy.

The following derivation illustrates the application of the Runge-Kutta method to the generalized equations of motion (eqs. (21)) for the simplified system considered in the section on generalized results. Since these equations can be readily reduced to the first order, they can be integrated by the step-by-step application of the general equations given on pages 301 and 302 of reference 6 for first-order simultaneous differential equations.

The generalized equations for the simplified system previously discussed (eqs. (21)) are

$$(u_1'-u_2')^2+u_1''=0$$

$$(u_1'-u_2')^2-u_2=0$$

$$u_1''+u_2=0$$

Inasmuch as any two of these equations are sufficient to describe the behavior of the system, only the last two equations are employed in this procedure. These equations can be reduced to a first-order system by introducing the new variable

$$w=u_1' \tag{A27}$$

so that

$$w'=u_1'' \tag{A28}$$

and the equations of motion become

$$\left.\begin{aligned}(w-u_2')^2-u_2&=0\\ w'+u_2&=0\end{aligned}\right\} \tag{A29}$$

Solving equations (A29) for u_2' and w', respectively, gives

$$u_2'=w-\sqrt{u_2} \tag{A30}$$

$$w'=-u_2 \tag{A31}$$

Applying the general procedure presented in the reference previously cited to the simultaneous equations (A27), (A30), and (A31) gives

$$\left.\begin{aligned}\Delta u_1=u_{1_n}-u_{1_{n-1}}&=\frac{1}{6}(k_1+2k_2+2k_3+k_4)\\ \Delta w=w_n-w_{n-1}&=\frac{1}{6}(l_1+2l_2+2l_3+l_4)\\ \Delta u_2=u_{2_n}-u_{2_{n-1}}&=\frac{1}{6}(m_1+2m_2+2m_3+m_4)\end{aligned}\right\} \tag{A32}$$

where

$$k_1=w_{n-1}\Delta\theta$$

$$k_2=\left(w_{n-1}+\frac{l_1}{2}\right)\Delta\theta$$

$$k_3=\left(w_{n-1}+\frac{l_2}{2}\right)\Delta\theta$$

$$k_4=(w_{n-1}+l_3)\Delta\theta$$

$$l_1=-u_{2_{n-1}}\Delta\theta$$

$$l_2=-\left(u_{2_{n-1}}+\frac{m_1}{2}\right)\Delta\theta$$

$$l_3=-\left(u_{2_{n-1}}+\frac{m_2}{2}\right)\Delta\theta$$

$$l_4=-(u_{2_{n-1}}+m_3)\Delta\theta$$

$$m_1=\left(w_{n-1}-\sqrt{u_{2_{n-1}}}\right)\Delta\theta=u_{2_{n-1}}'\Delta\theta$$

$$m_2=\left[\left(w_{n-1}+\frac{l_1}{2}\right)-\sqrt{u_{2_{n-1}}+\frac{m_1}{2}}\right]\Delta\theta$$

$$m_3=\left[\left(w_{n-1}+\frac{l_2}{2}\right)-\sqrt{u_{2_{n-1}}+\frac{m_2}{2}}\right]\Delta\theta$$

$$m_4=\left[(w_{n-1}+l_3)-\sqrt{u_{2_{n-1}}+m_3}\right]\Delta\theta$$

With this procedure, u_1, w, and u_2 can be calculated in step-by-step fashion from the values for the preceding interval, the procedure beginning with the initial conditions. From these values, u_1', u_1'', and u_2' can be calculated by means of equations (A27), (A28), and (A30), respectively.

APPENDIX B

SOURCE OF EXPERIMENTAL DATA

Following is a brief description of the apparatus and test specimen used in obtaining the experimental data presented in this report.

EQUIPMENT

The basic piece of equipment employed in the tests is the carriage of the Langley impact basin (ref. 7) which provides means for effecting the controlled descent of the test specimen. In these tests the impact-basin carriage was used in much the same manner as a conventional stationary landing-gear test jig (see ref. 8). In order to simulate mechanically the wing lift forces which sustain an airplane during landing the pneumatic cylinder and cam system incorporated in the carriage was used to apply a constant lift force to the dropping mass and landing gear during impact. The lift force in these tests was equal to the total dropping weight of 2,542 pounds.

TEST SPECIMEN

The landing gear used in the tests was originally designed for a small military training airplane having a gross weight of approximately 5,000 pounds. The gear is of conventional cantilever construction and incorporates a standard type of oleo-pneumatic shock strut. The wheel is fitted with a 27-inch type I (smooth-contour) tire, inflated to 32 pounds per square inch. The weight of the landing gear is 150 pounds. The weight of the lower mass (unsprung weight) is 131 pounds.

In the present investigation the gear was somewhat modified in that the metering pin was removed and the original orifice plate was replaced with one having a smaller orifice diameter. Figure 14 shows the internal arrangement of the shock strut and presents details of the orifice. Other pertinent dimensions are presented in table III. The strut was filled with specification AN–VV–O–366B hydraulic fluid. The inflation pressure with the strut fully extended was 43.5 pounds per square inch. In these tests the landing gear was mounted with the shock-strut axis vertical. Figure 15 is a photograph of the landing gear installed for testing.

TABLE III

IMPORTANT CHARACTERISTICS OF LANDING GEAR USED IN TESTS

A_a, sq ft	0.05761
A_h, sq ft	0.04708
A_o, sq ft	0.0005585
v_0, cu ft	0.03545
p_{a_0}, lb/sq ft	6,264
l_1, ft	0.5521
l_2, ft	2.22604
W_1, lb	2,411
W_2, lb	131

INSTRUMENTATION

A variety of time-history instrumentation was used during the tests. The vertical acceleration of the upper mass was measured by means of an oil-damped electrical strain-gage accelerometer having a range of $\pm 8g$ and a natural frequency of 85 cycles per second. A low-frequency (16.5 cycles per second) NACA air-damped optical-recording accelerometer, having a range of $-1g$ to $6g$, was used as a stand-by instrument and as a check against the strain-gage accelerometer. Another oil-damped strain-gage accelerometer, having a range of $\pm 12g$ and a natural frequency of 260 cycles per second, was used to determine the vertical acceleration of the lower mass. The vertical displacement of the lower mass (tire deflection) and the shock-strut stroke were measured separately by means of variable-resistance slide-wire potentiometers. The vertical displacement of the upper mass was determined by addition of the strut-stroke and tire-deflection measurements. The vertical velocity of the landing gear at the instant of ground contact was determined from the output of an elemental electromagnetic voltage generator. A time history of the vertical velocity of the upper mass was obtained by mechanically integrating the vertical acceleration of the upper mass subsequent to the instant of ground contact. Electrical differentiation of the current output of the strut-stroke circuit provided time-history measurements of the shock-strut telescoping velocity. The instant of ground contact was determined by means of a microswitch, recessed into the ground platform, which closed a circuit as long as the tire was in contact with the platform.

The electrical output of the instruments was recorded on a 14-channel oscillograph. The galvanometers were damped to approximately 0.7 critical damping and had natural frequencies high enough to produce virtually uniform response up to frequencies commensurate with those of the measuring instrumentation. A typical oscillograph record is shown in figure 16.

It is believed that the measurements obtained in the tests are accurate within the following limits:

Measurement	Accuracy
Upper-mass acceleration, g	± 0.2
Force on upper mass, lb	± 500
Lower-mass acceleration, g	± 0.3
Vertical velocity at ground contact, fps	± 0.1
Upper-mass velocity during impact, fps	± 0.5
Upper-mass displacement, ft	± 0.05
Lower-mass displacement, ft	± 0.03
Shock-strut stroke, ft	± 0.03
Shock-strut telescoping velocity, fps	± 0.5
Time after contact, sec	± 0.003

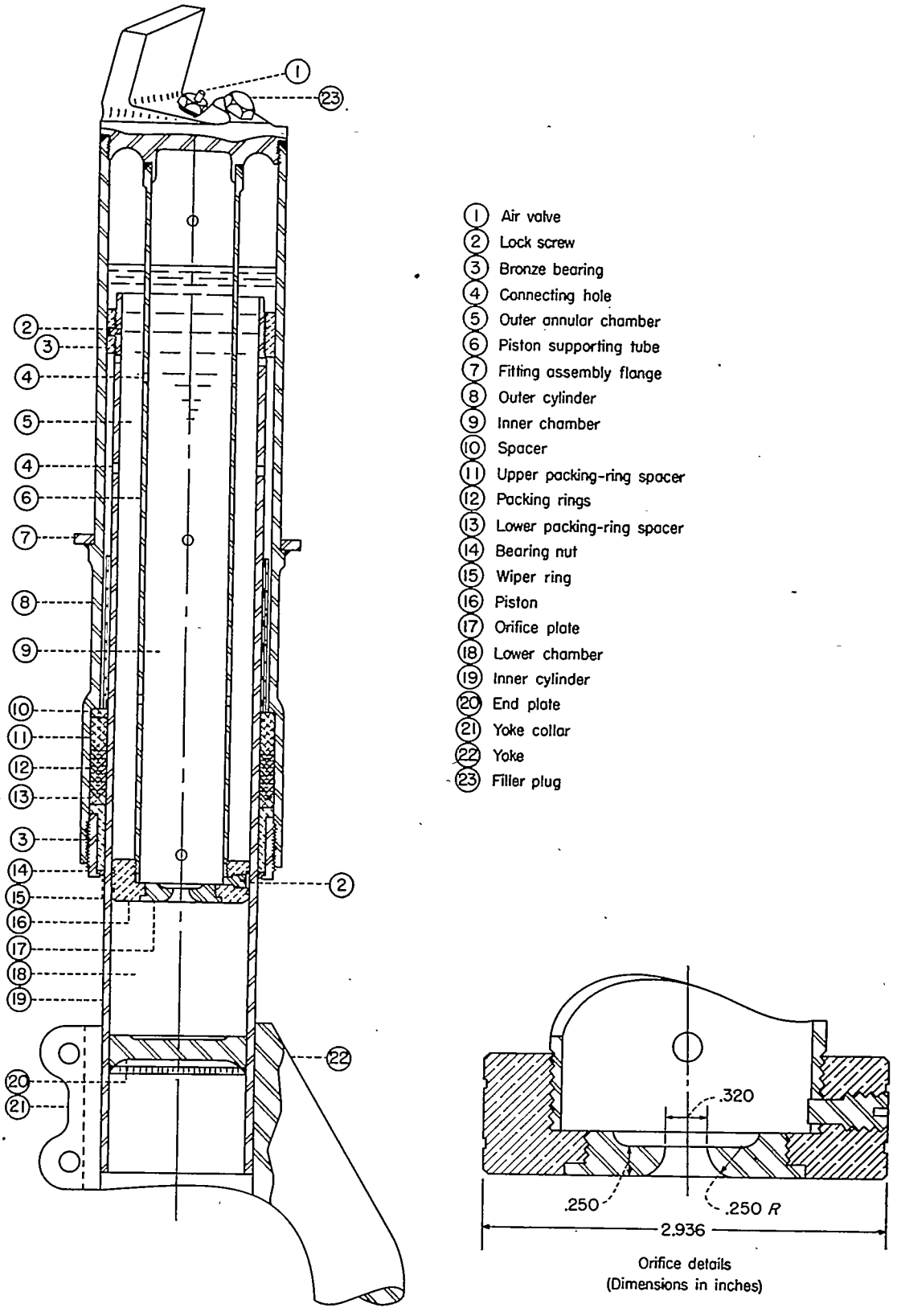

FIGURE 14.—Shock strut of landing gear tested at Langley impact basin.

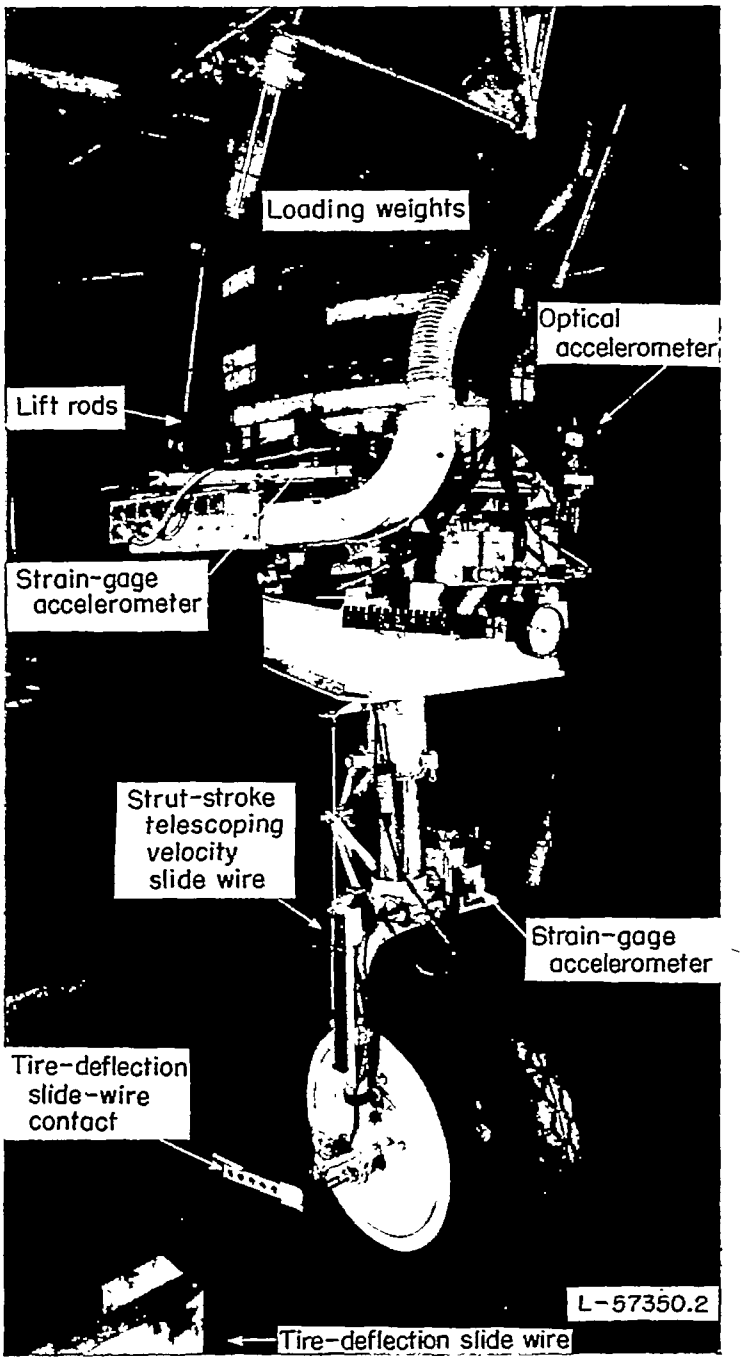

FIGURE 15.—View of landing gear and instrumentation.

REFERENCES

1. McPherson, Albert E., Evans, J., Jr., and Levy, Samuel: Influence of Wing Flexibility on Force-Time Relation in Shock Strut Following Vertical Landing Impact. NACA TN 1995, 1949.
2. Stowell, Elbridge Z., Houbolt, John C., and Batdorf, S. B.: An Evaluation of Some Approximate Methods of Computing Landing Stresses in Aircraft. NACA TN 1584, 1948.
3. Walls, James H.: Investigation of the Air-Compression Process During Drop Tests of an Oleo-Pneumatic Landing Gear. NACA TN 2477, 1951.
4. Hurty, Walter C.: A Study of the Response of an Airplane Landing Gear Using the Differential Analyzer. Jour. Aero. Sci., vol. 17, no. 12, Dec. 1950, pp. 756–764.
5. Southwell, R. V.: Relaxation Methods in Theoretical Physics. The Clarendon Press (Oxford), 1946.
6. Scarborough, James B.: Numerical Mathematical Analysis. Second ed., The Johns Hopkins Press (Baltimore), 1950.
7. Batterson, Sidney A.: The NACA Impact Basin and Water Landing Tests of a Float Model at Various Velocities and Weights. NACA Rep. 795, 1944. (Supersedes NACA ACR L4H15.)
8. Milwitzky, Benjamin, and Lindquist, Dean C.: Evaluation of the Reduced-Mass Method of Representing Wing-Lift Effects in Free-Fall Drop Tests of Landing Gears. NACA TN 2400, 1951.

BIBLIOGRAPHY

Callerio, Pietro: The Shock-Absorbing System of the Airplane Landing Gear. NACA TM 938, 1940.

Kochanowsky, W.: Landing and Taxying Shocks With Oleo Leg Undercarriages. British Ministry of Supply, TPR 3/TIB 2 Translation No. GDC 10/5250 T, Nov. 1944.

Stowell, Elbridge Z., Houbolt, John C., and Batdorf, S. B.: An Evaluation of Some Approximate Methods of Computing Landing Stresses in Aircraft. NACA TN 1584, 1948.

Schlaefke, K.: Zur Kenntnis der Kraftwegdiagramme von Flugzeugfederbeinen. (On Force-Deflection Diagrams of Airplane Spring Struts.)

1. Teilbericht: Vergleich von Diagrammen mit linearer und quadratischer Dämpfung. (Partial Rep. No. 1: Comparison of Diagrams With Linear and Quadratic Damping.) Tech. Berichte, Bd. 11, Heft 2, 1944, pp. 51–53. (Translation available from CADO, Wright-Patterson Air Force Base, as ATI 27004.)
2. Teilbericht: Näherungsverfahren zum Berechnen der Kraftwegdiagramme mit nichtlinearer Federkennlinie und linearer oder quadratischer Dämpfung. (Partial Rep. No. 2: Approximation Method for the Calculation of Force-Deflection Diagrams With a Non-Linear Spring Chart and Linear or Quadratic Damping.) Tech. Berichte, Bd. 11, Heft 4, 1944, pp. 105–109. (Translation available from CADO, Wright-Patterson Air Force Base, as ATI 27031.)
3. Teilbericht: Der Landestoss von Ölluftfederbeinen. (The Landing Impact of Air-Oil Shock Absorbers.) Tech. Berichte, Bd. 11, Heft 5, May 15, 1944, pp. 137–141.

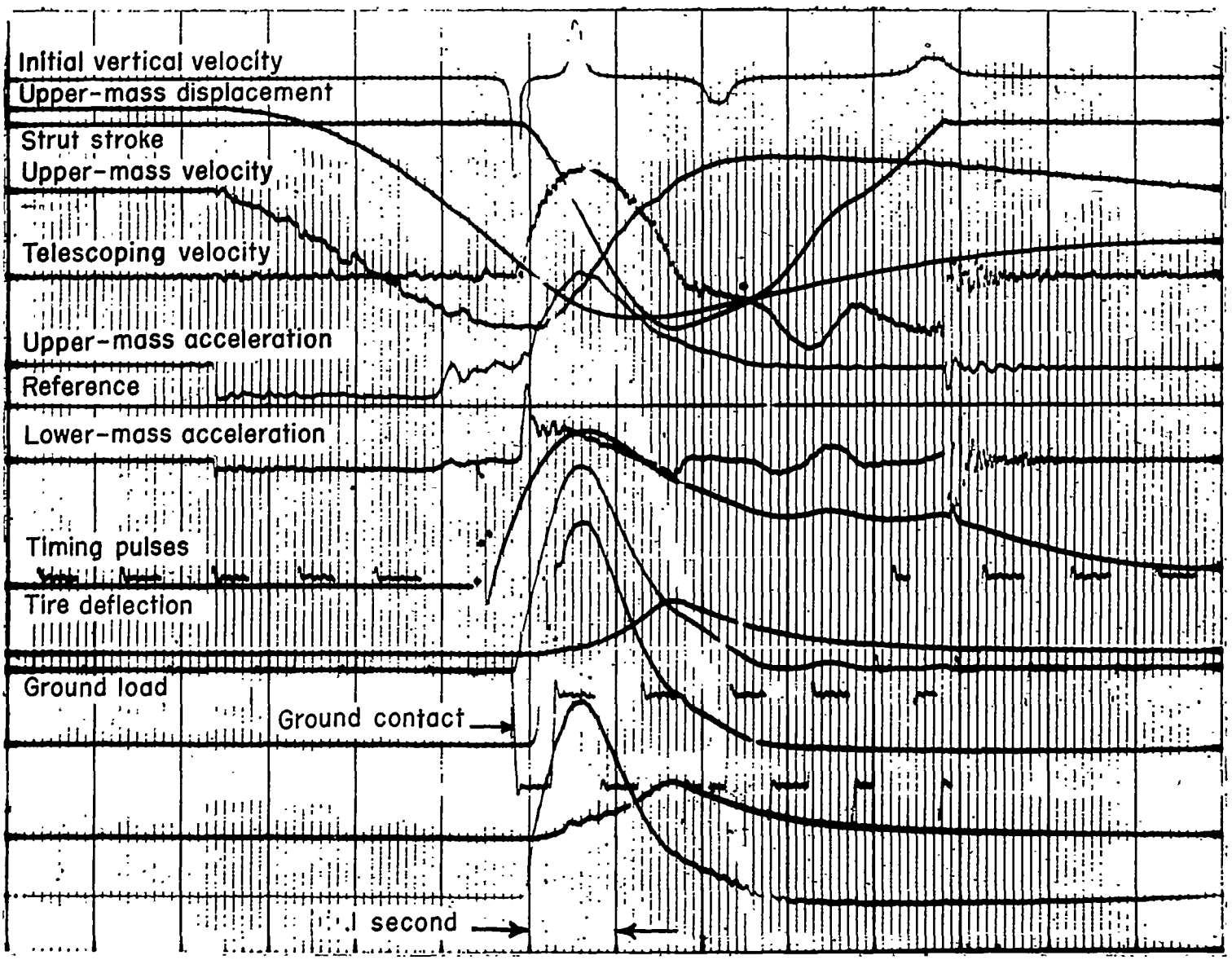

FIGURE 16.—Typical oscillograph record obtained during test in Langley impact basin.

Schlaefke, K.: Zur Kenntnis der Wechselwirkungen zwischen Federbein und Reifen beim Landestoss von Flugzeugfahrwerken. (On Reciprocal Effects Between Landing Gear and Tire in Landing Impact of Airplane Undercarriages.) Tech. Berichte, Bd. 10, Heft 11, Nov. 15, 1943, pp. 363–367.

Marquard, E., and Meyer zur Capellen, W.: Näherungsweise Berechnung der zwischen Fahrgestell und Rumpf beim Landen auftretenden Federkräfte. (Approximate Calculation of the Shock-Strut Forces Occurring Between Landing Gear and Fuselage in Landing.) FB Nr. 1737, Deutsche Luftfahrtforschung (Berlin-Adlershof), 1942.

Marquard, E., and Meyer zur Capellen, W.: Näherungsweise Berechnung der zwischen Fahrgestell und Rumpf beim Landen auftretenden Federungskräfte. (Approximate Calculation of the Shock-Strut Forces Occurring Between Landing Gear and Fuselage in Landing.) FB Nr. 1737/2, Deutsche Luftfahrtforschung (Berlin-Adlershof), 1943.

Yorgiadis, Alexander J.: Graphical Analysis of Performance of Hydraulic Shock Absorbers in Aircraft Landing Gears. Jour. Aero. Sci., vol. 12, no. 4, Oct. 1945, pp. 421–428.

Temple, G.: Prediction of Undercarriage Reactions. R. & M. No. 1927, British A.R.C., Sept. 1944.

Makovski, S. A.: A Method of Shock Absorber Performance Prediction With a Note on Its Application to Tricycle Aeroplanes. TN No. S.M.E. 183, British R.A.E., Sept. 1943.

Frankland, J. M.: Ground Loads in Carrier Aircraft. Rep. No. 7992, Chance Vought Aircraft, Div. of United Aircraft Corp. (Dallas, Tex.), Oct. 20, 1949.

Readey, W. B., and LaFavor, S. A.: An Analytical Method for the Design of Metering Pins and Prediction of Load Stroke History of Landing Gears. Rep. No. 1688, McDonnell Aircraft Corp., May 12, 1950.

Berry, F. R., and Frick, R. P.: Theoretical Development of Load Factor Vs. Time Curves for the DC–6 Main Gear. Rep. No. 21546, Douglas Aircraft Co., Inc., Sept. 1, 1950.

Hurty, Walter C.: A Study of the Response of an Airplane Landing Gear Using the Differential Analyzer. Jour. Aero. Sci., vol. 17, no. 12, Dec. 1950, pp. 756–764.

Masaki, Mamoru, Smilg, Ben, and Moore, C. K.: The Prediction of Vertical Two-Wheel Landing Loads. MR No. TSEAC5–4595–2–10, Air Materiel Command, Eng. Div., U. S. Air Force, May 28, 1946.

Flügge, W.: Landing-Gear Impact. NACA TN 2743, 1952.